CECÍLIA GALLOTTINI DE MAGALHÃES

Investigating lens placode development in vivo

Dissertação apresentada ao Programa de Pós-graduação em Biologia Celular e Tecidual do Instituto de Ciências Biomédicas da Universidade de São Paulo, para obtenção do Título de Mestre em Ciências.

Área de concentração: Biologia Celular e Tecidual

Orientadora: Profa. Dra. Chao Yun Irene Yan

São Paulo

2019

ABSTRACT

Magalhães, C. G. Investigating lens placode development in vivo. 2019. 93 p. Dissertação (Mestrado em Biologia Celular e Tecidual) – Instituto de Ciências Biomédicas, Universidade de São Paulo São Paulo, 2019.

The correct shape, position and alignment of optic components are defined through a series of complex morphological changes during the embryogenesis of the eye. The retina originates from the neural tube´s optic vesicle while the lens precursor cells arise from the ectoderm that overlie the apex of the optic vesicle. This ectoderm is molecularly delimited as pre-placodal and undergoes a series of morphogenic events during its initial development to form the lens placode and subsequently the lens vesicle. The lens placode arises from the thickening of the pre-placodal ectoderm. Subsequently, the placode invaginates to form the vesicle of the lens. During the invagination of the placode, the ectodermal cells that surround the placode (peri-placodal cells) also move to close the opening of the lens that invaginated and reconstruct the surface ectoderm. Here we focus on two processes of eye development. We investigated the role of the extracellular matrix in the lens placode thickening and the dynamics of the emission of membrane protrusions by the peri-placodal cells during the lens placode invagination. The extracellular matrix plays a relevant role in placodal morphogenesis. For example, Fibronectin in the extracellular matrix between the optic vesicle and the pre-placodal ectoderm is required for the formation of lens placode. However, the dynamics of the Fibronectin architecture during placode formation is unknown. Thus, our first aim here was to investigate the architecture of Fibronectin and Laminin, two important components of the extracellular matrix, during thickening of lens placode through confocal 3D images. Our data suggest that both Fibronectin and Laminin present a diffuse and punctate pattern restricted to the placodal region. This pattern is maintained during thickening and invagination of the placode. We found a similar pattern of Laminin in the placodal region of the mouse embryo, suggesting the conservation of this architecture in this context. We also demonstrate that Noggin-mediated inhibition of BMP signalling, which disrupts the development of the eye, affects the organization of Fibronectin and Laminin, suggesting that BMP signalling regulates the organization of the extracellular matrix during the lens placode development. Our second objective was to analyse the emission of thin cellular protrusions by peri-placodal cells correlating with the lens invagination movement. Here we investigated the dynamics and

composition of the cytoskeleton of these protrusions to understand their function during the development of the eye. We observed a large number of protrusions in peri-satellite cells of chicken and mouse embryos. Our quantification results with chicken embryo protrusions showed no correlation between length and direction of emission or with half-life. We also analysed the diversity in the composition of the cytoskeleton, and we found protrusions positive for Cofilin and Tubulin. These data suggest a heterogeneous population of periplacodal protrusions. Finally, we have also identified these protrusions on other ectodermal surfaces of chicken and mouse embryos, suggesting that they play a role in the development of surface ectoderm.

Keywords: Lens placode. Eye development. Extracellular matrix, morphogenesis, thin membrane protrusion.

RESUMO

Magalhães, C. G. Investigating lens placode development in vivo. 2019. 93 p. Dissertação (Mestrado em Biologia Celular e Tecidual) – Instituto de Ciências Biomédicas, Universidade de São Paulo São Paulo, 2019.

O formato, posição e alinhamento corretos dos componentes oculares são definidos através de uma série de mudanças morfológicas complexas durante sua embriogênese. A retina se origina de células da vesícula óptica do tubo neural enquanto as células precursoras do cristalino surgem do ectoderma que reveste o ápice da vesícula óptica. Este ectoderma é delimitado molecularmente como pre-placoidal, sofre uma série de eventos morfogênicos durante o seu desenvolvimento inicial para formar o placóide do cristalino e, posteriormente, a vesícula do cristalino. O placóide do cristalino surge a partir do espessamento do ectoderma pre-placoidal. Posteriormente, o placóide invagina para formar a vesícula do cristalino. Durante a invaginação do placóide, as células da ectoderme que circundam o placóide (células periplacodais) também se movem para fechar a abertura do cristalino que invaginou e reconstruir o ectoderma da superfície. Aqui, nos concentramos em dois processos do desenvolvimento do olho. Nós investigamos o papel da matriz extracelular no espessamento do placóide do cristalino e a dinâmica da emissão de protrusões de membrana pelas células periplacodais durante a invaginação do placóide. A matriz extracelular desempenha papel relevante na morfogênese placodal. Por exemplo, a Fibronectina na matriz extracelular entre a vesícula óptica e o ectoderma pré-placoidal é necessária para a formação de placóide do cristalino. No entanto, a dinâmica da arquitetura de Fibronectina durante a formação do placóide é desconhecida. Assim, nosso primeiro objetivo aqui foi investigar a arquitetura da Fibronectina e da Laminina, dois importantes componentes da matriz extracelular, durante o espessamento do placóide do cristalino através de imagens confocais em 3D. Nossos dados sugerem que um padrão de Fibronectina e Laminina difuso e pontuado é restrito à região do placóide. Este padrão é mantido durante o espessamento e invaginação do placóide. Encontramos um padrão similar de Laminina na região do placóide de embrião de camundongo, sugerindo a conservação desta arquitetura neste contexto. Também demonstramos que a inibição mediada por Noggin (inibidor da sinalização de BMP), que interrompe o desenvolvimento do olho, afeta a organização da Fibronectina e da Laminina, sugerindo que a sinalização de BMP regula a organização da matriz extracelular durante o desenvolvimento do placóide do cristalino. Nosso segundo objetivo foi analisar a emissão de

protrusões celulares finas por células periplacodais correlacionando com o movimento de invaginação. Aqui, nós investigamos a dinâmica e composição do citoesqueleto dessas protrusões para entender sua função durante o desenvolvimento do olho. Observamos uma grande quantidade de protrusões em células periplacodais de embriões de galinha e de camundongo. Nossos resultados de quantificação com protrusões de embriões de galinha não mostraram correlação entre comprimento e direção de emissão ou com meia-vida. Nós também analisamos a diversidade na composição do citoesqueleto, uma vez que encontramos protrusões positivas para Cofilina e Tubulina. Estes dados sugerem uma população heterogênea de protrusões finas de membrana periplacodais. Finalmente, também identificamos essas protrusões em outras superfícies ectodérmicas de embriões de galinha e de camundongo, sugerindo que elas desempenham um papel no desenvolvimento de ectoderme superficial.

Palavras-chave: Placóide do cristalino. Desenvolvimento do olho. Matrix extracelular, morfogênese, protrusão fina de membrana, dinâmica.

1 GENERAL INTRODUCTION

The adult eye is composed of different tissues and has a complex shape. Three main cellular tissues are in the light path of the mature vertebrate eye: the cornea, the most distal transparent and convex layer that covers its outer surface; the lens, also a transparent tissue that is avascular, non- innervated and biconvex; and the retina, the third and most proximal structure that is the neural sensitive component of the eye (Fig. 1). The cornea allows the light to enter in the eye chamber and is the first refractive element that light encounters. It is composed by a simple layer of epithelium cells, stroma and an innermost endothelium layer (Lwigale, 2015). The lens refracts the light rays and directs them onto the retina. The retina is a cup -shaped tissue composed by the neural retina. It contains the photoreceptors (rods and cones), who transduce the luminous stimulus into neural signals that are further processed by additional neural layers of the retina (Cholkar et al., 2013).

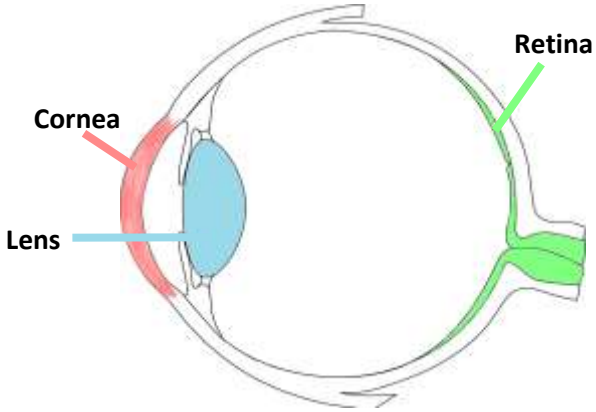

Figure 1. Simplified scheme of an adult human eye.

The anatomy of the eye is crucial for its function, since at the end of the light path a focused image must be formed on the retina.

Its shape and the correct position and alignment of its component tissues are formed through a series of complex tissue changes. For this reason, it has been widely used as a classical model to investigate tissue-shape changes and induction events during embryogenesis. The control of tissue size and shape changes during embryo development is also known as morphogenesis.

1.2 MORPHOLOGICAL EVENTS DURING EYE DEVELOPMENT

The first morphogenetic movement of the eye development begins after neurulation, when the diencephalon of the forebrain extends outwards bilaterally and forms the optic vesicle at stage HH9 (Fig. 2 A-C and F-H). The optic vesicle will form the retina and the retina pigmented

epithelium. As it extends further outwards, the optic vesicle contacts the overlying ectoderm that will form the future lens placode (Fig. 2 A, F and K).

Between stage HH13 and 14, the lens placode is morphologically defined by a cell height increase (Fig. 2C and H). With thus, the lens placode converts from a simple cuboidal epithelium into a pseudostratified epithelium that reaches a thickness of about 36 µm in chick embryos, In contrast, the non-placodal ectoderm remains at the height of 7 µm (Schook, 1980). This transition from a cuboidal monolayer tissue into a thickened pseudostratified placode is characterized by extensive cytoskeletal reorganization. Electron microscopy images demonstrates a rearrangement of the cytoskeleton during lens placode thickening where the microtubules become organized parallel to the apico-basal axis of the cells, following cell elongation (Byers and Porter, 1964).

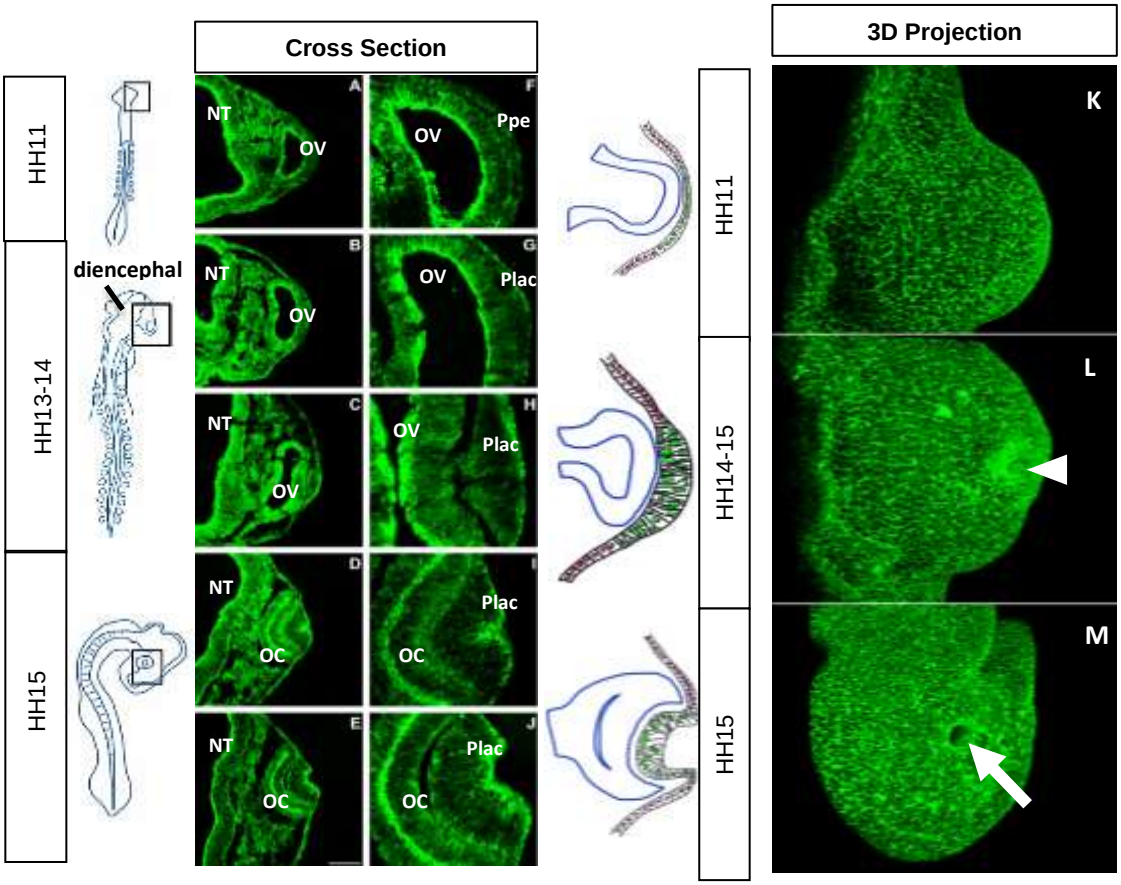

Figure 2. Early eye development (A-J) Cross section of the chick embryo at the eye region in different stages (HH11-HH15) and stained for actin with phalloidin. **(A-E)** Lower magnification of the right side of the head with the neural tube on the left and the optic vesicle, ectoderm and lens placode on the right side. **(F-J)** higher magnification of eye from the same section. **(A and F)** Stage HH11/12: the pre-placodal cells (cephalic ectoderm) adjacent to the optic vesicle are cuboidal and actin labelling is diffuse. **(B and G)** Stage HH13: thickening of placodal cells begins and the transition from pre-placode to placode starts to become visible. Also, actin labelling in the placodal cells is apical. **(C and H)** Stage HH14: the placode is now morphologically defined and the cells have grown in the apical-basal axis. Actin remains apical. **(D and I)** Stage HH15 lens placode undergoes apical constriction and starts to invaginate while the optic vesicle bends inwards following its movement. **(E and J)** End of stage HH15. Scale bar: 100 µm. NT: neural tube; OV: optic vesicle; OC: optic cup; Ppe: pre placode ectoderm; Plac: lens placode. **(K-M)** 3D projection of images obtained in confocal microscopy of chick embryo stained with phalloidin in different eye development stages. The optical slices were taken apically and the 3D projection was turned. **(K)** Stage HH11, the placode is not formed and the surface has a dome shape. **(L)** Stage between HH14 and HH15 where placode is formed and the surface starts to deform in the centre of the placode where the lens pit arises(with arrowhead). **(M)**The lens placode invaginates and the lens pit deepens (white arrow points to the invagination centre). Images were taken on confocal microscopy. Scale bar (bottom right corner of image E): 100 µm.

During lens placode formation, there is an increase in cell density through placodal cell proliferation combined with a disproportionately lesser expansion in placodal area. In this process, the volume of an individual cell does not change, and increase in cell density results in cell packing and in the height of the placodal tissue, which can be seen as its thickening (Mckeehan, 1951; Hendrix & Zwaan, 1973; Shook, 1980). After cell height increase, actomyosin filaments accumulate in the apical domain (Fig. 2B-E and G-J, Borges et al., 2011). The accumulation of actin in the apical domain is not sufficient for apical constriction and placode invagination (Jidigam et al., 2015; Melo et al., 2017). After lens placode formation, Rho pathway is activated (Borges et al., 2011). Rho GTAses also are located in the apical domain and its activity is necessary for the accumulation of myosin that activates contraction of the apical cell domain (Borges et al., 2011). Contraction of the apical actomyosin cytoskeleton reduces apical area (Fig. 2 D-E and I-J; Borges et al., 2011; Plageman et al., 2011). This process is known as apical constriction and results in the lens placode invagination. The inhibition of actin-myosin function prevents apical constriction and interferes with epithelial invagination (Borges et al., 2011).

The thickness of lens placode remains constant during invagination (Schook, 1980). Also, during lens placode thickening and invagination, blebs are found in the apical surface of the tissue. These blebs are no longer present after invagination is complete (Schook, 1980). Thus, it has been suggested that blebbing is a mechanism complementary to apical constriction to reduce the apical membrane surface area.

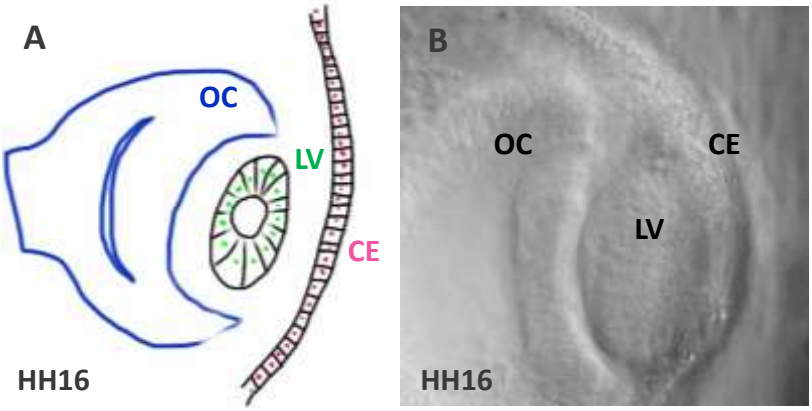

Figure 3. Chick eye at stage HH16. (A) Schematic representation of the embrionic eye. Cells with the green nucleus correspond to lens vesicle (LV). Cells of the ectoderm with the pink nucleus correspond to the periplacodal cells, which will later form the cornea epithelium (CE). The optic cup is outlined in blue (OC). **(B)** One optical slice from confocal image of the eye.

After its invagination, the lens placode reaches maximum lumen constriction and separates from the ectoderm, forming the lens vesicle (Fig. 3). Electron microscopy analysis shows pycnotic nuclear fragments at the borders of the detaching lens vesicle which indicate cell death in apical surface at this stage (Schook, 1980). Cell death is also observed at the borders of the neural tube during chick neural tube invagination (Weil et al., 1997). Caspase inhibition results in neural tube closure deficiency, suggesting that programmed cell death is required for the dissociation of the invaginating tissue for its original ectodermal (Weil et al., 1997).

Meanwhile, the optic vesicle also invaginates inwards, resulting in the formation of a cup shaped-tissue (Fig. 2 D-E). The optic cup is now formed by bilayer epithelium that will derivate the neural retina and retinal pigmented epithelium (Fig. 3).

During lens invagination, the ectodermal cells that surround the placode (periplacodal cells) also move in to close the lens aperture and rebuild the surface ectoderm over the recently formed lens vesicle (Fig. 3). These regions will later form the transparent corneal epithelium (Fig. 3). At the end of these morphogenetic processes, the basic components of the mature eye are stablished.

1.3 MOLECULAR EVENTS DURING EYE DEVELOPMENT

1.3.1 Pre-placodal region

The location of placode precursors is specified in early stages of the vertebrate embryo. After gastrulation, when the three germ layers have formed (ectoderm, mesoderm and endoderm), the ectoderm is divided in neural plate, neural plate border and epidermal ectoderm (Fig. 4 A-C). Variations in the levels of bone morphogenic protein (BMP) concentration is one of the major molecular factors that play a role in the differentiation of ectoderm. BMP is a ligand from the TGF-β family and an important morphogen present in various developmental processes. High levels of BMP lead to the differentiation of ectoderm into epidermis, while low levels direct ectoderm to a neural fate (reviewed in Hintze et al., 2017). The pre-placodal region is determined by intermediate levels of BMP at the neural plate border (Fig. 4B; Linker et al., 2009; Patthey et al., 2009; reviewed in Hintze et al., 2017). Fibroblast growth factor proteins (FGF) are also required for specifying the neural plate border in ectodermal cells and for pre-placodal region induction (reviewed in Andrea Streit, 2008; Hintze et al., 2017). Together, BMP and FGF signalling regulate neural and non-neural territories.

At

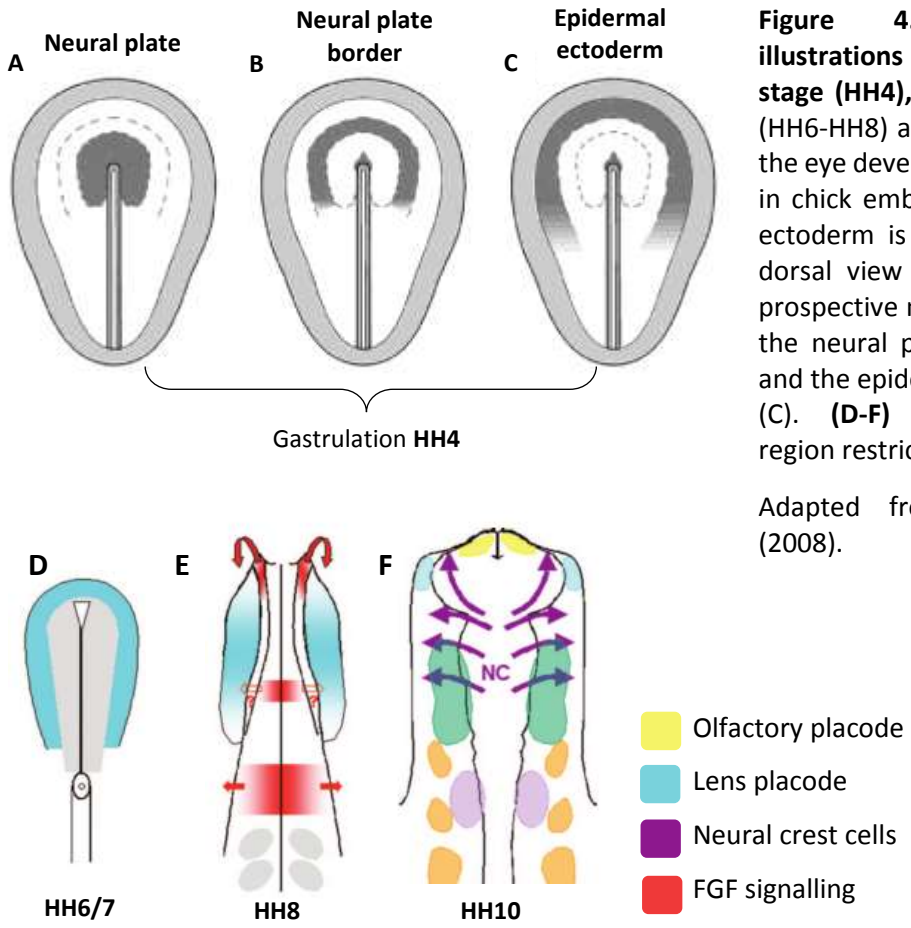

Figure 4. Schematic illustrations of late gastrula stage (HH4), neurula stages (HH6-HH8) and beginning of the eye development (HH10) in chick embryos. **(A-C)** The ectoderm is represented in dorsal view and divided in prospective neural plate (A), the neural plate border (B) and the epidermal ectoderm (C). **(D-F)** Lens placode region restriction.

Adapted from Streit, A. (2008).

early stages (HH6), cells from pre-placodal region have the potential to form any sensory placode (Bailey et al., 2006), but they have an initial *default* competence to develop lens (reviewed in Streit, 2008). When cultivated *in vitro*, the pre-placodal ectoderm from different regions (HH6) express lens placode specific markers (Bailey et al., 2006).

Experiments with mesoderm transplants in chick embryo at stage HH6-7 showed that the head mesoderm and neural plate emits signals that induce the pre-placodal region. Transplantation of cells from the head mesoderm and the neural plate induced expression of pre-placodal cells specific markers in other ectodermal regions (Litsiou et al., 2005). The head mesoderm and the neural plate signals reduce BMP signalling to intermediate levels, which is essential for activation of pre placodal genes (Litsiou et al., 2005; Pieper et al., 2012; Hintze et al., 2017). Wnt signalling also restricts the placodes formation to the head and play an important role in the neural plate border cell fate (Hintze et al., 2017).

1.3.2 Lens placode region restriction

Since the early pre-placodal domain has a strong preference to form lens placode (Fig. 4D), the development of the lens can be viewed as a restriction of the lens fate to the ectoderm overlying the optic vesicle. Thus, after stage HH8, lens specification is suppressed everywhere except at ectoderm over the optic vesicle (Fig. 4E). The neural plate starts to invaginate and the anterior neural ridge secrets FGF, which induces olfactory placode specification (Fig. 4E; Bailey et al., 2006; Sjodal et al., 2007). Studies with chicken pre-placodal ectoderm culture showed that FGF signalling is necessary and sufficient for inducing olfactory fate (Bailey et al., 2006). When cultivated without FGF, cells from pre placodal region express lens specific markers. But, when the same cells are exposed to FGF, they only express olfactory specific markers (Bailey et al., 2006). In other words, the exposure of FGF in lens territory changes its fate and promotes expression of olfactory placode markers (Bailey et al., 2006). With this, FGF plays an important role in delimiting the lens placode region by repressing lens characteristics (Fig. 4E).

After the approximation of optic vesicle to the ectoderm (HH10), the restriction of lens character continues with the migration of neural crest cells (Fig. 4F; Bailey et al., 2006; reviewed in Andrea Streit, 2008). Neural crest cells derive from the neural plate and migrate after neural tube formation. Those cells are required for sustained repression of lens fates and their absence results in the formation of ectopic lens (Grocott et al., 2011; Litsiou et al., 2005; Bailey et al., 2006).

1.3.3 Lens placode specification in the ectoderm and the role of BMP signalling in lens placode development

BMP is produced by the optic vesicle and induces lens placode development. $BMP^{-/-}$ mice fail to develop lens (Furuta and Hogan, 1998; Wawersik et al., 1999). BMP expression from optic vesicle induces placode-specific gene expression, like Sox2 and Pax6 (Furuta and Hogan, 1998; Wawersik et al., 1999). Further, chick explant assays of placodal cell differentiation, (Sjodal et al. 2007) demonstrated that the duration of exposure to BMP signals is also important for lens placode specification. When exposed for longer and uninterrupted time to BMP4 the pre-placodal ectoderm cells *in vitro* developed lens placode characters (Sjodal et al., 2007).

Other studies have also demonstrated that BMP signalling is not only required for lens placode specification, but also for pre-placodal ectoderm thickening and cytoskeletal organization. The

pre-placodal ectoderm BMP4-/- of mouse embryos do not undergo cell height increase, remaining cuboidal (Furuta and Hogan, 1998). Not only the induction by BMP signalling is important, but the expression of BMP receptors is also crucial for lens morphogenesis. When BMP receptors were conditionally deleted in the pre-placodal ectoderm of mouse embryos and the lens failure morphogenesis. In addition, in those mice, the cytoskeleton rearrangement necessary for apical constriction did not occur (Rajagopal et al., 2009).

In chick embryos, inhibition of BMP signalling in pre-placodal ectoderm also showed that BMP is essential for lens morphogenesis. To inhibit BMP signalling, chick embryos were electroporated with a plasmid construct expressing the BMP antagonist Noggin at stage HH11 in pre-placodal cells (Jidigam et al., 2015). Noggin overexpression repressed lens placode thickening, apical constriction and epithelial invagination (Jidigam et al., 2015; Figure 5). Further, inhibition of BMP signalling reduced apical accumulation of F-actin (Jidigam et al., 2015). This data demonstrates that the BMP pathway plays an important role in the conversion of the lens pre-placode to placode.

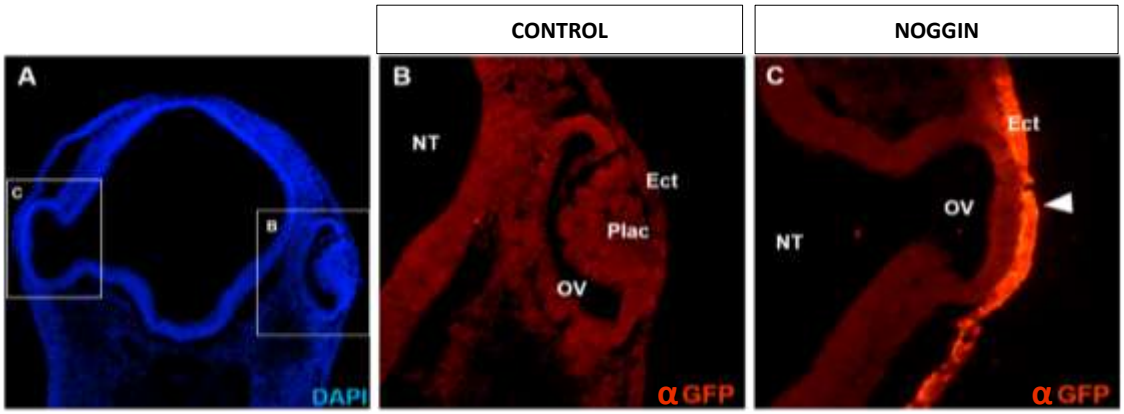

Figure 5. Noggin overexpression suppresses placode thickening. (A) Coronal cross section of chick embryo head at stage HH16 electroporated with Noggin on the right eye (left side of image) and stained with DAPI. **(B)** Higher magnification of the control left eye. The eye develops normally – the lens placode has invaginated and the overlying ectoderm has covered the lens vesicle to form the surface ectoderm that will differentiate into the corneal epithelium. **(C)** Noggin-electroporated cells lack a placode and the cephalic ectoderm remained cuboidal. The electroporated region is identified by the presence of GFP (stained redçarrowhead). NT: neural tube; OV: optic vesicle; Plac: placode; Ect: periplacodal ectoderm.

2 EXTRACELLULAR MATRIX CHANGES DURING LENS PLACODE DEVELOPMENT

2.1 INTRODUCTION

2.1.1 Extracellular matrix during embryo development

The extracellular matrix (ECM) is the acellular component that plays an important role in tissue shape, homeostasis and cell differentiation. The composition of the ECM determines its physical characteristics and signalling properties. Together, both the mechanical and molecular signals derived from the ECM can influence cell differentiation, behavior and polarity. Differences in the ECM architecture, its density and porosity regulates tissue shape and organization (Rozario and DeSimone, 2010; Mouw et al., 2015; Kleinman et al., 2003). Likewise, the cells in the overlying tissues are constantly changing and can affect ECM composition, altering their surrounding microenvironment through secretion of extracellular molecules, remodeling the ECM and its physical characteristics. Thus, the relationship between extracellular environment and cells is interrelated.

2.1.2 Extracellular matrix signalling: extracellular components (more on Fibronectin and Laminin)

The ECM is composed of water, polysaccharides and proteins (Alberts et al., 2010). The composition and physical characteristics of the ECM are dynamic and changes during embryonic development. Four main fibrous proteins compose the ECM: collagens, elastins, fibronectins and laminins (Alberts et al., 2010). Their distribution and assembly are responsible for physical characteristics that regulates tissue scaffolding and ultimately controls their shape. Here, we focused on Fibronectin and Laminin dynamics during chick eye development.

Fibronectin is a large secreted glycoprotein that displays binding motifs recognized by cell surface receptors and collagen (Fig. 6B; Mouw et al., 2014). It plays an important role in cell adhesion, migration and differentiation (Schwarzbauer and De Simone, 2011). Fibronectin has multiple domains that interact with cell receptors, collagen, proteoglycans and other Fibronectin molecules (Schwarzbauer and De Simone, 2011). It can regulate cellular cytoskeleton organization through its interactions with cell receptors, such as Integrins (Meo and Schwarzbauer, 2005). Briefly, compacted Fibronectin binds to Integrins (see Item 2.1.3) that are associated to actin filaments. This provides a structural connection to transmit

mechanical signals from the ECM to the cell. Indeed, Fibronectin can act as an extracellular mechanorregulator of cell behavior. Fibronectin has molecular motifs that can participate in the conversion of mechanical force to biochemical signals (Jalali et al., 2001; Vogel and Sheetz, 2006; Smith at al., 2007). When stretched, Fibronectin deforms, exposing additional sites that can bind to additional isoforms of Integrin (reviewed in Frantz et al., 2010;Mao and Schwarzbauer, 2005). The exposed domains interact with cellular membrane receptors that modulate intracellular signalling pathways and cytoskeletal organization, thus triggering intracellular signalling pathways that change cell behavior. With this, Fibronectin modulates cell migration and shape through interactions with cellular membrane receptors (Vogel and Sheetz, 2006).

Fibronectin plays important role in embryonic development. During heart development, pre-cardiac cells migrate along gradients of Fibronectin, which act as a guide for specific migration (Linask and Lash, 1986). Also, during neural crest cell migration, Fibronectin stablishes migration routes. In cell culture studies, trunk neural crest cells do not synthesize Fibronectin, but their adjacent cell do (Newgreen and Thiery, 1980; French-Constant and Hynes, 1988). Migrating neural crest cells express Integrin receptors that interact with Fibronectin domains (French-Constant and Hynes, 1988). This suggests that non-crest cells secret Fibronectin that is necessary for stablish migration routes for the neural crest cells.

Conversely, extracellular Fibronectin assembly can be modulated by cell traction movements. Vascular endothelial cell lines studies show that mechanical stretching induces collagen and Fibronectin synthesis (O'Callaghan and Williams 2000).

Another important component of the ECM is the Laminin. Laminin is a heterodimer composed of three long polypeptide chains (Fig. 6A). In early embryos, Laminin is the major component of the basement membrane, the portion of ECM that supports the entire epithelium in the organism and has a critical role in body architecture (Alberts, 2010). Disruption of Laminin interaction with other ECM components perturbs the basement membrane and affects morphogenesis processes (Kadoya et al., 1997). For instance, transgenic mouse embryos with knockout for chain ϒ1 of Laminin fail to develop and die after stage E5.5, since they could not produce basement membrane (Smyth, et al., 1999). The knockout of chain ϒ1 results in the non-formation of several types of Laminin, resulting in the absence of basement membrane, with no or little labelling of matrix components in early stages (E4.5 dpc).

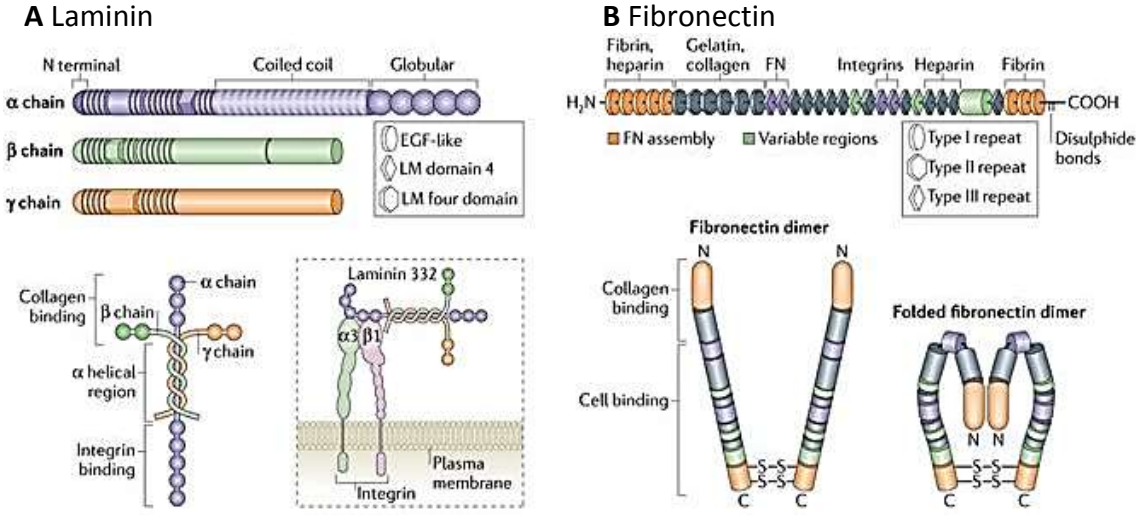

Figure 6. Schematic representation of Laminin and Fibronectin molecules. (A) Tree chains (upper) that compose the Laminin molecule (bottom left). Laminin association with Integrin (bottom right). **(B)** Fibronectin molecule with binding sites (upper) and Fibronectin dimer relaxed (bottom left) and folded (bottom right). EGF, epidermal growth factor; LM domain, Laminin domain. Adapted from Mouw et al., 2014.

Antibody used here for Fibronectin labelling is derived from chicken embryo fibroblasts culture and do not have its target epitopes mapped. Antibody used here for Laminin labelling recognizes the subunit alpha-1 (alpha chain).

2.1.3 ECM signalling: membrane receptors

The ECM membrane receptors transduce changes from the extracellular environment into changes in cell behaviour. On the extracellular domain, those receptors recognize the ECM components and, on the intra-cellular domain, they interact with the cytoskeleton. One of the main ECM receptors are the Integrins. Integrins are heterodimers composed by two subunits (α and β). They play important roles in mechanobiology and morphogenesis processes.

In vascular endothelial cells, mechanical stress induce Integrins expression that bind to specific ECM ligands and regulates cellular response (Jalali et al. 2001). When plated in different ECM mediums and then exposed to shear stress, vascular endothelial cells will adapt their Integrins expression accordingly. For instance, when plated in Fibronectin (ligand for α5β1 and αvβ3), they express Integrin β1 and, in Vitronectin (ligand for αvβ3), they express Integrin β3 (Jalali et al. 2001). In other words, there is a dynamic remodelling of Integrin expression profile at the membrane triggered by shear stress in conjunction with changes in ECM composition. This example also implies that the interaction between Integrins and their respective ligands in the ECM is very specific, thus requiring remodelling of the Integrin profile to respond to

changes in the ECM. This specificity and remodelling are crucial for the cell response to the physical modulations of the extracellular medium. After blocking the specific Integrin-binding sites of ECM ligands, the signals induced by shear stress to intracellular pathways are abolished (Jalali et al. 2001).

In chick development, Integrins are required for neural crest migration. Inhibition of Integrin interaction with Fibronectin results in reduction in the number of migrating neural crest cells (reviewed in Bokel and Brown, 2002).

The cell also responds to the effects of the extracellular medium by modulating it. During Xenopus gastrulation, blocking Integrin-binding sites that interact with Fibronectin results in deficiency in Fibronectin deposition at the blastocoel roof (Marsden and DeSimone, 2001). The cell rearrangement and cells organization is severely modified (Marsden and DeSimone, 2001). This data shows the importance of the interactions between Integrins and ECM components in regulating cell shape and tissue organization.

Growth factors signalling pathways illustrate well the interaction between intracellular signalling and ECM. When secreted, TGF-β complexes with extracellular LAP protein (latency-associated protein) which contains Integrin-binding sites (RGD) (Fig 7C; revised by Munger and Sheppard, 2011). The interaction of the extracellular TGF-β-LAP complex through its RGD domain with cellular Integrins can activate intracellular TGF-β signalling pathway (Fig. 7C). In this scenario, TGF-β activates its pathway not through its own receptor, but through the interaction of LAP with Integrins. Therefore, TGF-β signals can be modulated by interactions between Integrins and ECM (Fig. 7C; revised by Munger and Sheppard, 2011).

As Integrins transmit mechanical signals from the ECM to the cell, TGF-β pathway can also be modulated by mechanical changes. *In vitro* assays demonstrate that changes in contractile forces can modulate release of TGF-β molecules (reviewed in Rozario and DeSimone, 2010). In rat cardiac fibroblast cell culture, intense stretching increases the levels of TGF-β (Lee et al. 1999). Furthermore, during mammary gland development, ECM degradation can release TGF-β, which regulates branching and ductal growth (Sternlicht et al., 2006). In other words, the ECM remodeling can influence TGF-β cellular signalling, release or storage in the extracellular environment.

The importance of the interaction between BMP and collagen IV has been shown in Drosophila development (reviewed in Lecuit, 2007). The interaction between collagen IV and Dpp (BMP homologue) enhances Dpp interaction with its receptor, activating the BMP pathway. Thus, extracellular collagen IV regulates the gradient of available BMP during dorsoventral axis and wing formation (reviewed in Lecuit, 2007).

On the other hand, TGF-β can also change ECM composition in a feed-back loop. Smooth muscle cells submitted to cyclic stretch increase TGF-β expression. This increase ultimately results in increase of collagen IV and Fibronectin deposition, remodeling the ECM (Joki et al., 2000). Other growth factors, such as FGF, can also induce ECM components synthesis during mechanical stress (Chiquet, 1999).

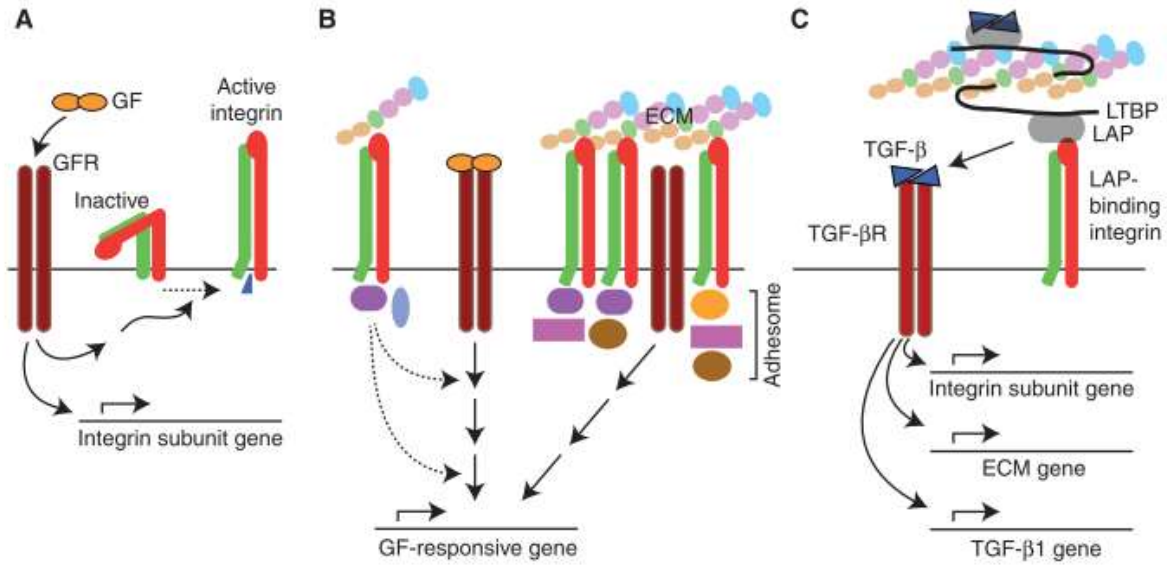

Figure 7. Cross talk between Integrins and growth factors. (A) Growth factors signalling can activate Integrins receptors and change Integrins subunit expression (the two subunits are differentiated by green and red). **(B)** Integrins binds to ECM molecules (collared balls) and affect growth factor receptor signalling, acting on downstream components of the growth factor pathway. **(C)** TGF-β binds to LAP, which in associated with LTBP, a component of the ECM. TGFβ-LAP complexes interact with Integrins and regulate gene expression. GF: growth factor; GFR: Growth factor receptor; LAP: latency-associated peptide; LTBP: latent TGF-β binding protein. Adapted from Munger and Sheppard, 2011.

2.1.4 ECM in embryonic development

Embryonic axis elongation is a well-studied morphogenetic process and it involves both cytoskeletal and ECM remodeling. As such, it is a good example of the importance of ECM in

embryonic shape changes. In zebrafish, Laminin and Fibronectin are important for proper embryo elongation as it regulates the notochord, somites and neural tube extensions (reviewed in Rozario and DeSimone, 2010). In zebrafish mutants for Laminin, the notochord failed to differentiate (Parsons et al., 2002). The extracellular matrix between mesoderm and neural plate regulate morphogenetic movements in early neurulation stages of zebrafish embryos (Araya et al., 2016). When Laminin and Fibronectin levels were reduced by antisense morpholino treatment, the neural plate did not form a properly shaped neural tube. Instead, the cells formed disorder aggregates (Araya et al., 2016).

In Xenopus embryos, knockdown of Integrin subunits that contain Laminin binding sites also result in neurulation failure (Lallier and DeSimone, 2000). Interestingly, in this study the neurulation induction was not affected as there was no changes in gene expression, but its morphogenesis process was severely disturbed (Lallier and DeSimone, 2000).

In chick embryo studies, the dynamic of ECM was observed during paraxial mesoderm and somite development. This study demonstrated that Fibronectin and Laminin matrix follows pre-somitic mesoderm maturation. The organization of Fibronectin changes during somite development, changing from globular architecture to a fibrillar matrix with higher complexity (Rifes and Thorsteinsdóttir, 2012).

2.1.5 ECM during eye morphogenesis

The presence of ECM components as Fibronectin, Laminin and Collagen IV throughout late eye development is described in detail; however little is known about the evolution of ECM architecture during early eye morphogenesis (reviewed in Kristen M. Kwan, 2014).

Histochemical methods showed the presence of glycoproteins and glycosaminoglycan between pre-placodal ectoderm and optic vesicle. The density of interfacial matrix increases during lens induction (Hendrix and Zwann, 1975).

Immunostaining with Laminin and Fibronectin antibodies followed the presence of these proteins in cross sections during chick lens development. At stage HH13, both Laminin and Fibronectin are intensely labelled between the optic vesicle and pre-placode ectoderm (Hilfer and Randolph, 1993). At stage HH15, Fibronectin staining seems to form particles between the optic cup and lens placode (Hilfer and Randolph, 1993). Also, after lens placode

invagination, both Laminin and Fibronectin staining are less intense between lens vesicle and optic cup when compared to the ECM surface ectoderm (Hilfer and Randolph, 1993).

Previous work has shown that morphological changes during lens formation depend on the quality of the ECM (Rozario, T. and DeSimone, D. W., 2010; reviewed in Kristen M. Kwan, 2014; Diaz-de-la-Loza et al., 2018). Experiments with mutant mouse embryos showed that Fibronectin is essential for lens placode development (Huang et al., 2011). Mutant mice with lens-specific knockout of Fibronectin did not develop lens placodse. Placodal thickening and lens pit invagination did not occur (Huang et al., 2011). The pre-placodal ectoderm remained cuboidal but, interestingly, there was actin accumulation in the apical membrane (Huang et al., 2011). This suggests that while Fibronectin in the basal membrane is necessary for the increase in cell height it may not be required for apical actin accumulation. Also, this data shows that placode thickening is a prerequisite for invagination. Together, these data underscore the importance of the placodal ECM in its morphogenesis and suggest that cell height increase is Fibronectin-dependent.

Although studies showed that Fibronectin is present during and is essential for lens placode development, how its architecture is modified during morphogenetic processes has not been investigated. Since ECM is very dynamic and maintains a close interaction with the cell, our objective here was to understand the importance of ECM architecture during lens placode morphogenesis.

2.2 MATERIALS AND METHODS

2.2.1 Obtaining and incubating embryonated eggs

Fertilized Leghorn chicken eggs were obtained from Granja Yamaguishi, Jaguariúna – SP (for embryos used in experiments in University of São Paulo) and Henry Stewart & Co. (for embryos used in experiments in University of Oxford). The eggs were incubated at approximately 37.7 ° C and 50% relative humidity for 36-38 hours to obtain embryos at stage HH10-11, 42-45 hours to obtain embryos at stage HH14 and 50h hours to obtain embryos at stage HH15. After *in ovo* electroporation, the embryos were incubated for 6-18 hours according to the stage desired in the experiment (Hamburger, 1992).

2.2.2 Obtaining and dissecting Mouse embryos

We obtained embryos at stages between E9.0 and 10.0 resulting from the cross of two lines: ROSA26mT-mG and ROSA-Cre/ERt2 transgenic line (see Methods chapter 3, item 3.2.5). We collected the embryos in M2 media (Sigma) cultured in a 1:1 mix of CMRL (Invitrogen) and KnockOut Serum (Gibco). Embryos were kept at 37°C in 5% CO2 until fixation.

2.2.3 Immunofluorescence

Chicken and mouse embryos were staged and dissected in PBS. We removed all the extra-embryonic membranes and collected the head. They were fixed in paraformaldehyde (PFA) 4% for 25-30 minutes (chick embryos) and 2-3 hours (mouse embryos) and washed for 10 minutes, 3 times in PBS 1x. They were permeabilized in 1% Triton X-100 in PBS for 30 minutes and incubated in 5% bovine serum albumin (BSA) in PBS for 3h at room temperature as described by Rifes and Thorsteinsdóttir, 2012. We used the following primary antibodies: mouse monoclonal anti-chicken Fibronectin (DSHB, clone B3/D6, diluted 5-1 ng/ml; chick embryos only), rabbit polyclonal anti-green fluorescence protein (Life, A6455, diluted 1:200), and rabbit polyclonal anti-Laminin (Sigma, L9393, diluted 1:60 – donated by Shankar). All primary antibodies were diluted in PBS 1x with 1% BSA and 0.1% Triton X-100. Embryos were incubated with primary antibodies for 48h at 4°C and washed for 10 minutes, 3 times in PBS 1x (Rifes and Thorsteinsdóttir, 2012). Subsequently, they were incubated with secondary antibodies, phalloidin coupled to different fluorophores (Thermo Life Scientific, 1:100) and DAPI (Invitrogen, 1 mg/ml, diluted 1:1000) for 24h at 4°C. Secondary antibodies used were: anti-mouse Alexa Fluor 568 or Alexa Fluor 647 and anti-rabbit Alexa Fluor 488, all diluted in

PBS 1x (Invitrogen, diluted 1:600). The embryos were maintained under mild agitation during all washes and incubations.

2.2.4 Electroporation in ovo

After incubation to the right stage, the eggs were exposed through an opening in the shell and the chicken embryos were contrasted by non-toxic Indian ink injection at the vitelline membrane (10% in Howard Ringer's saline). Close to the optic vesicle on the right side of the embryo, a puncture was made with a glass capillary microneedle and approximately 1 ml of Ringer's saline solution was applied over the embryo to facilitate electric conduction. Platinum electrodes (4 mm apart) were positioned so that the positive electrode was on the left side and the negative electrode on the right side of the embryo. Injection of a solution stained with 0.1% Fast Green containing one or two plasmids of interest, was targeted through a glass microneedle to the external surface of the ectoderm of the right eye. The electric pulses were applied simultaneous to plasmid injection with the following parameters: 5 pulses of 9 V with duration of 50ms in intervals of 100 ms. We used the plasmids pcS2+-Noggin (donated by Chenbei Chang, University of Alabama at Birmingham, USA) and pcDNA3.1-mGFP ressuspended in H_2O at a concentration of 1,5-3,0 µg/µl. The mGFP sequence is a modified GFP containing the palmitoylation domain from GAP43. This domain is sufficient for membrane association of the resulting fusion protein (Okada et al., 1999). We subcloned mGFP into the plasmid pcDNA3.1 by digesting pCAG-mGFP (Addgene plasmid #14757) with NotI and EcoRI and inserting in pcDNA3.1 at the same sites. After electroporation, the eggs were sealed with nontoxic packing tape and incubated again to the proper stage.

2.2.5 Mounting fixed embryos

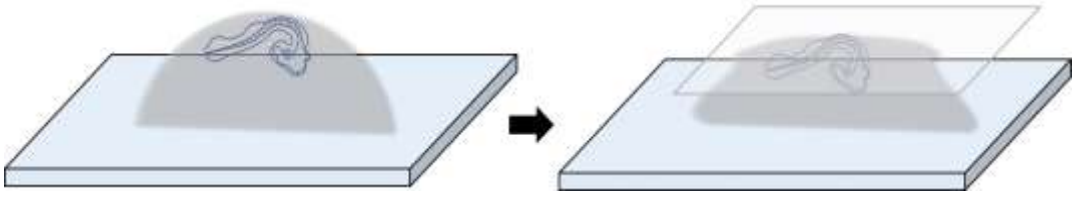

Figure 8. Schematic representation of mounting the chick embryo in agarose low melt disk. The embryo is placed in melted low melt agarose, without sinking (left). Immediately, a coverslip is placed on the top, so that, after the agarose hardens, the embryo will be close to the flat surface of the disc (right).

To position the chicken and mouse embryos at the correct angle for imaging, we placed them in a drop of 2% low melt agarose made in water at 42°C. Before the agarose hardened completely, we placed a glass cover slip on top of the drop to create a flat horizontal surface (Fig. 8). The embryo was placed as close as possible to the objective of the microscope. After hardening, the agarose flat disk containing the embryo was turned upside down in petri dish with glass cover slip at the bottom and imaged in an inverted confocal microscope. To avoid dehydration, the agarose flat disks were maintained in PBS before placing at the microscope.

We also used Methyl Cellulose (MC; Sigma, M0387) as an alternative medium to mount the embryos in a petri dish with coverslip in the bottom (MatTek P35G-1.0-14-C). In this method, the embryo was positioned on the coverslip and all liquid medium was removed, allowing the embryo to remain close to the cover sheet by surface tension. Then we covered the embryo with the MC solution. The MC was diluted in water to 2-3%: 0,02 g/ml MC, 4,5 g/ml glucose, HEPES (1mM:10ml) , 25% PBS1x, 0,25% fungizone. To make the MC solution, the powder was slowly added to 65°C MilliQ water with constant stirring and left shaking at 4°C overnight. The other components (at 2X concentration) were added on the next day in a 1:1 proportion while hand mixing the solution. The final solution was aliquoted with a syringe and frozen for long-term storage.

2.2.6 Confocal imaging

Confocal images were acquired on a Zeiss LSM-780 NLO (CEFAP, ICB – USP, FAPESP 2009/53994-8) and on Zeiss 880 Airyscan fast (Srinivas Laboratory, University of Oxford). In Zeiss LSM-780 NLO, we used a 60x 1.4 NA oil immersion lens (Objective Plan-ApoChromat 63x / 1.40 Oil Infinity/0.17). In Zeiss 880 Airyscan fast, we used 40x 1.2 NA oil immersion lens (Objective C-Apochromat 40x/1.20 W Korr M27) with 1.5 digital zoom. Images were obtained with 1 µm stack interval, generating a 3D image.

2.2.7 Image analysis

Analysis of the images obtained in confocal microscopy was performed by Fiji (ImageJ version 2.0.0-rc-49/1.51p). Stacks were merged into 2D images using Z Project tool, with the methods of maximum intensity and sum of pixel values. For the supplementary movie, we used the 3D Projection tool.

2.2.8 Chicken eye dissection for RNA isolation

We dissected chick eyes electroporated with pCS2+-Noggin 20-24 hours after electroporation, when the embryos where at stage HH15-16. In all dissections, we separated the lens placode attached to the optic vesicle with RNAse free materials in 1x PBS with DEPC (1:1000) and on ice. (Figure XX). After dissection, the tissue pieces were placed in 30 µl Extraction Buffer solution from the PicoPure RNA Isolation Kit (Applied Biosystems). The RNA was isolated on a column with the PicoPure kit. After isolation, the RNA was stored in a freezer at -80° C until used in the reverse transcription reaction to obtain cDNA. For each group, 3 replicates were performed (see Table below).

	POOL	Nº OF DISSECTED EYES
HH15-16 ELECTROPORATED WITH NOGGIN (EXPERIMENTAL + CONTROL)	1	5+5
	2	7+7
	3	8+8

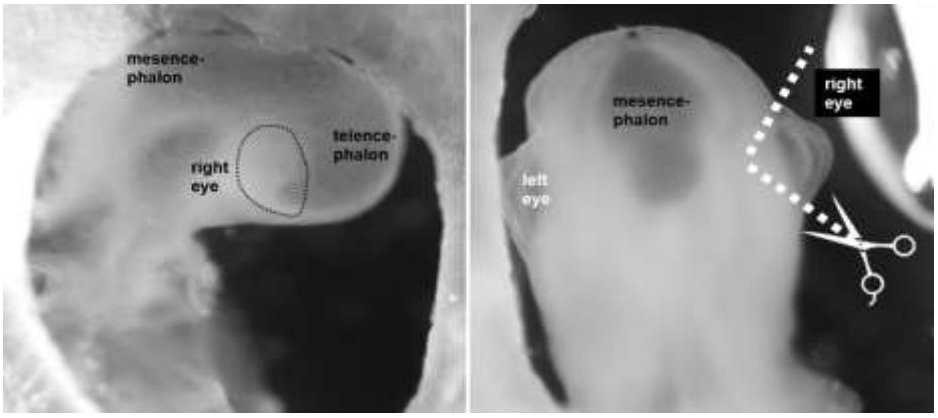

Figure 9. Chicken eye dissection scheme. A. Chicken embryo at stage HH14 positioned laterally. **B.** For the dissection of the eyes, we placed the embryo dorsally and initially perform two cuts with microscopes at the border of the eye (dotted white line). After these first cuts, we removed as much as possible of the peripheral ectodermal tissue.

2.2.9 qRT-PCR

The cDNA synthesis reaction was performed with Oligo-DT using the enzyme SMARTScribe Reverse Transcriptase (ClonTech) and 1 µg of total RNA (quantified using Epoch BioTek). Real-time PCR analysis (40 cycles, 95 ° C for 15 seconds, 60 ° C for 1 minute) was performed in the presence of SYBR-Green (Applied Biosystems) with the StepOnePlus instrument (Applied Biosystems). Each reaction was performed in triplicates with variation

between Ct values less than 0.5. In each well we used 5 µl of the cDNA reaction at a concentration from 11 to 14 ng/µl, 5 µl of each primer pair at 20 µM and 10 µl of SYBR-Green. For the blank, we used H_2O instead of cDNA.

- **Primers design**

Firstly, we identified extracellular matrix proteins that could be in the region between the placode and the optic vesicle through an extensive analysis of the classical literature on the composition of the extracellular matrix in this region in chicken and mouse embryos. We also screened the gene expression database for chicken embryo (Geisha) to look for genes from the extracellular matrix that were enriched in the optical region by *in situ* hybridization experiments. Then, we searched for the genomic sequences of Integrin subunits, Laminin, Fibronectin and BMP receptors on chicken genome (Genome Browser UCSC – genome version g6a/galGal6). We designed specific primers for the amplification of the 5' portion of the target genes (Table). We chose sequences that were conserved in all isoforms of the selected proteins. The sequences of the primers also corresponded to the 5’ portion of an exon with the 3’ portion of the next exon.

To validate the primers, we performed a first qPCR assay using cDNA obtained from whole chicken embryo heads at stages HH11, HH14 and HH15. We analysed the amplification efficiency and the curve Ct profile to validate the use of the primers. We selected only primers that presented the Ct values between 20 and 30. The target genes selected for expression analysis were Integrin α2 (isoforms x1 and X2), Integrin α5 and Laminin α1.

Tabel 1. Targets genes and their designed primers

Target Gene	Code	Primer forward	Primer reverse	Start and end nucleotide	Amplification Efficiency (E_{target}*)
Cadherin 1	NM_001039258	Tccgcaatgatgtg gcccc	gctgccttcaggttc tcgtcg	2478-2545	Not used
Integrin α2 (x1 e X2)	XM015277561	Tggcacggccaca aataatg	agcacatgccgaa gttccaa	6445-6549	1.8787
Integrin α4	XM421974	Caccacaccaaaa gccaact	aacccacgttagct ctccaa	4452-4509	Not used
Integrin α5	KC439457	Tggtgacggggct gcagtg	agcccagcttgtag aggccg	3215-3306	2,1883
Laminin α1	NM001199806	Tgtgggaggactcc ccatag	tgccaatgcaggca ggaata	8600-8638	1.8604
Laminin γ1	XM_001234658.4	Ccacagtacgtgcc ttcact	cattttgttcaccgc cccag	7100-7200	Not used
Fibronectin	NM001198712	accaagttggaga gcagtggc	aacgccagccctgc tgt	7276-7323	Not used
BMP receptor II	AB006785/nm001001465.1	Aacatgacaacatt gcccgc	cacccagtcacttg tgtgga	977-1078	Not used

* E_{target}= 10 ^ [-1/slope]. The slope was obtained from Mean CT Value at three concentrations of cDNA: 24, 12 and 6 ng/µl (see FigureXX).

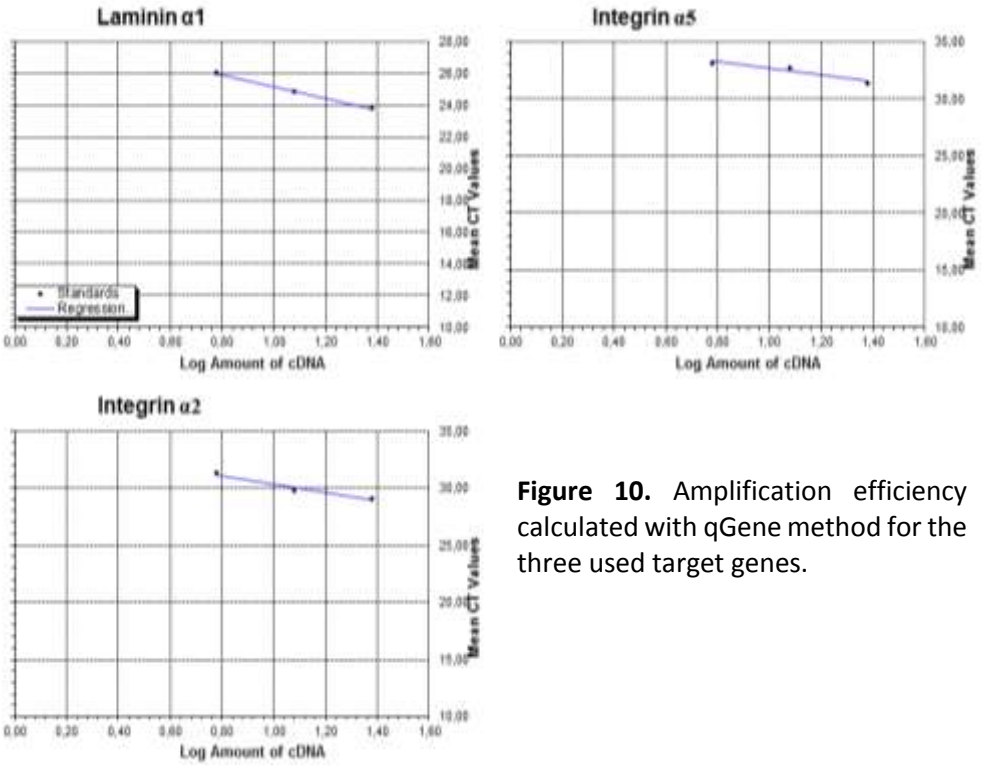

Figure 10. Amplification efficiency calculated with qGene method for the three used target genes.

- **qPCR data analysis**

Normalized expression data were obtained after processing the Ct values (cycle threshold) by the Q-Gene method of relative quantification (Muller et al., 2002). We used the Q-Gene Core Module file (qgene96.xls) that is structured into four worksheets. In the "Setup" worksheet, the plate sample is listed, linking the sample names with that of the target genes. In the "Q-PCR Reaction" worksheet, there is information about the PCR reagents (their concentrations and volumes). In the "Amplification Efficiency Plot" worksheet the amplification efficiency of the target gene and the reference gene (Etarget and Eref) is calculated. We used GAPDH as the reference gene. The last worksheet is the "Data Analysis", where the normalized expression is calculated based on Ct-values, Etarget and Eref. The Ct-values obtained in real-time PCR assay of the target and reference gene were entered manually. All mean normalized expression (MNE) data were obtained with the mean of the normalized expression values of the triplicates. Lastly, Values of SD and mean were calculated using GraphPrism software (version 7).

2.3 RESULTS

2.3.1 Fibronectin immunostaining pattern during chick eye development

Our first question was if the Fibronectin architecture changes during eye development in chick embryo. During eye development, the placodal region undergoes intense morphological remodelling whilst the non-placodal region does not. Since the ECM quality and composition are important in tissue morphogenesis, our hypothesis was that the Fibronectin immunostaining would have a different pattern in the lens placodal region when compared to non-placode regions, outside of the optic vesicle.

To investigate if the Fibronectin pattern evolves during window of time of lens placode thickening, we analysed embryos at pre placodal ectoderm stages (HH10-11), placodal stages (HH14) and during placode invagination (HH15).

Before lens placode thickening (HH11), the Fibronectin in the ECM between the optic vesicle and surface ectoderm presented a different staining pattern when compared to its surrounding regions, outside the optic vesicle region (Fig. 11 A-B'). In the peri-placodal region, the Fibronectin presented a fibrillar organization (Fig. 11 B-B', cyan arrowhead). At the pre-placodal region, we observed a more diffuse and punctate pattern (Fig. 11 B-B', magenta arrowhead). These two differing patterns are also observed at stage HH14, when placodal cells have already grown in the apical-basal axis but have not undergone apical constriction or invagination. In the ECM underlying the lens placode region the Fibronectin was diffuse and punctate (Fig. 11 C-D', magenta arrowhead). In the ECM underlying the non-placodal region, the fibrillar pattern was more evident, with a thick fibrillar pattern arranged circumferentially to the placodal border (Fig. 11 D-D', cyan arrowhead). Together, these data suggest that a more diffuse ECM architecture underlying the lens placode region is important for placode development.

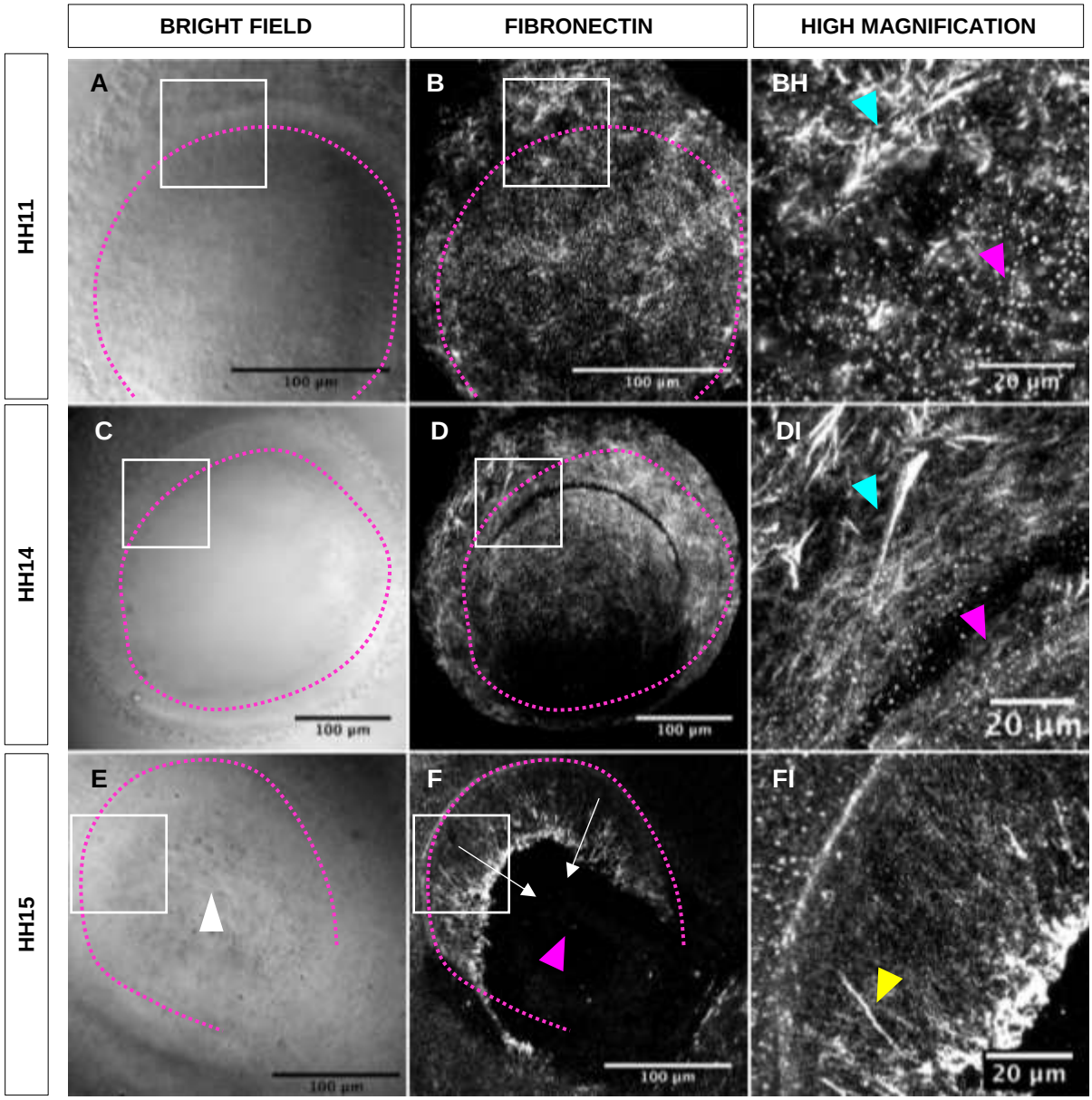

Figure 11. Fibronectin pattern differs on placodal and extra-placodal regions. (A-F) Z-projection in maximum intensity of apical view of the eye in different stages. The dotted magenta line delimits the optic vesicle borders that lies under the placodal region. **(A, C and E)** Bright field (grayscale) of one optical slice. **(B, D and F)** Immunostaining for Fibronectin (white). **(B', D' and F')** High magnification of the white square in the first and second column. **(A-B')** At stage HH11 the placode is not yet formed (A). At this stage, the ECM between the pre placode ectoderm and the optic vesicle displays a diffuse and punctate Fibronectin immunostaining pattern (magenta arrowhead). The ECM of regions outside of the optic vesicle present a fibrillar organization (far from the dotted line; cyan arrowhead). **(C-D')** At HH14 stage the placode is formed and the difference of Fibronectin immunostaining pattern is more evident. There is a diffuse and punctate Fibronectin immunostaining pattern at the ECM immediately overlying the optic vesicle (inside the dotted circle, magenta arrowhead), while periplacodal regions present a fibrillar organization (outside the dotted circle, cyan arrowhead). **(E-F')** At stage HH15, during lens placode invagination, the diffuse and punctate pattern of Fibronectin in the placodal region is maintained (magenta arrowhead). While the lens placode invaginates the periplacodal ectoderm approximates to the invagination centre (white arrowhead) to close the tissue and form the cornea. The ECM in this region has a different Fibronectin pattern, which is fibrillary and parallel (yellow arrowhead) to the invagination movement (white arrows).

During lens placode invagination (HH15), the Fibronectin in the ECM between the invagination placode and the optic vesicle remained diffuse (Fig. 11 E-F', magenta arrowhead). Interestingly, a new Fibronectin staining pattern appeared in the ECM under the periplacodal cells that will become the future cornea. At this region, non-placode ectodermal cells are following the lens invagination movement to close the tissue. The Fibronectin displayed a fibrillar pattern organized in parallel arrays pointing from the base of the future cornea towards the centre of the lens placode entry point (Fig. 11 F-F', yellow arrowhead). The Fibronectin that surrounded the optic vesicle had evolved to densely packed thick bundles (Fig. 11 F).

In conclusion, the Fibronectin immunostaining pattern was more diffuse in the lens placode when compared to regions periplacodal regions. This architectural diversity that might be important for lens placode morphogenesis.

2.3.2 Laminin immunostaining pattern during chick and mouse eye development

Differently to Fibronectin immune assays at stage HH11, the Laminin in the ECM between the optic vesicle and pre placodal ectoderm presented similar pattern when compared to non-placode regions (Fig. 12 A, C and E, yellow arrowhead). We observed a fibrillar pattern of Laminin inside and outside the optic vesicle region, with no clear difference in the lens placode region (Fig. 12 E, yellow arrowhead). On the other hand, at stage HH14, the Laminin in the thick placodal region was diffuse when compared to non-placodal regions (Fig. 13 D-E). In 3D projection images, the thick dark region (Fig 13 E) corresponds to region with diffuse staining of Laminin (Fig. 13 C). At stage HH15, the Laminin in the ECM between the invagination placode and the optic vesicle remains diffuse (Fig. 12 F, white arrowhead) whereas the ECM that surrounds the lens placode invagination contains dense thick Laminin fibrils and bundles (Fig. 12 F, magenta arrowhead).

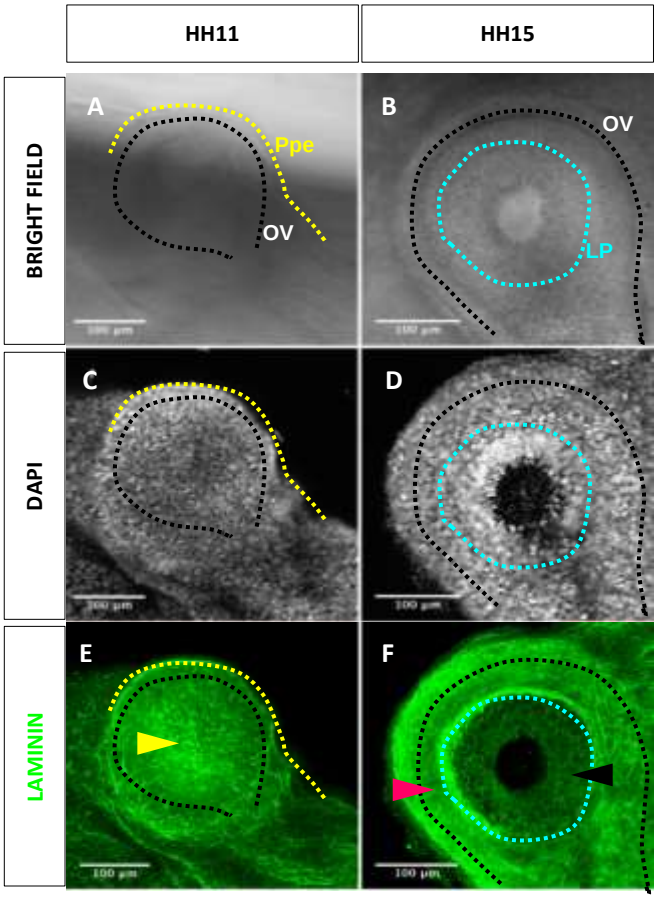

Figure 12. Laminin staining pattern differs from the placode and periplacode regions **(A-F)** Apical view from optic region at two different stages, pre placode ectoderm (first column; yellow dotted line) and invaginating placode (second column; cyan dotted line); white dotted line delimits the optic vesicle. **(A-B)** Bright field of the last optical slice (most basal optic section). **(C-D)** Z-projection in maximum intensity. Staining for nucleus (grayscale) with DAPI. **(E-F)** Immunostaining for Laminin (green). **(E)** At stage HH11, the ECM between pre placodal ectoderm (yellow dotted line) and optic vesicle, the Laminin immunostaining shows a fibrillar and dense pattern and the same pattern is found outside the optic vesicle region (purple arrowhead). **(F)** At stage HH15, the placode is formed and invaginating. The ECM in the boundaries and outside of the optic vesicle displays a fibrillar pattern (magenta arrowhead) and diffuse pattern in the placode region (white arrowhead).

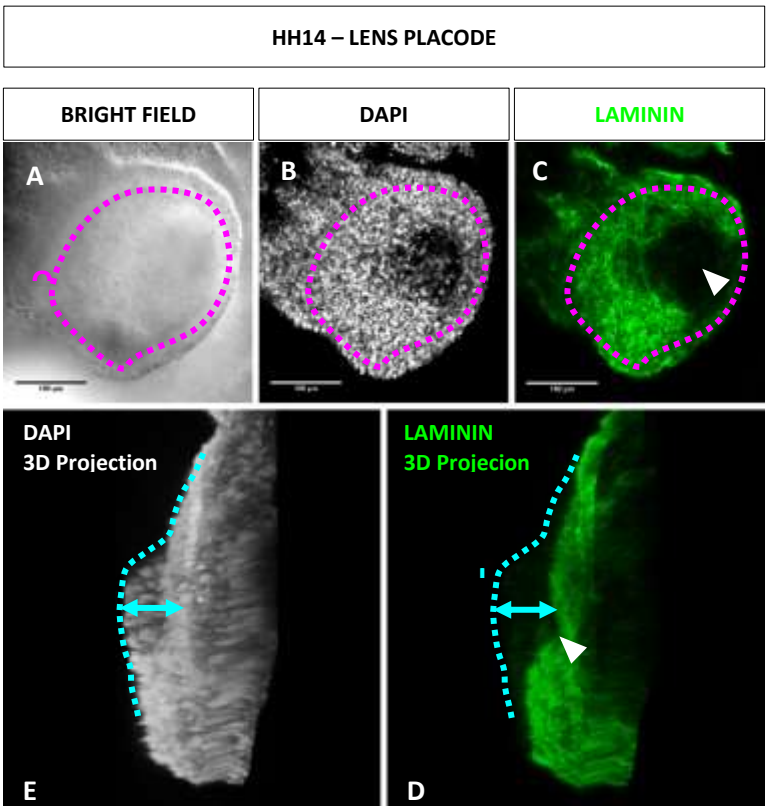

Figure 13. Laminin is diffused and punctate in the thick placodal region at stage HH14. **(A-C)** Z-projection in maximum intensity of apical view form eye region. **(A)** Bright field of the last optical slice (most basal optic slice) Optic vesicle is delimited by magenta dotted line. **(B)** Staining for nucleus (grayscale) with DAPI. **(C)** Immunostaining for Laminin (green) shows a diffuse pattern in the placode region (white arrowhead). **(D-E)** 3D Projection rotation of DAPI (D) and Laminin images (E). **(E)** With 3D view, it is able to analyse the thick lens placode region (cyan double-arrow). Cyan dotted line delimits the placode and non-placode ectoderm apical surface.

This data suggest that Laminin and Fibronectin have a very similar architecture during eye development. At stage HH14, when lens placode is thick, both had a diffuse and punctate pattern in the ECM between the optic vesicle and the placodal ectoderm. At stage HH15, during lens placode invagination, Fibronectin and Laminin showed a fibrillar pattern in peri-placodal regions, in the ECM outside of the optic cup region and between optic cup and non-placodal ectoderm (Fig. 11-13).

Next, in order to investigate if this pattern is also conserved in other vertebrate models, we analysed the Laminin immunostaining pattern in mouse embryos at stage E9.5. As the eye development is conserved among vertebrates, our hypothesis was that we would observe a similar evolution of Laminin immunostaining pattern during placode formation in the mouse embryo. We found it difficult to define if the lens placode was already thick or not in E9.5 mouse embryos. This is because, in mouse embryos, the lens placode are very close to the optic vesicle, and they remain attached to each other by filopodia (Chauhan et al., 2009;

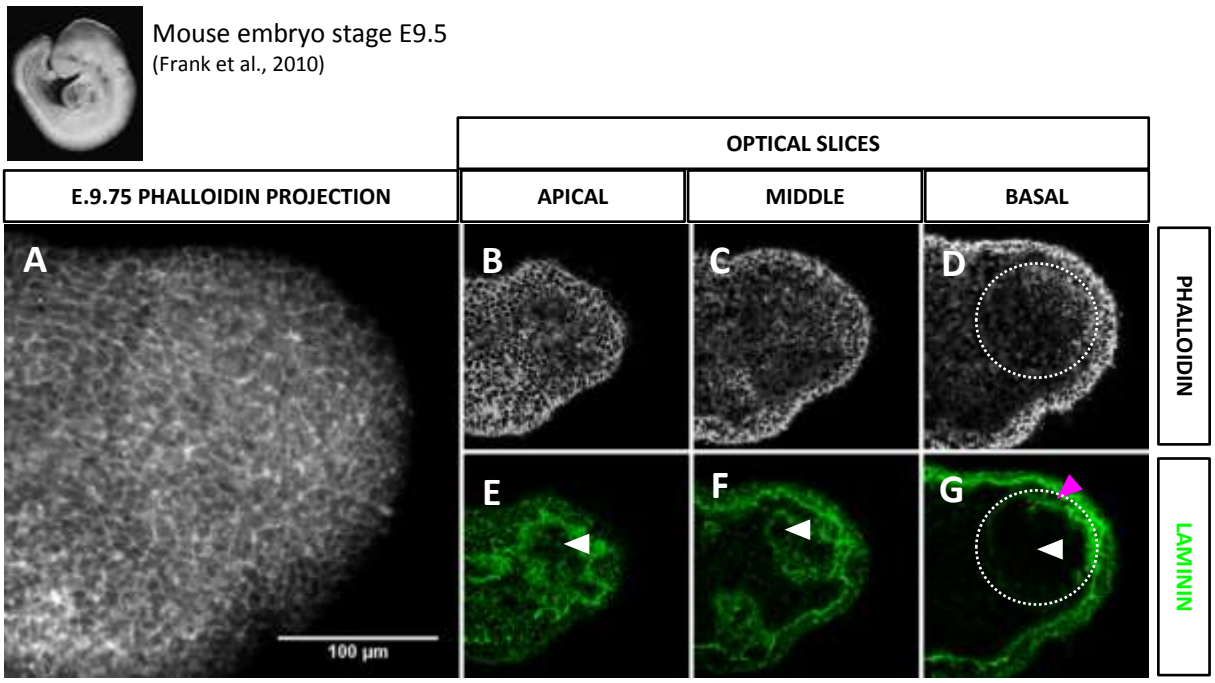

Figure 14. Laminin is organized in bundles and has a degraded aspect in placodal region in mouse. (A-G) Apical view form eye region of mouse embryo stage E9.75. **(A)** Z-projection of phalloidin staining. (B-G) Different optical slices (stacks in Z), from apical (B and E) to basal (D and G). **(B-D)** Phalloidin staining shows irregular staining pattern of cells boundaries inside the optic vesicle region (dotted white line delimits the optical vesicle), at the region underlying the lens placode. **(E-G)** Laminin immunostaining shows different pattern in lens placode region (white arrowhead) compared to the periplacodal regions (magenta arrowhead). In lens placode region the Laminin staining pattern is more diffuse, while outside the lens region there is a fibrillar and dense labelling.

reviewed in Kwan 2014). The proximity between the tissues results in a concave shape and hinders the proper alignment of the embryo for 3D projection imaging. However, by analysing the optical sections separately, we observed two distinct patterns of Laminin immunolabeling. (Fig. 14). Between the optic vesicle and placodal ectoderm, Laminin is organized in bundles, but has a degraded aspect and there were regions where staining was absent, as discontinuities in a layer (Fig. 14 E-F, white arrowhead). In regions outside the optic vesicle, Laminin immunostaining shows a more fibrillar pattern (Fig. 14 E-F, magenta arrowhead).

2.3.3 Effects of BMP inhibition in Laminin and Fibronectin immunostaining pattern

Since BMP signalling is a pre-requisite for progressing from pre-placodal to placodal state, we investigated the importance of BMP signalling on the architecture of Fibronectin during lens placode morphogenesis. Here, our hypothesis was that BMP signalling is upstream ECM organization and its inhibition would change Fibronectin and Laminin pattern in chick embryos.

To investigate this, we optimized Noggin overexpression in one eye of the chick embryo at stage HH10-11. Noggin overexpression inhibits BMP signalling and arrests eye development (see Fig. 5; Jidigam et al., 2015). Pre-placodal cells (HH10-11) were co-electroporated with Noggin and mGFP (Fig. 5).

Embryos electroporated with Noggin did not develop a placode and both Fibronectin and Laminin staining were significantly different when compared to the control (Fig. 15). In the lateral view of pre placodal ectoderm and optic vesicle at stage HH11 it is already possible to analyse the effect of Noggin overexpression. In the control embryo, the Fibronectin in the lens placode precursor region has a slightly more punctate pattern (Fig. 15 B', magenta arrowhead), than in the rest of the tissue (Fig. 15 B and B', cyan arrowhead), whereas in the experimental embryo, Fibronectin appears to be organized in bundles throughout the tissue (Fig. 15 D and D').

Later at stage HH15, the lateral view of control embryo show a diffuse and punctate pattern of Fibronectin immunostaining between the invaginating placode and optic cup (Fig. X15 F and F', magenta arrowhead). As analysed in the results already shown in Fig. 15, in the ECM underlying the non-placodal region, Fibronectin displays a fibrillar pattern (Fig. 15 E-F', cyan arrowhead). Close to the invaginating placode, the fibrillar pattern of Fibronectin is organized

in parallel arrays pointing towards the centre of the lens placode entry point (Fig. 15 F-F', yellow arrowhead). At this stage, embryos electroporated with Noggin did not develop lens placode (Fig. 15 G) and Fibronectin was organized in disordered fibrillar aggregates and formed sparse bundles under the putative placodal region (Fig. 15 H and H').

Next, we analysed if the Laminin immunostaining pattern is also changed after BMP signalling inhibition. Indeed, as in Fibronectin analyses, chick embryos electroporated with Noggin have fibrillar pattern of Laminin in the optic vesicle region (Fig. 16 B and D), yellow arrowhead). At stage HH14 and HH15, in the ECM between optic vesicle and Noggin positive ectoderm, Laminin immunostaining has a fibrillar pattern.

In conclusion, Noggin-treated embryos did not display a diffuse and punctate pattern of Fibronectin and Laminin and there is no difference in the staining of the extra placodal and pre-placodal regions (Fig. 15 and 16). Observed changes in Fibronectin and Laminin organization suggests that BMP signalling could regulate the organization of the extracellular matrix during lens development.

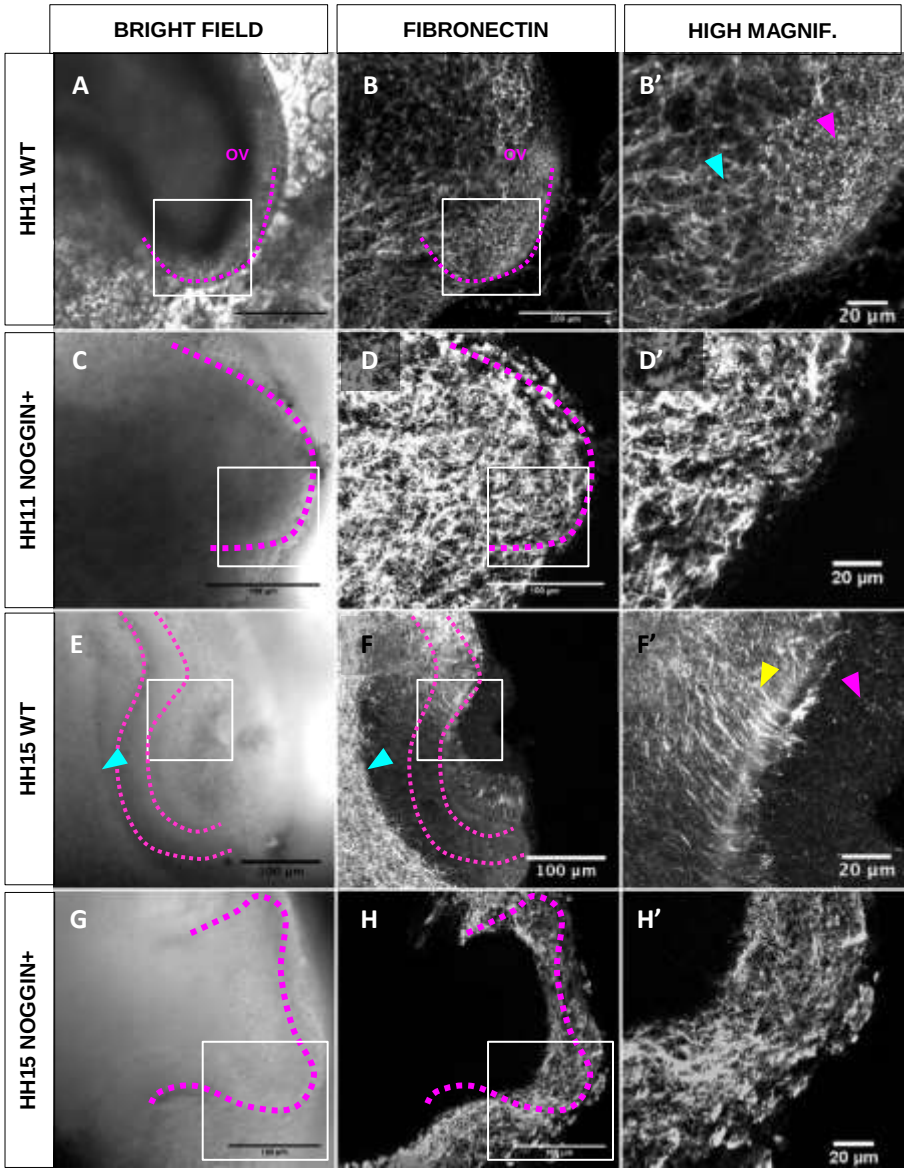

Figure 15. Noggin overexpression changes Fibronectin organization. Lateral view of the right eye of chick embryos electroporated with Noggin at stage HH9-11 and collected 4 hours (E-F') and one day after electroporation (G-H'). **(A, C, E and G)** Bright field of most basal optical slice. Magenta dotted line delimits the optic vesicle. **(B, D, F and H)** Z-projection in maximum intensity lateral view of immunostaining for Fibronectin (grayscale). **(B', D', F' and H')** High magnification of immunostaining for Fibronectin; the magnified area corresponds to the white square in the first and second column. **(B-B')** At HH11 the ECM between the pre-placode ectoderm and the optic vesicle displays a dense and punctate Fibronectin immunostaining pattern (magenta arrowhead). The ECM of regions outside of the optic vesicle present a fibrillar organization (cyan arrowhead). **(C-C')** The lateral view of the invaginating placode shows a dense and fibrillar network of Fibronectin in the ECM, outside of the optic vesicle (cyan arrowhead). There is a diffuse and punctate Fibronectin immunostaining pattern at the ECM in the invagination placode region (magenta arrowhead). The ECM between the periplacodal ectoderm that approximates to the invagination centre, following the placodes movement, shows fibrillary and parallel pattern of Fibronectin (yellow arrowhead). OV: optic vesicle. **(E-H')** Noggin overexpression supressed lens placode development (E and G) and modified the Fibronectin immunostaining to a more fibrillar and disordered pattern when compared to the placodal regions in control embryos.

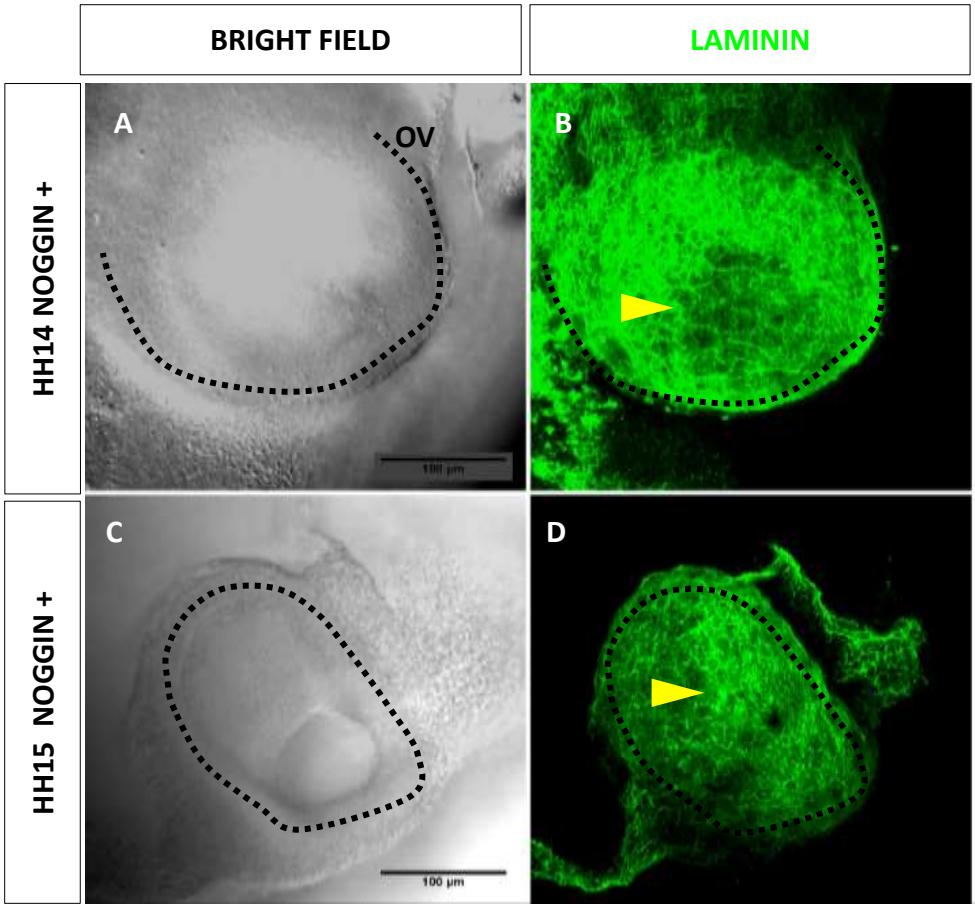

Figure 16. Laminin shows a fibrillar pattern in optic vesicle region after Noggin overexpression. **(A-D)** Apical view from eye region at two different stages, HH14 (first line) and HH15. **(A and C)** Bright field of the last optical slice (most basal Z stack). **(B and D)** Immunostaining for Laminin (green). Noggin overexpression supressed lens placode development and modified the Laminin immunostaining pattern to a more fibrillar pattern in the optic vesicle domain (yellow arrowhead; white dotted lines). OV: optic vesicle.

2.3.4 qRT-PCR analysis for expression of ECM factors

In this study, the use of antibodies to investigate the expression and protein conformation of ECM factors was essential. However, the vast majority of available antibodies target human or mouse proteins and, often, the recognized epitopes of the proteins are not conserved in chicken. Thus, we used the qRT-PCR technique as an alternative way to analyse the expression of additional ECM factors.

We analysed the expression of the genes encoding Laminin α1, Integrin α2 and Integrin α5 in two different groups of tissues: the optic region from the control non-electroporated eye and from the Noggin-electroporated eye. The expression of Laminin α1 was decreased slightly after Noggin overexpression (Fig. 17). On the other hand, there was a increase in the expression of Integrins α2 and α5 increased with Noggin treatment (Fig. 17).

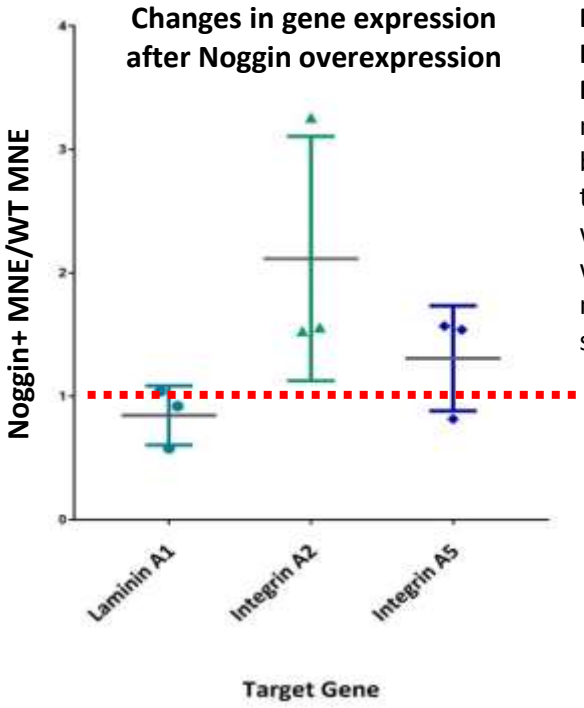

Figure 17. Laminin α1 is down regulated and Integrin α2 and Integrin α5 are up regulated after Noggin overexpression. Comparison between mean normalized expression (MNE) values between noggin-overexpressing and control optic tissues. Red dotted line refers to the value 1, where there was no difference between MNE of wildtype and Noggin. Values above indicate an noggin-induced increase in expression. Error bars: standard deviation (SD). Horizontal lines: mean.

2.4 DISCUSSION

The ECM changes dynamically during embryonic development. The architecture and components of the ECM can change prior to or during the morphogenesis and differentiation of each tissue. The importance of the ECM in optic development can be illustrated by the removal of Fibronectin. Mice with lens-specific knockout of Fibronectin do not develop lens placode and the surface epithelium remains cuboidal (Huang et al., 2011). These data suggest that placodal apical-basal growth is Fibronectin-dependent and that changes in Fibronectin distribution/availability should occur prior to placodal thickening. Here, we focused on investigating the dynamics of two main components of the ECM: Fibronectin and Laminin, during lens placode thickening and invagination.

We observed two distinct Fibronectin architectures after the optic vesicle contacted the overlying surface ectoderm: a diffuse and punctate pattern in the pre-placodal/placodal region, and a fibrillar network in the periplacodal region, underlying the non-placodal ectoderm. The diffuse staining under lens placode region remained thus throughout the invagination process. The persistent differences in Fibronectin architecture of the placodal and periplacodal regions suggest that this conformation is relevant for the establishment and progression of lens placode morphogenesis.

Similarly, Laminin staining also showed different staining patterns after placodal thickening. Both during placodal stages and its invagination, there were two distinct Laminin architectures: A less intense and punctate pattern in the lens placodal region and a fibrillar network in non-placodal regions. Thus, this study extends the original observations that were reported briefly in the past, where immunostaining for Laminin and Fibronectin seems to be less intense in the ECM between lens placode and optic cup when compared with non-placodal regions (Hilfer and Randolph, 1993). In this previous work, a punctate pattern was also described after staining for Fibronectin between optic cup and placode during lens placode invagination (Hilfer and Randolph, 1993). The puncta were present in both the basal surfaces of the optic cup and the lens placode and in the middle of the extracellular space. Here, we repeated the experiment showing a new perspective into this information using a new method that allows us to analyse the complete architecture of Fibronectin and Laminin from 3D image acquisition. We observed regional differences in the mouse embryo optical ECM as well. The results from the mouse embryos also strengthens the similarities in eye

development amongst amniotes and reinforce the importance of ECM architecture, during lens placode development. There are many studies showing the importance of the ECM in the lens fibers development in mouse embryos. Laminin and Collagen IV are present in the basal membrane between the optic vesicle and the overlying ectoderm in mouse embryos, but the staining is less intense in the apex of the optic vesicle, where it is closer to the ectoderm (Svoboda and O'Shea, 1987; Matsuda and Keino, 2001). Likewise, collagen IV is also present in this region, with weaker labelling in the pre-placode ectoderm basal membrane compared to its surrounding regions (Svoboda and O'Shea, 1987). After lens placode invagination, Laminin, Fibronectin and collagen IV remain present in the basal membrane surrounding the optic cup and lens vesicle in mouse embryos (Svoboda and O'Shea, 1987; reviewed in Kwan, 2014). In mouse, the Laminin-rich ECM between the placode and the optic vesicle might be important to sustain filopodia emission from the basal surface of placodal cells. These filopodia tether the lens placode to the optic cup during their concomitant invagination (Chauhan et al., 2009). Inhibition of filopodia formation by placode cells resulted in a significant decrease in invagination depth (Chauhan et al., 2009). However, the formation of these filopodia has not yet been correlated with the quality of the ECM.

Here, our hypothesis is that the two patterns, fibrillar and diffuse, of Fibronectin and Laminin are crucial for lens placode morphogenesis. This hypothesis is in agreement with previously reported influences of ECM organization in embryonic morphogenesis. Live imaging analysis of the posterior axis elongation of chick embryo at stage HH5 shows a relation between Fibronectin expression pattern and cell motility (Loganathan et al., 2016). Where Fibronectin forms a fibrillar pattern, cells movement is organized, while, where the Fibronectin pattern is diffuse, cellular movements are random (Loganathan et al., 2016). Also, during Drosophila wing development, remodulation of ECM is necessary for the initiation of wing cells height increase (Diaz-de-la-Loza et al., 2018). Live imaging of wing development revealed ECM degradation before cell height increase (Diaz-de-la-Loza et al., 2018). Without the degradation of those ECM components, the imaginal disks do not thicken (Diaz-de-la-Loza et al., 2018).

Our results also showed that BMP inhibition changes ECM architecture. After Noggin treatment, the diffuse and punctate seen in control eyes was disrupted, showing that reduction of BMP signalling alters Fibronectin and Laminin architecture. These results suggest that BMP signalling acts up-stream to ECM changes. Lens placode morphogenesis is highly

dependent on BMP signalling (Furuta and Hogan, 1998; Wawersik et al., 1999; Bailey et al., 2006; Sjodal et al., 2007; Rajagopal et al., 2009; Jidigam et al., 2015). Noggin overexpression represses lens placode cell height increase, apical accumulation of F-actin and invagination (Jidigam et al., 2015). Similarly, removal of Fibronectin also represses placodal thickening. Importantly, lack of Fibronectin does not affect BMP signalling, as seen by the amount of nuclearly-localized phosphorylated Smad1/5/8does not change (Huang et al., 2011). Together, this data agrees to our hypothesis that BMP signalling is upstream of Fibronectin and Laminin changes

In our experimental paradigm, expression levels of Laminin α1 mRNA did not seem to change with noggin overexpression, suggesting that the fibrillar or diffuse pattern of Laminin does not result from the decrease in Laminin transcription, but from a change in its conformation/accessibility to the antibody or to its half-life in the extracellular *millieu*.

In the former possibility, the different staining patterns could be explained by alterations in how Laminin or Fibronectin are deposited and assembled in the ECM. Both Laminin and Fibronectin can self-assemble through their various domains (reviewed in Mao and Schwarzbauer, 2005; Hamill et al, 2009). The assembly of both proteins is a cell-mediated process, but the involvement of Integrin is clearer in the case of Fibronectin than in the case of Laminin. Clustering of Fibronectin-Integrin complexes at the cell membrane help organize Fibronectin into short fibrils. This interaction also exposes additional domains that can modulate subsequent steps of Fibronectin fibrils formation. As this process progresses, longer fibrils are formed and interaction with integrins are no longer necessary. In contrast, Laminin assembly seems to be more independent of cell receptors and it is unclear how it responds to cell-triggered changes (Hamill, 2009). Irrespective of these differences, it is very clear that both Laminin and Fibronectin assembly can be modulated by changes in availability of their different isoforms that contain distinct domains mediating self-interaction. Thus, it is possible that changes in the placodal ECM are driven by secretion of different isoforms of Laminin and Fibronectin and/or changes in placodal cell Integrin composition and behavior. Unfortunately, our experimental system does not allow identification of specific isoforms of Laminin, Fibronectin or Integrin.

Another possibility is that BMP pathway modulate extracellular degradation of the ECM. This possibility is supported by our images from mouse embryo eye development. We observed

irregular rips and holes in the Laminin layer under the placodal region but not in the periplacodal region. The irregularity of the Laminin holes suggest an ongoing active degradation process. In agreement with this idea, studies with mouse mammary gland shows that changes in the ECM through matrix degradation are essential for morphogenic signals during branching morphogenesis (reviewed in Fata, 2004). In primary mammary epithelial organoids culture, metalloproteinases are crucial for morphogenesis process (Simian et al., 2001). The cultivation of mammary epithelial cells with growth factors and metalloproteinases was sufficient to drive branching morphogenesis *in vitro* (Simian et al., 2011). Also, inhibition of metalloproteinases activity prevented branching morphogenesis (Simian et al., 2011). In addition, metalloproteinase proteolytic activity not only regulate ECM assembly and remodel it, but can also release growth factors important for the mammary gland development during ECM remodelling.

The relationship between BMP signalling and ECM could be a positive feedback loop in that BMP-triggered ECM changes could further enhance BMP signalling in the placode. In other words, the ECM architecture alteration could contribute for towards sustained BMP signalling in the placode. As mentioned previously, lens placode specification *in vitro* requires long-term exposure to BMP (Sjodal et al., 2007).

Indeed, there are examples where ECM modifications can modulate BMP signalling. ECM components can bind to BMP and modulate the steepness of the BMP gradient (reviewed in Plouhinec et al., 2011). For instance, Dpp, a BMP2/4 homologue, binds to Collagen IV and this interaction facilitates the Dpp flow necessary for dorsal-ventral patterning in Drosophila (Wang et al. 2008). In this context, changes in Fibronectin and Laminin organization could affect lens development through interference with BMP signalling by restricting BMP availability to the placode region. Thus, the different in Fibronectin and Laminin organization in periplacodal and placode regions could result in differences in the concentration of extracellular BMP.

In our proposed model (Fig. 18), BMP signalling and ECM organization would be interconnected in a feedback loop. The pre-placodal region at the border of the neural plate that has been exposed to BMP will be competent to form lens placode (Bailey et al., 2006)). Restriction of this competence in the context of the embryo is done through FGF and Wnt signalling (reviewed in Streit, 2008). In the pre-placodal region that has not received FGF or

Wnt signalling, and upon prolonged exposure to optic vesicle-secreted BMP (Furuta and Hogan, 1998) the cells would progress further into the lens placodal fate. As a result, only the pre-placodal cells modify their underlying ECM. This alteration could be through Integrin-mediated changes in the pattern of deposition of newly synthesized Fibronectin/Laminin or increased degradation of previously deposited Fibronectin/Laminin. Or both. The changes in the placodal basement membrane would increase the availability of extracellular BMP that is trapped in its components. Thereafter, the increase in ECM-derived BMP signalling drives the placode towards the subsequent steps of its morphogenesis: cell height increase and invagination. Alternatively, it is also possible that the optic vesicle cells contribute towards ECM remodeling.

Pax6 is also crucial for lens specification and cytoskeletal reorganization (Rajagopal et al., 2009; Plageman et al., 2010). Prior to lens placode formation, Pax6 is uniformly expressed in the cephalic ectoderm (Bailey et al., 2006). During lens placode induction Pax6 levels increase in the ectoderm and becomes restricted to the optical region (Lang, 2004). Expression of Pax6 seems to be relevant for ECM evolution in the optic region. In Pax6-knockout mouse embryos, lens placode formation is inhibited and the quality of the ECM between the optic vesicle and the ectoderm is altered (Huang et al, 2011). Staining for Periodic Acid-Schiff (PAS) and Alcian Blue (AB), which labels ECM molecules, was intense in wild type embryos placodal basement membrane, but decreased in Pax6-knouckout (Huang et al., 2011). On the other hand, in Fibronectin-knockout mouse, Pax6 was not decreased and the apical localization of the actin cytoskeleton was not affected, suggesting that the molecular specification for lens placode does not depend on ECM (Huang et al., 2011). Also, gene expression for several transcripts encoding ECM components, such as fibronectin1, versican, tenascin-C, hyaluronan synthase 2, leprecan-like 1 and the α1 chain of collagen type 13 decreases in Pax6-knockout mouse (Huang et al., 2011). These data suggest that both Pax6 and BMP signalling are upstream of ECM changes. As In turn, ECM changes would be upstream of a “second-wave” of BMP signalling that is required for placode height increase.

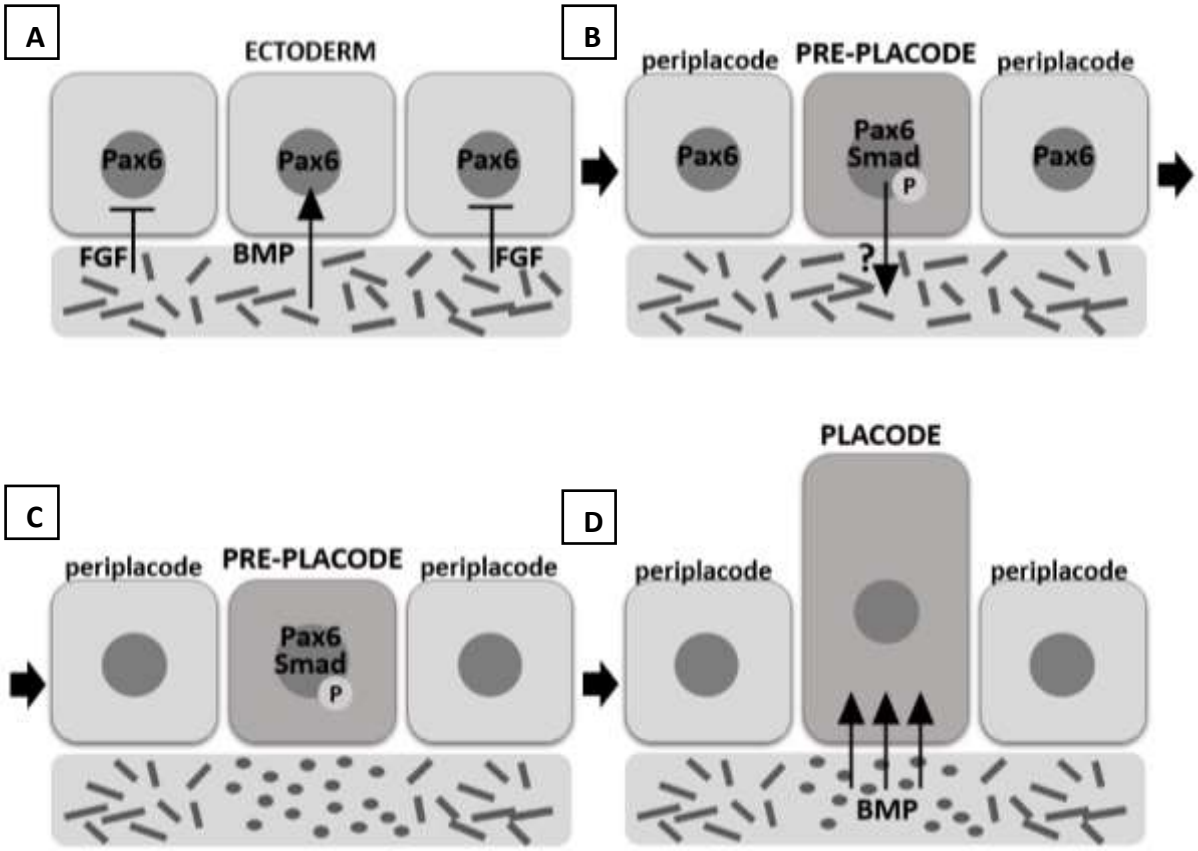

Figure 18. Summary scheme of the hypothesis on BMP signalling and ECM conformation during lens placode thickening. (A) Pax6 is expressed in ectodermal cells ate the pre placodal domain (Bailey et al., 2006). FGF delimits lens placode region by repressing lens characteristics (Bailey et al., 2006). BMP signalling is required for lens placode induction and specification (Furuta and Hogan, 1998). At this stage, the ECM has an homogeneous conformation in all pre placodal domain. **(B)** Lens placodal region is specified and BMP signaliing is activated (Smad is fosforilated in the nucleus) in pre placodal cells. **(C)** After lens placode molecular specification, the ECM organization is changed to a diffuse and punctate pattern between pre placodal ectoderm and the optic vesicle and remains fibrillar in periplacodal regions. **(D)** Changes in the ECM realeses BMP molecules, keeping its exposure to lens placode cells. Changes in ECM and BMP signalling (Rajagopal et al., 2009; Jidigam et al., 2015) are both required for lens placode thickening.

2.5 CONCLUSION

Our results showed that Fibronectin and Laminin immunostaining pattern is more diffuse in the lens placode region when compared to non-placodal regions at placode thickening stages. The diffuse and punctate pattern of those ECM components were maintained during lens placode invagination. Together, our data provide evidence that Fibronectin and Laminin organization evolve during lens placode morphogenesis. Most likely, this is an evolutionarily conserved phenomena in eye development, as we also observed a similar pattern of Laminin staining in the lens placode region in mouse embryos. In conclusion, BMP signalling in early lens development is upstream of Fibronectin and Laminin architecture, which in turn might be important to regulate BMP signalling.

3 DYNAMICS OF PERIPLACODAL CELLS THIN MEMBRANE PROTRUSIONS

3.1 INTRODUCTION

3.1.1 Cornea epithelium development

While the induction and morphogenesis of the lens has been intensely studied, the same is not true for the corneal epithelium. The vertebrate mature cornea has three cellular layers: the stratified corneal epithelium that covers the outermost surface, the middle layers that occupy the largest volume that forms the stroma and the innermost single layer endothelium (Lwigale, 2015). The precursors of the corneal epithelium arise from cells adjacent to the lens placode. In neurula stages (HH8), the anterior portion of cephalic ectoderm will give rise to four domains: oral, olfactory, lens and the corneal epithelium. The lens and cornea precursors derive from the pre-placodal ectoderm, adjacent to the lens vesicle (Collomb et al., 2013). Also, both lens and cornea precursors are Pax6-positive (Bailey et al., 2006; Dhouailly et al., 2014; reviewed in Lwigale, 2015). Experiments in chick embryo showed that the surgical removal of lens pre-placodal ectoderm induces migration of corneal precursor cells that were capable of developing new lens placode (Collomb et al., 2013). Together, this data reinforces the idea that corneal epithelium precursors share the potential to form lens.

The cornea becomes a continuous epithelial layer after the lens placode completes its invagination (Fig. 3). As the lens pit deepens, the periplacodal cells move in concert to close the outer edge of the lens vesicle and heal the perimeter of the entry point. Preliminary live imaging experiments from our laboratory showed an intense protrusion emission by periplacodal cells during lens placode invagination. Here we investigate further the dynamics and cytoskeletal composition of those protrusions in order to understand their function and role during eye development.

3.1.2 Intercellular communication by thin membrane protrusions

In recent years, a novel mechanism of cell-cell communication by thin membrane protrusions has been increasingly explored. The name "thin membrane protrusions" is because such structures have a much smaller diameter than other protrusions already well described in the literature, such as filopodia and lamellipodia. This kind of intercellular communication is widely observed in cell line studies, but its presence and functions in embryonic models are

still being elucidated. Several authors argue that cellular protrusions are an efficient means of communication in the context of embryonic development, since the target is much more specific and information flow is more restricted. This model of specific and localized information exchange would explain development processes not elucidated by classical models of secretion and diffusion of molecular signalling (reviewed in Pröls et al., 2015; reviewed in Thomas B. Kornberg, 2017; reviewed in Yamashita et al., 2018).

Thin membrane protrusions can be divided into three distinct classes: cytonemes, tunnelling nanotube (TNT)-like protrusions and microtubule-based nanotubes (MT nanotubes) (reviewed in Yamashita et al., 2018). All of these structures have been shown to be involved in intercellular communications (Fig. 19).

Cytonemes were first observed in developing Drosophila imaginal discs (Ramırez-Weber & Kornberg 1999). Later, they were characterized as structures similar to filopodia as they contain actin and require actin regulators factors for their formation (Roy et al., 2014). This study shows specific and localized deposition of Decapentaplegic (Dpp), a Drosophila morphogen signalling protein, through cytonemes, where cells emit the protrusions to exchange signalling proteins (Roy et al., 2014). In mutant Drosophila with reduced cytonemes formation, Dpp signalling was impaired (Roy et al., 2014).

The TNTs were exclusively described in cell line studies where trafficking of vesicular organelles was observed between two cells. They are actin-based structures and have a diameter between 50 and 200 µm. TNTs are described as similar to invadopodia by their functional and morphological characteristics (reviewed in Yamashita et al., 2018).

The MT nanotubes were first observed in Drosophila germline stem cells (Inaba et al. 2015; reviewed in Yamashita et al., 2018). They are composed by microtubules (Tubulin-positive), have a diameter smaller than 1.5 µm and their formation does not require actin cytoskeleton regulators (Inaba et al. 2015; reviewed in Yamashita et al., 2018). Studies with Drosophila germ line cells showed that MT nanotubes are required for morphogen signalling activation and maintenance of the cell line molecular characteristics (Inaba et al., 2015). Unlike cytonemes and TNTs, MT nanotubes are extended and encapsulated by another cell. The tip of the protrusions carry specific receptors that interact with ligands expressed by the target cell (Inaba et al. 2015).

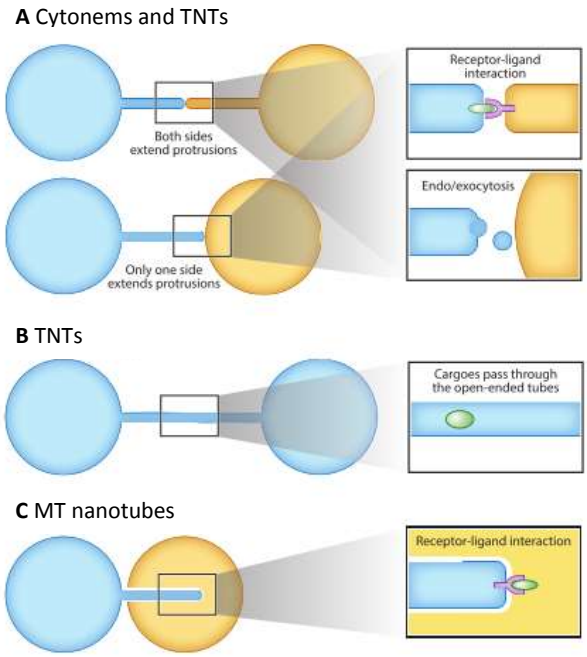

Figure 19. Thin membrane protrusions structures. (A) In cytoneme and TNT-mediated intercellular communication, one or both cells can extend the protrusion where ligand and receptors interact. Also, the exchange of molecules can be through exo or endocitoses. **(B)** TNTs can form an open bridge structure, connecting the cytoplasm of two cells directly and or mediate vesicle exchange. **(C)** MT nanotubes can be encapsulated by another cell and specific receptors interact with ligands expressed by the target cell. Adapted from Yamashita et al., 2018.

Despite different characteristics, all of these classes of protrusion are involved in molecular signalling and inter-cellular communication. Cytonemes and TNTs are longer and more involved in long-range intercellular communication while MTs are shorter and involved exclusively in short-range communication.

3.1.3 Thin membrane protrusions signalling in chick embryos

Cytonemes have been shown to be involved in vertebrate embryos intercellular communication. Filopodia-like protrusions were recently described involved in long-range communication in zebrafish, xenopus and chick embryos (Sanders et al., 2013; Danilchik et al., 2013; Luz et al., 2014; Sagar et al., 2015; Stanganelho et al., 2015).

Specifically, in the chick embryo, thin membrane protrusion intercellular communication are in developing limb mesenchymal cells and in somite epithelial cells. The protrusions were labelled with Cofilin and fascin, both actin-associated proteins. Microtubule associated proteins were found only in the proximal portion of the protrusions. In addition, these protrusions participate on Shh transport (Sanders et al., 2013). Cellular protrusions were also found between the dermomyotome and the adjacent ectoderm. These protrusions arose from somite epithelial cells, and were actin and Tubulin positive and transported frizzled 7 (Wnt receptor) molecules. Although the authors did not pursue this point, these protrusions very likely are involved in vesicular transport as they were actin- and Tubulin- positive and had tubular motor proteins (Sagar et al., 2015).

3.2 MATERIALS AND METHODS

3.2.1 Obtaining and incubating embryonated eggs

Fertilized Leghorn chicken eggs were obtained from Granja Yamaguishi, Jaguariúna – SP (for embryos used in experiments in University of São Paulo) and Henry Stewart & Co. (for embryos used in experiments in University of Oxford). The eggs were incubated at approximately 37.7 ° C and 50% relative humidity for 36-38 hours to obtain embryos at stage HH10-11, 42-45 hours to obtain embryos at stage HH14 and 50h hours to obtain embryos at stage HH15. After *in ovo* electroporation, the embryos were incubate for 6-18 hours according to the stage desired in the experiment (Hamburger, 1992).

3.2.2 Electroporation in ovo of chick embryo (stages HH9-11)

After incubation, the eggs were exposed through an opening in the shell and the chicken embryos were contrasted by non-toxic Indian ink injection (10% in Howard Ringer's saline). Close to the optic vesicle on the right side of the embryo, a puncture was made with a glass capillary microneedle and approximately 1 ml of Ringer's saline solution was applied over the embryo to facilitate electric conduction. Platinum electrodes (4 mm apart) were positioned so that the positive electrode was on the left side and the negative electrode on the right side of the embryo. Injection of a solution stained with 0.1% Fast Green containing one or two plasmids of interest, was targeted by through a glass microneedle to the external surface of the ectoderm of the right eye. The electric pulses were applied simultaneous to plasmid injection with the following parameters: 5 pulses of 9 V with duration of 50ms in intervals of 100 ms. We used the plasmids pcDNA3.1-mGFP, pCAG-Tubulin-GFP (Addgene plasmid #66105) e pEGFP-N1-hCofilin (Addgene plasmid #50859) and pLifeAct-RFP (Ibidi 60102) diluted in H2O (1,5-3,0 µg/µl). The mGFP sequence is a modified GFP with sequence for Palmitoylation of GAP43, required for membrane association (Okada et al., 1999). We cloned this sequence in the plasmid pcDNA3.1 by digesting pCAG-mGFP (Addgene plasmid #14757) with NotI and EcoRI and inserting in pcDNA3.1, also cut at the same sites. After electroporation, the eggs were sealed with nontoxic packing tape and incubated again to the proper stage.

3.2.3 Electroporation ex ovo of early chick embryos (stages HH5-7)

To obtain embryos for live imaging experiments at pre-placodal ectoderm stages (HH11-12) we adapted an *ex ovo* electroporation system in embryos at stages HH6-8 (Prof. Andrea Streit Department of Craniofacial Development in King´s College University, U.K. personal communication).

The embryos were collected at stage HH6-8 using filter paper technique with Whatmann Filter Paper n°3 - cut in a square with a single hole in the centre, slightly larger than the embryo- in Pannet-Compton solution (Chapman et al., 2001; Streit and Stern, 2008). For the electroporation, the embryo was positioned on top of the electroporation chamber with dorsal portion facing upwards. The chamber contained a square positive electrode, and it was filled with Tyrode´s solution. A solution stained with 0.1% Fast Green containing the plasmids of interest (2-3 μg/μl), was injected with the microneedle between the extra-embryonic membrane and the embryonic membrane in the cephalic right region. After injection, we positioned the negative electrode on the top the embryo and stimulated with 4 pulses of 4-6 V, with duration of 50ms in intervals of 780 ms. The distance between the electrodes was 4 mm (Voiculescu et al., 2008; Fig. 20B).

3.2.4 Ex ovo culture of the chick embryo

After ex ovo electroporation, we cultured the embryos using the modified Cornish pasty method (Nagai et al., 2011), an *ex-ovo* chick embryo culture technique. The filter paper and the extra-embryonic membrane were removed in Pannet-Compton solution (Fig. 20A), at room temperature and the embryonic membrane in a circle shape was folded in a half-moon shape, with the ventral portion inside (Fig. 20B). The anteroposterior axis of the embryo was at the straight edge of the cornish pasty. Embryos were then transferred to a plate containing medium (a 2:1 mixture of thin albumen and Pannet-Compton solution with penicillin and streptomycin 5000 U/ml). The cultures were grown at 37°C incubator to stage HH11-12 for live imaging analyses.

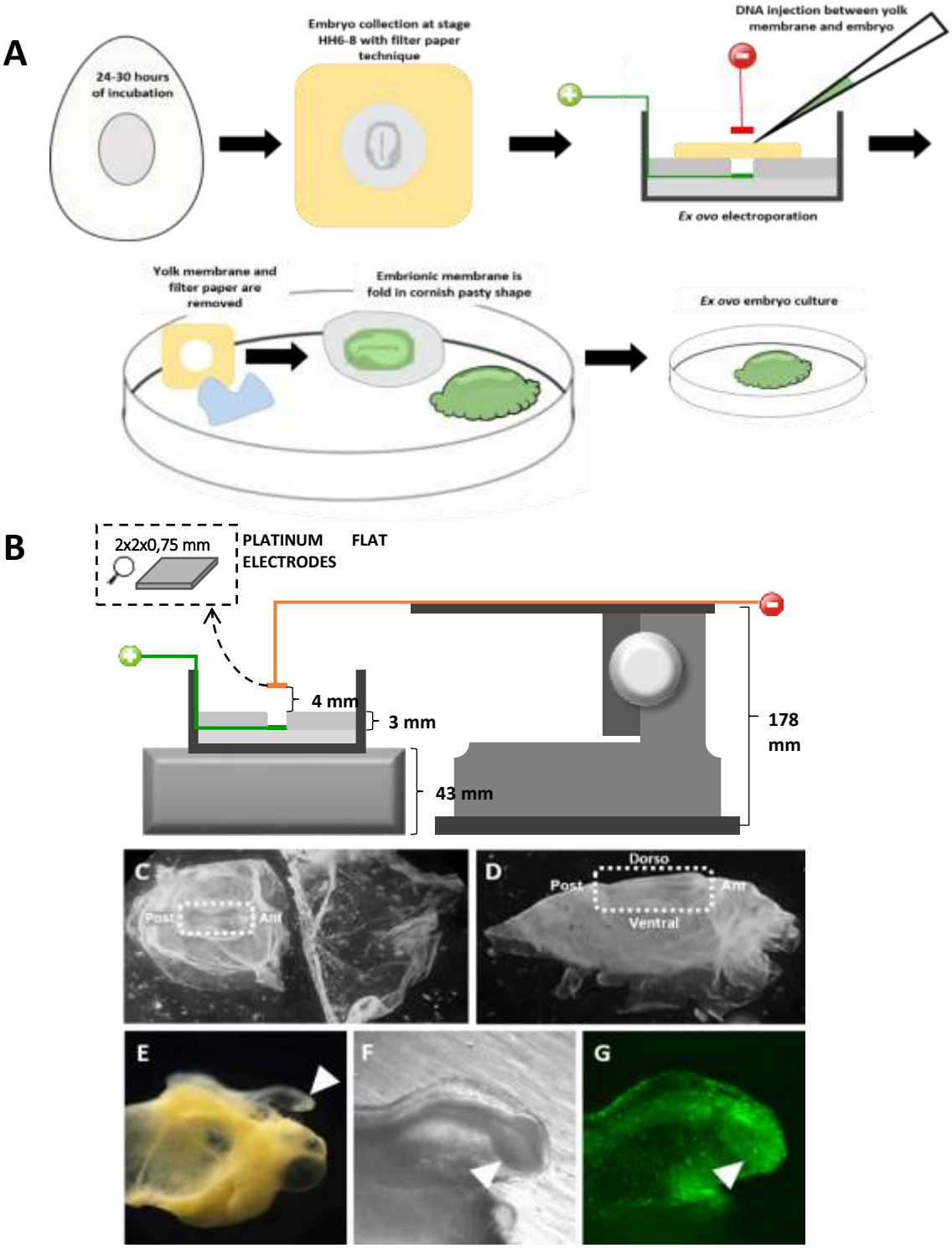

Figure 20. *Ex ovo* electroporation system and culture. A. Collection, electroporation and ex ovo chicken embryo culture, as described in the text **B.** Scheme of electroporation system; the positive electrode (green) is inside the chamber and the negative (red) is outside, on top of the embryo. The embryo is positioned in the chamber, with the are to be electroporated on top of the positive electrode. A micromanipulator (on the right) is used to regulate the negative electrode position after DNA injection. **C.** After ex ovo electroporation, the embryo (white dotted line) is collected and the yolk membrane is separated (right) from the embryonic membrane. **D.** Embryonic membrane is folded with the ventral portion inside the semi-circle. **E.** Embryo at stage HH10, 14 hours after electroporation (embryo head is pointed by white arrowhead). **F-G.** Bright field (F) and green channel (G) of embryo at stage HH9, 12 hours after electroporation.

3.2.5 Obtaining and dissecting mouse embryos

To visualize the cellular protrusions in the embryonic tissue, we required contrast between single cells and their surroundings, best obtained with tissues labelled in a mosaic pattern. To obtain a transgenic mouse with such a pattern, we crossed two lines: ROSA26mT-mG and ROSA-Cre/ERt2 transgenic lines. The mT-mG line expresses membrane-targeted tandem dimer Tomato (mT) flanked by Lox sites. A mGFP gene is downstream of mT and is not expressed unless mT is removed through Cre-mediated recombination. The CreERt2 line expresses the Cre protein constitutively in all tissues, but requires exposure to Tamoxifen for its activation (Friedrich and Soriano, 1991). This is because the Cre recombinase sequence is fused to the sequence of a human estrogen receptor which is highly sensitive to tamoxifen (Indra et al., 1999). Thus, in the presence of tamoxifen, the Cre enzyme is activated, the mT is removed, allowing the expression of mG (membrane-targeted green fluorescent protein) (Muzumdar et al., 2007). The ideal level of mosaicism for our experiments was obtained by injecting tamoxifen 40% (calculated amount based on weight, 0,06mg/gm) 24-36 hours before collecting the embryos at stage E9.0 to E9.75. We dissected embryos in M2 media (Sigma) cultured in a 1:1 mix of CMRL (Invitrogen) and KnockOut Serum (Gibco),and cultured at 37°C in 5% CO2 until live imaging experiments. All the extracellular membrane was removed and the embryos head collected for the live imaging experiments.

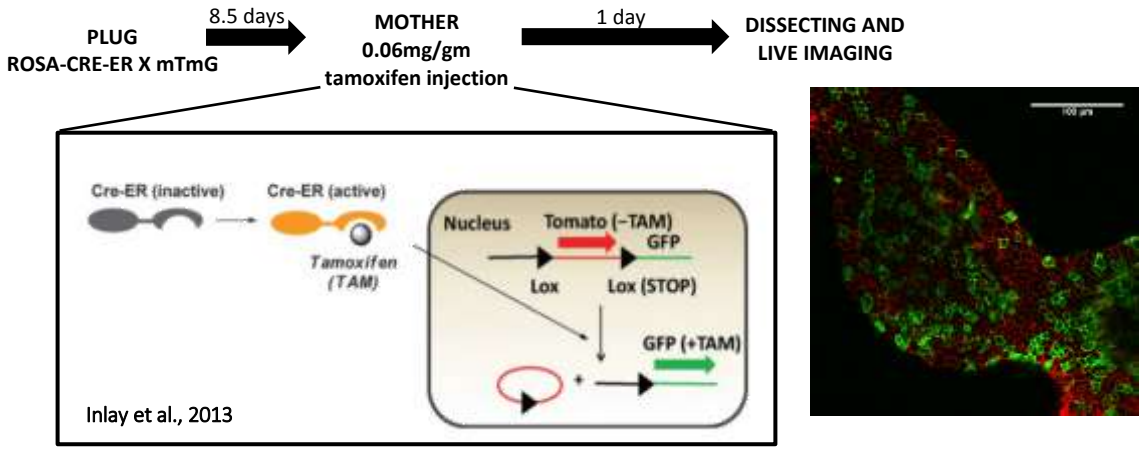

Figure 21. Generation of mosaic mouse for mTomato and mGFP. Crosses and tamoxifen treatment as described in the text. On the right, image obtained in confocal microscopy of the red (mTomato) and green (mGFP) channels whosing the obtained mosaic expression at the optic region.

3.2.6 Mounting chick and mouse embryos for microscopy analyses

After dissecting the chick embryos, we cut the head in the neck region and positioned in the petri dish with glass coverslip at the bottom (MatTek P35G-1.0-14-C). To stabilize the embryos, we used vaseline jelly to build a small bed around the head. After positioning the embryo in the centre, we filled the plate with albumin. The embryos were kept in a heated, humified chambers with CO_2 control for the duration of the imaging experiments.

For the experiments in Oxford University, we also used Methy Cellulose (MC; Sigma, M0387) as medium to mount chick and mouse embryos in the petri dish. In this method, the embryo was positioned on the coverslip and all liquid medium was removed, allowing the embryo to remain close to the cover sheet by surface tension. Then we covered the embryo with the MC solution at 2% in Tyrode's solution.

3.2.7 Confocal live imaging

Confocal images were acquired on a Zeiss LSM-780 NLO (CEFAP, ICB – USP, FAPESP 2009/53994-8) and on Zeiss 880 Airyscan fast (Srinivas Laboratory, University of Oxford). In Zeiss LSM-780 NLO, we used 60x 1.4 NA oil immersion lens (Objective Plan-ApoChromat 63x / 1.40 Oil Infinity/0.17). In Zeiss 880 Airyscan fast, we used 40x 1.2 NA oil immersion lens (Objective C-Apochromat 40x/1.20 W Korr M27) with 1.5 digital zoom. Images were obtained with 1 µm Z-stack interval and 1-minute interval per frame (total duration of 20 to 60 minutes). For live imaging experiments, we used least possible laser intensity in order to reduce phototoxicity and photobleaching without losing contrast, so as not to interfere with the normal cell biology of the cellular protrusions.

3.2.8 Live imaging analyses

Analysis of the images obtained in confocal microscopy was performed by Fiji (ImageJ version 2.0.0-rc-49/1.51p). For each 4D image, we analysed only the cells that did not divide during the experiment and were inside the x-y and z fields in all frames. The protrusions were measured using the drawing tools in Fiji.

For each frame we measured the cell area using the freehand tool, annotated the z-start and z-end of the cell and we also measured the angle of the cell relative to the placode invagination centre, always using the fluorescence and the bright fields as guidance (Figure 22).

For each protrusion, we noted the frame and the stacks in Z where it was observed along with the length and angle measurements from the centre of the cell to the periphery (Figure 22). It was very important to analyse the optical slices separately to understand the start and end of the protrusions.

In summary, we obtained the measures of angle, size and position in Z for all frames of each protrusion from all analysed cells.

With this data, we carry out our analysis of stability, protrusion emission angle and cellular region in which these protrusions occur.

- Calculation of extension/retraction dynamics: Defined as variation in protrusion length with time. Calculations are of changes from a frame relative to its previous frame, including the first extension and total retraction (first and last lengths measured). For this calculation, we have the variations of the protrusion lengths given by the modular value of the difference in length between one frame and the next one. We calculated the average of variation and related this value with the maximum length of the protrusion. We only performed this calculation for protrusions that arose and disappeared during our movies. In other words, we did not include for protrusions that were present from the beginning of the 4D image acquisition or remained after the end of the movie.

n= frame

$D_n = |length_{(n)} - length_{(n-1)}|$

$\text{Average} = \frac{\sum_{i=2}^{n} \Delta i}{(n-1)}$

- Calculation of half-life in relation to the length: Defined as the time (number of frames) that the protrusion was present. For this we counted for how many frames the protrusions was present and divided the value for its maximum length.

- Calculation of the angle of the protrusion relative to lens placode centre: with the drawing tool in Fiji, we determined the angle of each protrusion relative to the bottom of the image. We also measured the angle of the cell centre in relation to the centre of placode invagination, tracing a straight line from the estimated centre of the cell to the centre of the invagination. Because the cells that were analysed were spread at all angles relative to the invagination centre, we need to calculate the angle of the all the protrusions relative to the centre of the invagination point. In other words, we needed to set the invagination point as zero for all cells. Thus, we normalized the angles of all the protrusions in a single cell with the angle of the cell to the lens placode centre with the above formula.

Ang_p = protrusion angle relative to bottom axis of image (raw data obtained in FIJI).

Ang_c= angle of the cell to the lens placode center relative to bottom axis of image (raw data obtained in FIJI).

$NAng_p$= protrusion angle normalized with the lens placode invagination center as zero.

$$NAngp= Ang_{p-} Ang_c$$

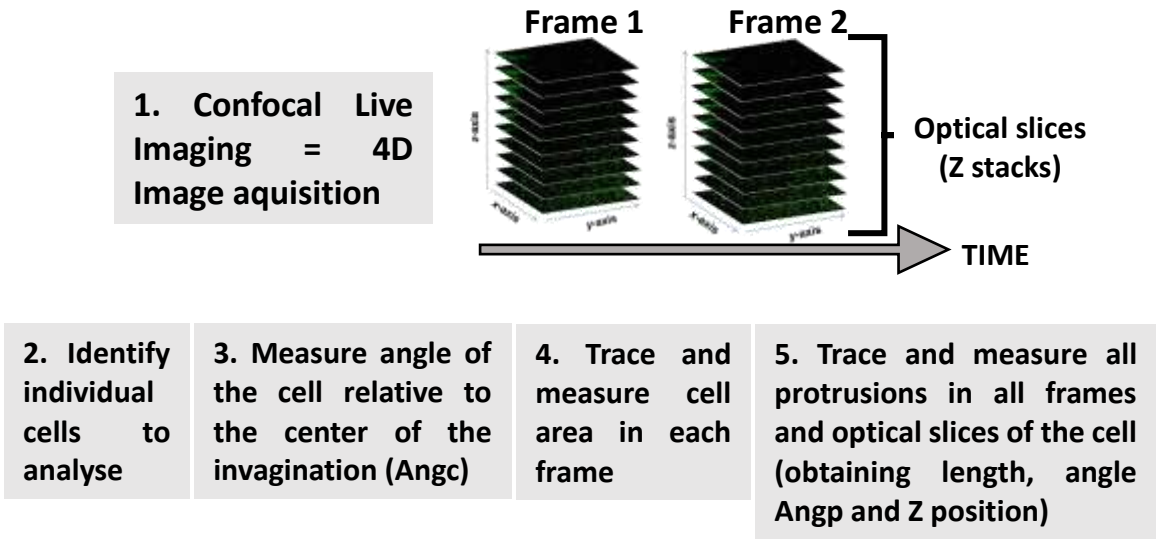

Figure 22. 4D Image analyses. After the 4D image acquisition on confocal microscopy, we identify cells suitable for analysis (do not divide, do not die, are present during all frames). We then measure the angle of the chosen cell relative to the centre of placode invagination by drawing a straight line (orange lines). The angle is automatically calculated by the software (yellow). With the free hand tool, we measure the cell area in all frames (cell outline in cyan) and note the first and last optical slice in which the cell is observed. We draw a straight line on all the protrusions found (cyan), measuring length, angle (pink and yellow) and also note the optical slice in which each protrusion was observed. Ang_c = Angle from cell centre to the centre of placode invagination. Ang_p =Angle of each protrusion in relation to centre of invagination.

3.3 RESULTS

3.3.1 Live imaging data analysis of cellular protrusion emission during eye development in chick embryos

3.3.1.1 Thin membrane protrusions labelled with mGFP

We electroporated the cephalic ectoderm with pcDNA3.1-mGFP which contains a modified sequence of green fluorescence protein (GFP) which targets the protein to the membrane (see Methods; Okada et al., 1999). We chose this method based on previously published studies with live imaging in the chick embryo, where membrane markers were more effective in labelling of protrusions (Sanders et al., 2013). The electroporation technique generates a mosaic expression pattern, which creates the contrast between cell and background necessary for the visualization of the protrusions (see Methods; Fig. 23). We acquired live imaging data in the confocal microscope and our images showed intense protrusions emission by periplacodal cells during the invagination of the lens placode (Fig. 24). There was a large amount of protrusions (Fig. 24, green arrowheads), with great diversity in size and dynamics (Fig. 24, B and D). During the imaging process, care was taken to minimize the effects of phototoxicity. Nevertheless, we observed occasional cell debris, but that did not increase in frequency in prolonged experiments. As a preliminary quantitative data, we measured the length of the protrusions. We noted a large range in size (Fig. 24). We obtained lengths varying between 0.7 and 22 µm, with a mean of 3.5 nm. Most protrusions have a size below 5 µm (Fig. 25).

Also, detailed analysis of the live imaging data showed membrane puncta travelling through these protrusions (Fig. 24E, white arrowhead). We measured the displacement of the membrane puncta and we divide it by the value of the interval between the frames to calculate their velocity. We obtained a speed of vesicular transport around 80nm/s.

The high heterogeneity of cellular protrusions together with the membrane puncta transport led us to focus on the function of these protrusions in the context of eye development. Our

aim here is to characterize molecular and physically the periplacodal protrusions and determine if they have a mechanical or signalling function.

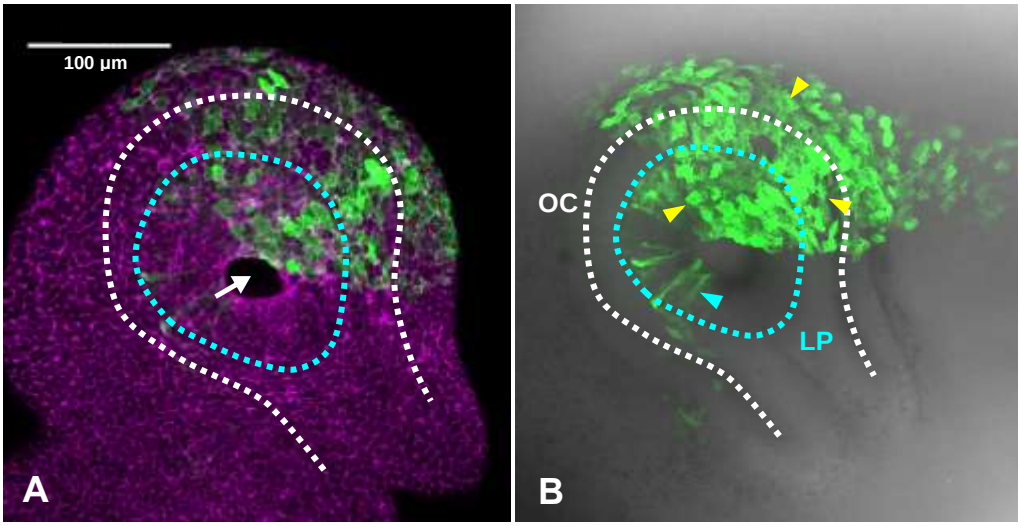

Figure 23. Mosaic expression pattern of GFP after electroporation of chick embryo eye region. (A-B) Apical view form eye region at stage HH15. Withe dotted line: optic cup (OC); cyan dotted line: lens placode during invagination (LP). **(A)** Phalloidin label (magenta) and GFP-positive cells (green). White arrow: centre of lens placode invagination. **(B)** Bright field of the last optical slice (most basal) and GFP-positive cells. Yellow arrowhead: GFP-positive periplacodal cells; cyan arrowhead: GFP-positive lens placode cells.

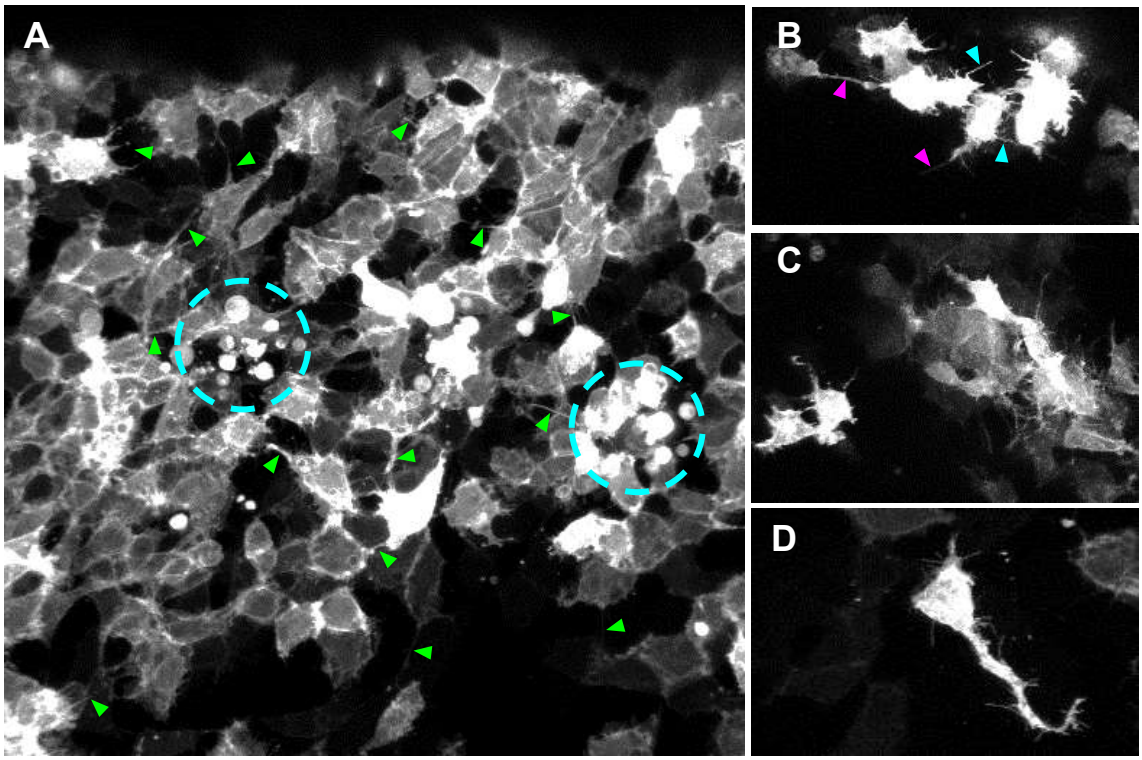

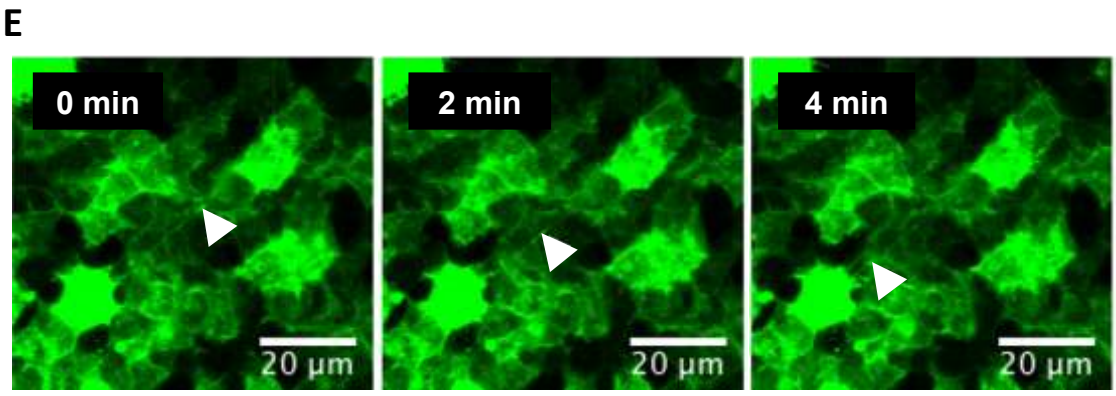

Figure 24. Intense emission of protrusion by periplacodal cells in chick embryo. (A-E) Confocal live imaging of periplacodal cells electroporated with mGFP. **(A)** The mosaic pattern expression of mGFP makes it possible to see numerous protrusions (green arrowheads). During the experiment, we observed some cases of cell death and blebbing (cyan dotted circles). **(B-D)** Large numbers of protrusions are emitted by a single cell and they are diverse in length. There are longer protrusions (magenta arrowheads) and shorter protrusions (cyan arrowhead) that appear to be more numerous. There are also protrusions that are linking one cell to another (yellow arrowhead). **(E)** Sequence of three frames showing the transport of membrane puncta between two cells (tip of white arrowhead).

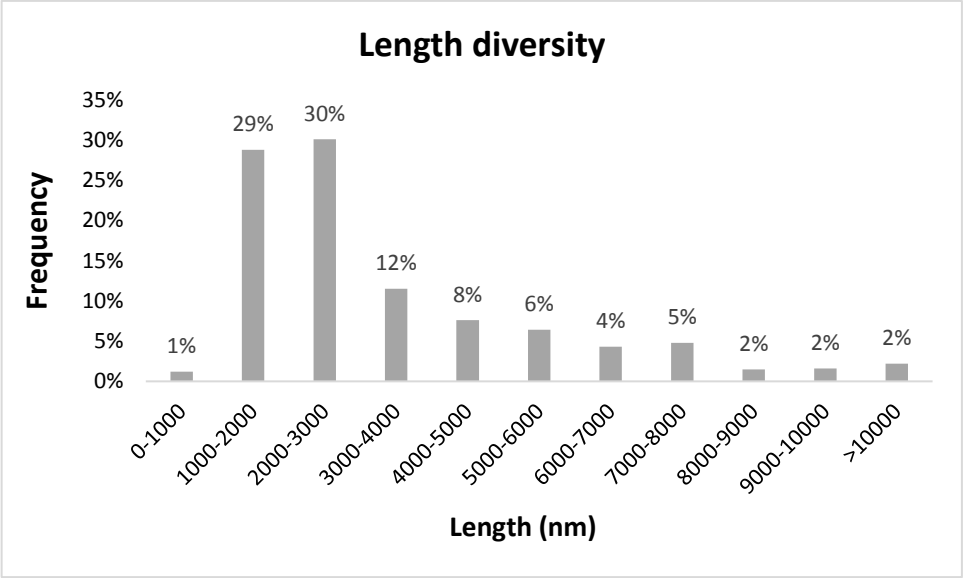

Figure 25. mGFP-positive protrusions measurements showed a great diversity in length. Most of the protrusions have length between 1000 and 3000 nm.

3.3.1.2. Molecular characterization of cellular protrusions

We then investigated the cytoskeletal composition of the protrusions in periplacodal cells. Firstly, we compared the cellular protrusion on cells expressing both mGFP and LifeAct. The latter has a high affinity for actin filament (Riedl et al., 2008), fused to red fluorescent protein (LifeAct-RFP). With mGFP labelling, the protrusions were longer than with LifeAct-RFP (Fig. 26). LifeAct-RFP labelled only the proximal end of the protrusions (Fig. 26, blue arrowheads). Furthermore, with mGFP, both short and long protrusions were labelled, thus increasing the range of protrusions lengths that were imaged (Fig. 26, white arrowheads).

The differences obtained with actin and mGFP labelling led us to hypothesize that the periplacodal protrusions were diverse in their cytoskeleton composition. Thus, we used the plasmids pCAG-Tubulin:: GFP and pEGFP-N1-hCofilin to label the protrusions. Cofilin is an actin-interacting protein (Ohashi, 2015) and its fusion with EGFP is another way of labelling the actin cytoskeleton.

In an initial analysis of the Tubulin-positive cells, we observed fewer labelled cellular extensions when compared to the labelling pattern obtained in experiments with mGFP and it appears to label preferentially longer protrusions (Fig. 27, white arrows). In addition, protrusions that are closer to the invagination centre seemed to be organized tangentially to the lens placode (Fig. 27, yellow dotted line).

In Cofilin-positive cells, few protrusions were labelled, all of which were short (Fig. 28). Unlike Tubulin-positive protrusions, Cofilin-positive protrusions did not seem present any type of organization in relation to the lens placode (Fig. 28).

Also, there seems to be a difference in the diameters between the Tubulin- and Cofilin-positive protrusions. Cofilin-positive protrusions appeared in a smaller number of optically tangential slices in comparison to Tubulin-positive protrusions (Fig. 28 C; Fig. 27 C). For example, in Figure 28C the same Cofilin-positive protrusions appeared in 5 optical slices in the *Z-axis* (cyan arrowhead). Whereas the Tubulin-positive protrusion in Figure 27C can be seen in 8 optical slices (cyan arrowhead).

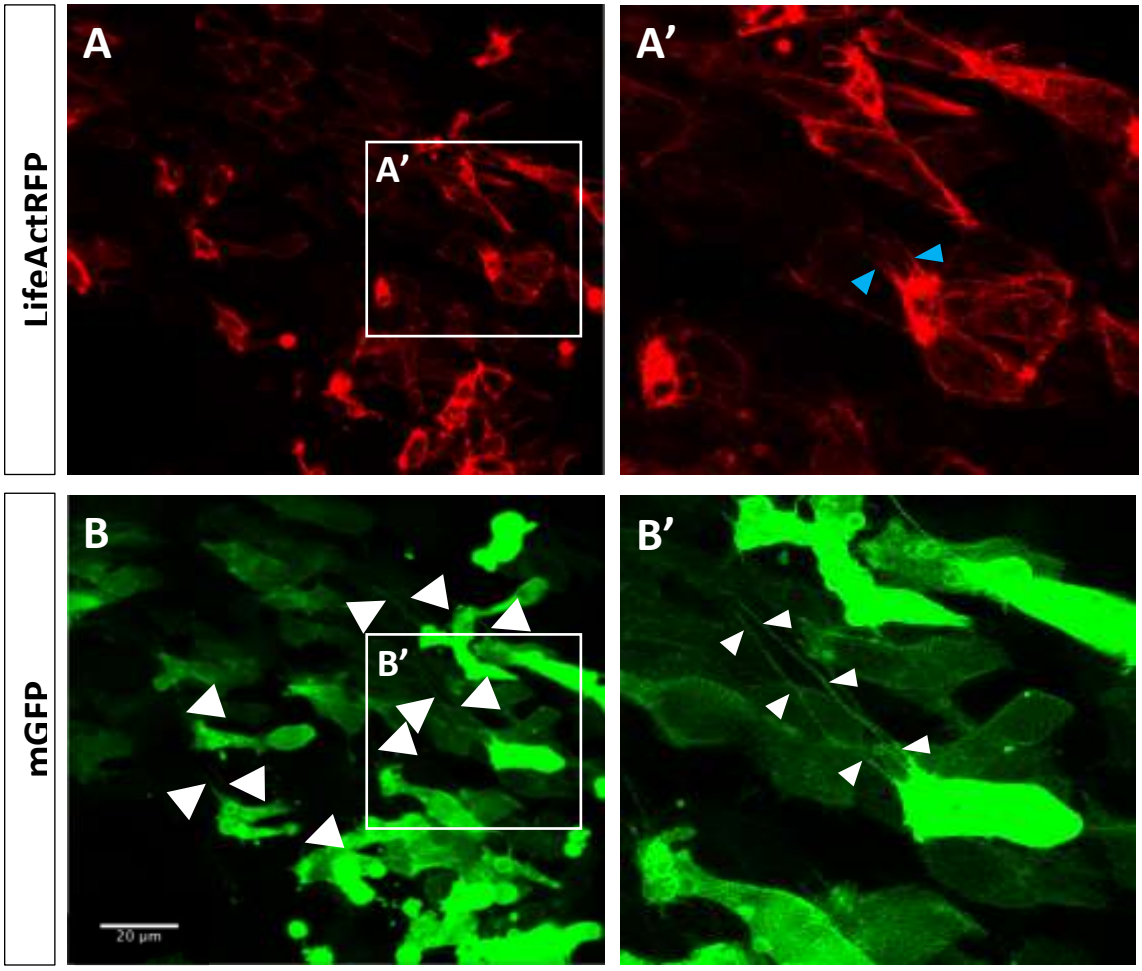

Figure 26. LifeAct labelled only the proximal end of the protrusions. (A-B') Confocal live imaging of chick embryo stage HH15. Periplacodal cells were electroporated with LifeAct-RFP (red) and mGFP (green). **(A-A')** LifeAct labelling showed protrusion emission, but only the proximal end was labelled (inset magnified in A', blue arrowheads). **(B-B')** The mGFP labelled the same structures as LifeAct, but it labelled a longer extension of the protrusions (inset magnified in B´, white arrowheads).

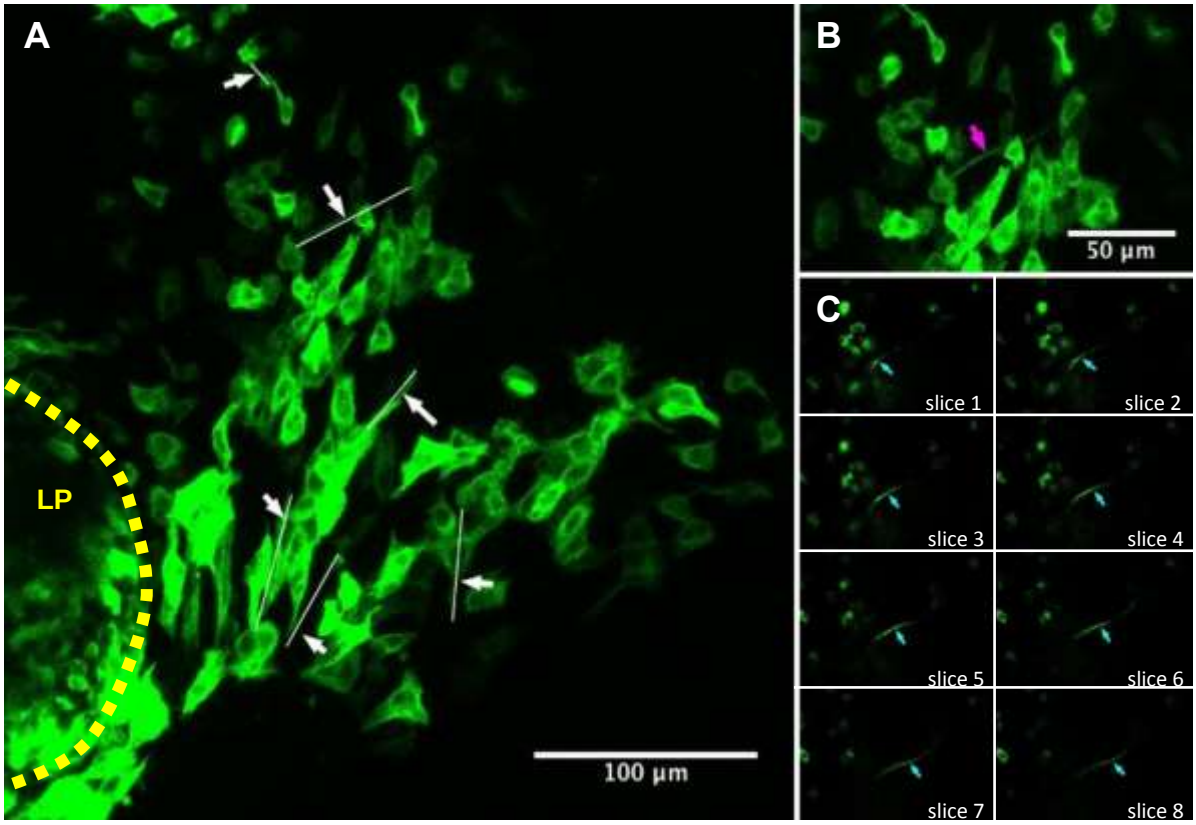

Figure 27. Tubulin appears to label preferentially longer protrusions. (A-C) Confocal live imaging of chick embryo periplacodal cells electroporated with Tubulin-GFP at stage HH15. **(A)** Z-projection of one frame from live imaging experiment. Tubulin labelled long protrusions (white arrows and lines). Protrusion closer to the lens placode invagination (yellow dotted line) appear to be directed tangentially to the placode area. **(B)** Region of figure A placed in prominence, highlighting a long intercellular protrusion (magenta arrow). **(C)** Sequence of optical slices from figure B. The long protrusion appears in slice 1 and continues until slice 10 (cyan arrow). This image was acquired with 1 µm between slices.

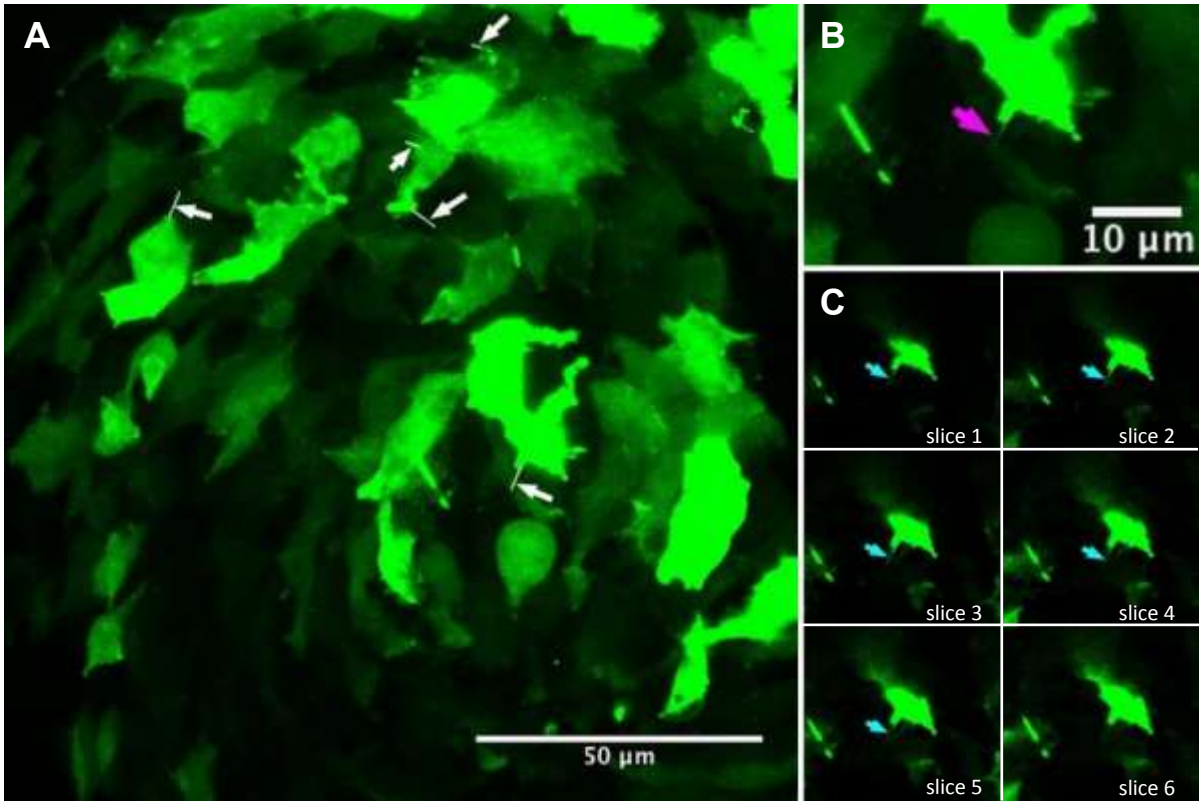

Figure 28. Cofilin appears to label only short protrusions. (A-C) Confocal live imaging of chick embryo periplacodal cells electroporated with Cofilin-GFP at stage HH14. **(A)** Z-projection of one frame from live imaging experiment. Cofilin labelled short protrusions (white arrows). The protrusions do not seem to have a specific direction of emission. **(B)** Region of figure A placed in prominence, highlighting a short protrusion (magenta arrow). **(C)** Sequence of optical slices from figure B. The short protrusion appears in slice 1 until slice 5 (cyan arrow) and disappears in slice 6. This image was acquired with 1 µm between slices.

3.3.2 Quantitative analyses of periplacodal cellular protrusions dynamics

To quantify the dynamics of periplacodal cellular protrusions, we measured all the different parameters during placode invagination (HH15) and calculated protrusions stability, extension/retraction dynamics and direction of emission.

3.3.2.1 Dynamics of extension and retraction activity

Given the variation in protrusion lengths, there are two possibilities regarding their establishment: the growth speed is homogenous independent of the length or there is a heterogeneity in the growth speed of longer and shorter protrusions. Thus, we calculated the dynamics of extension and retraction by correlating the variation of protrusions length during all frames with the maximum length of the protrusion (see Methods). All the results were obtained from mGFP-labelled protrusions.

Our results showed that there is a direct relationship between maximum protrusion length and its velocity (Fig. 29). The longer the protrusion, the higher the average length variation (Fig. 29). In other words, long protrusions extend and retract rapidly, while shorter protrusions tend to be slower, taking more image frames to cover the same distance.

However, this analysis does not provide the information regarding the half-life of the protrusion. Longer protrusions could be established quickly but remain for longer periods whilst the shorter protrusions could be established slowly and have a shorter half-life. Or vice-versa.

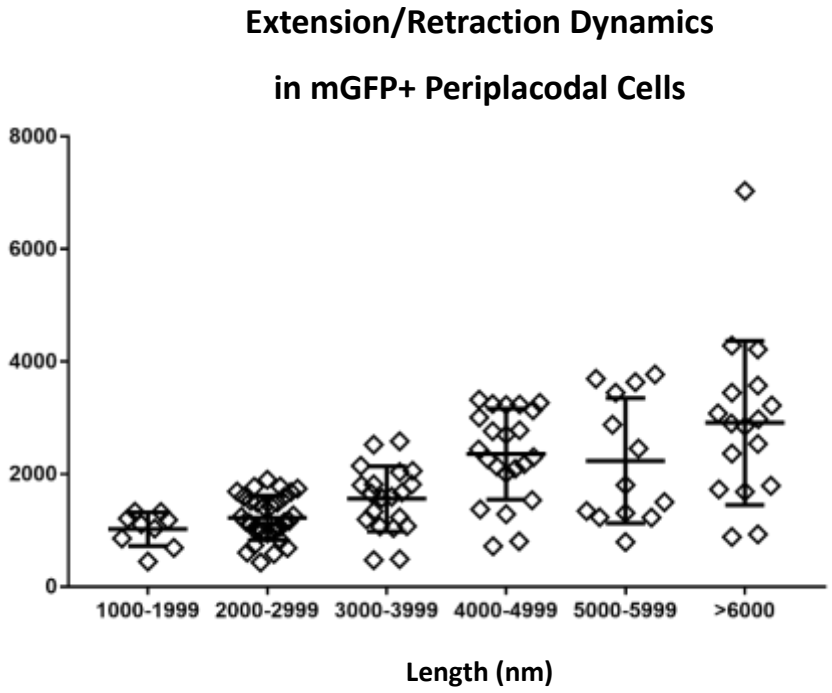

Figure 29. Long protrusions extend and retract rapidly and shorter protrusions are slower. Graph of the relation between maximum length (x axis) and dynamic of extension and retraction movements. The longer the protrusion, the higher the extension/retraction dynamic. Error bars: standard deviation (SD). Horizontal lines: mean. Values of SD and mean were calculated using GraphPrism software.

3.3.2.2 Half-life of cellular protrusions

To distinguish between these possibilities, we investigated if there was a relation between maximal length of the protrusion and its permanence (as seen by its presence in all frames) irrespective of its length in that particular moment. Our results show no clear relation between length and half-life (Fig. 30).

Subsequently, we performed the same analysis of in protrusions expressing Cofilin and Tubulin. Here our objective was to investigate if there is a relation between dynamics, length and cytoskeletal composition Our hypothesis was that the protrusions labelled with Tubulin had longer half-lives, while those labelled with Cofilin would be shorter-lived.

Protrusions labelled with Tubulin presented great variation of length, varying between 3 and 100 µm (Fig. XX). These protrusions were also quite stable, since the great majority did not show variation of extension and retraction during the experiment (Fig. 30). The protrusions labelled with Cofilin were shorter, varying between 3 and 8 µm, and were short-lived (Fig. 30).

3.3.2.3 Directionality of protrusion emission

Next, we analysed if there was a relation between length and direction of the protrusion emission. Here, we hypothesized that the protrusions help maintain tension or movement direction of the periplacodal tissue during placode invagination. In the case of a mechanical function, we expected the longer protrusions to be organized in an opposite or parallel way to the centre of the movement. To investigate if there was a relation between size and direction of emission, we measured the length and angle of each protrusion in relation to the lens placode invagination centre. We repeated these measurements with mGFP, Cofilin and Tubulin-labelled cells to investigate if it is possible to relate direction/length with cytoskeleton composition.

The results with mGFP do not show a preferential direction of emission of the protrusions and there is no clear relation between length and angle (Fig. 31). Both long and short protrusions were found in all quadrants without favouring a specific region relative to the invagination centre (Fig. 31). Similar to observed in mGFP labelled cells, the results with Cofilin or Tubulin-labelled protrusions do not show preferential directionality relative to the invagination centre (Fig. 31).

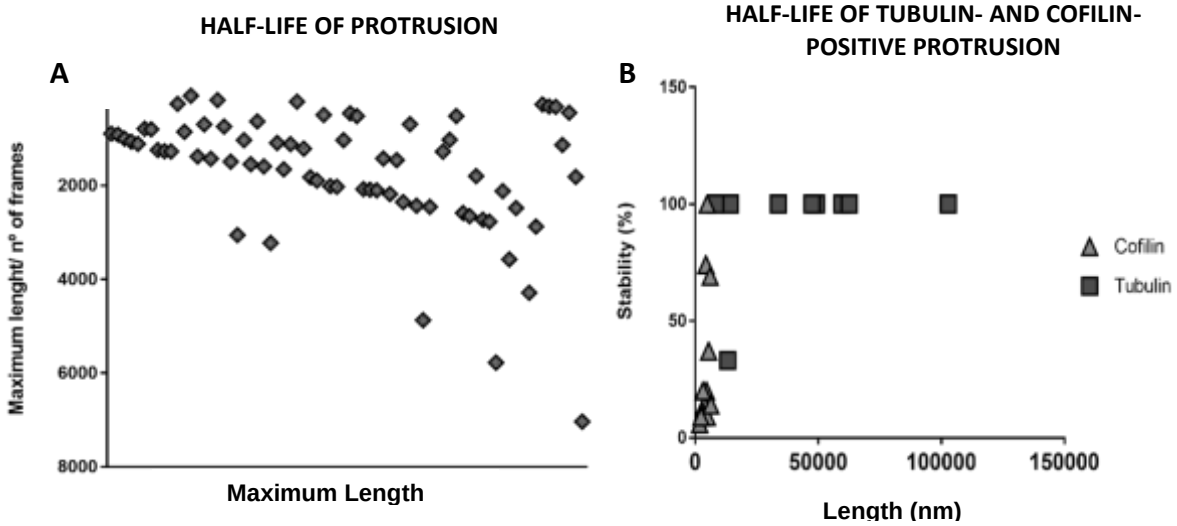

Figure 30. There is no relation between half-life and maximum length of protrusions, but Tubulin-positive protrusions have a longer half-life than Cofilin. (A-B) Graphs relating half-life (y axis) and maximum length (x axis) of periplacodal protrusions. **(A)** mGFP positive periplacodal protrusions showed a tendency for longer protrusions to have a half-life greater than the shorter ones. However, there is a great diversity of lengths of protrusions that have short half-lives. **(B)** In Cofilin and Tubulin-positive protrusions, there is no correlation between the half-life and maximum length. However, most of Cofilin-positive protrusions have a small half-life while most of Tubulin-positive protrusions have a long half-life.

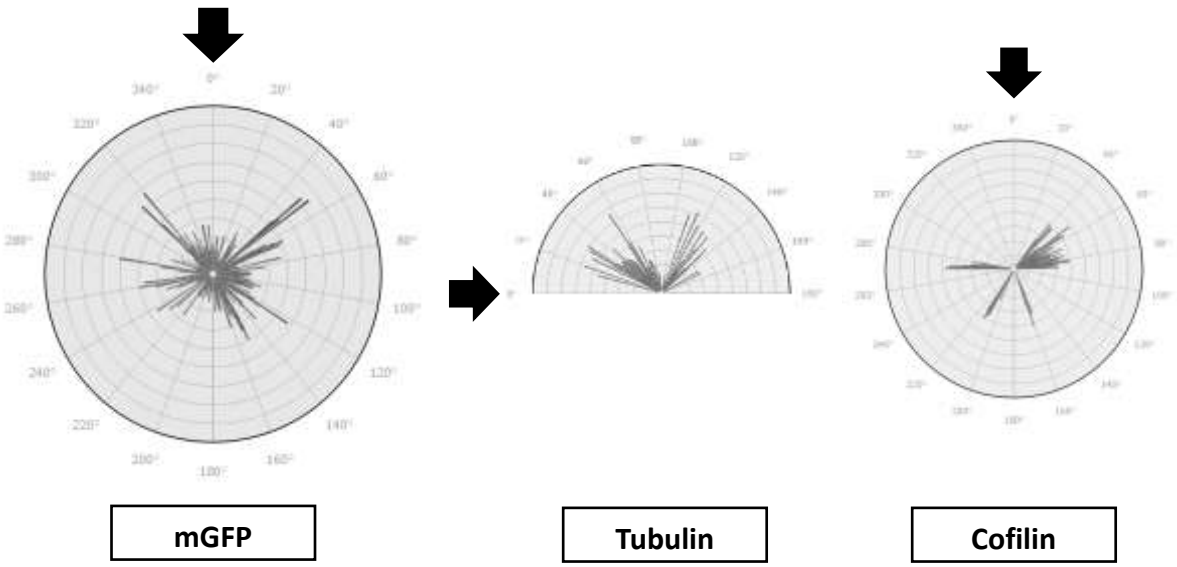

Figure 31. There is no specific direction of protrusion emission and no relation between angle and length. Graphs of distribution of emission angulation measured with mGFP-, Tubulin- and Cofilin-positive protrusions. The black arrow points to the angle 0°, relative to the direction of the lens placode invagination centre. The size of the lines corresponds to the length of the protrusions. In all graphs, there is no clear relation between the protrusion length and the angle of emission. Also, the angle is independent of the cytoskeleton composition. Tubulin-positive protrusions graph ranged from 0° to 180° degrees because measurements were performed only in one embryo, where only one side of the lens placode was visualized.

3.3.3 Evolutionary conservation of periplacodal protrusions in mouse embryos

If the periplacodal cellular protrusions play an important role in optic development, it is likely that they are evolutionarily conserved in amniotes. Thus, we investigated their occurrence in mouse embryos. To visualize the cellular protrusions in the mouse embryonic tissue, we crossed two transgenic mouse lines to obtain embryos with a expression of fluorescent proteins in mosaic pattern (see Methods).

Our results showed a high density of periplacodal protrusions emission (Fig. 32 and 33). As in chick embryo live imaging data, we also observed a great diversity of length, dynamics and membrane puncta transport. The amount of protrusions interfered with their visualization in Z-projection of the optical slices (Fig. 32 A). In our first analyses, we analysed the optical slices separately and identified extension and retraction activity at short time intervals (approximately 1 min). This was seen in both long and short protrusions (Fig. 32 C-E; white arrows ‘a’ and ‘b’). We also saw stable protrusions with no activity of retraction and extension during the frames (Fig. 32, magenta arrows).

Next, we analysed areas where there were fewer GFP-positive cells (Fig. 33). We observe a large number of periplacodal protrusions emission with different lengths and dynamics. There were stable protrusions, with no extension and retraction movements during frames (Fig. 33, magenta arrows) and unstable protrusions, whose length varies over the frames (Fig. 33, white arrows). In Figure 33 C, protrusion ‘a’ seems to be an intercellular communication, as there is a traveling membrane puncta (Fig. 33 C-C’’’ tip of magenta arrow ‘a’). Other protrusions have an intense extension and retraction activity, varying in length between the frames (Fig. 33 C-C’’’, protrusion ‘b’; Fig. 33 D-D’’’, protrusions ‘c’ and ‘e’; Fig. 33 E-E’’’, protrusion ‘f’). Protrusion ‘b’ extend between frame 1 and 9 (C-C’’), when in reaches a great length of approximately 29,5 μm, and retracts in frame 14 (C’’’).

Further, we observed protrusions linking to other ones. (Fig. 33 D-D’’’, cyan arrows). Protrusion ‘d’ seems to be linked to another protrusion in frame 1 and 5 (D-D’) and retracts between frame 9 and 14, when they lose contact (D’’-D’’’). During contact and retraction there seems to be a membrane puncta exchange (tip of cyan arrow ‘d’).

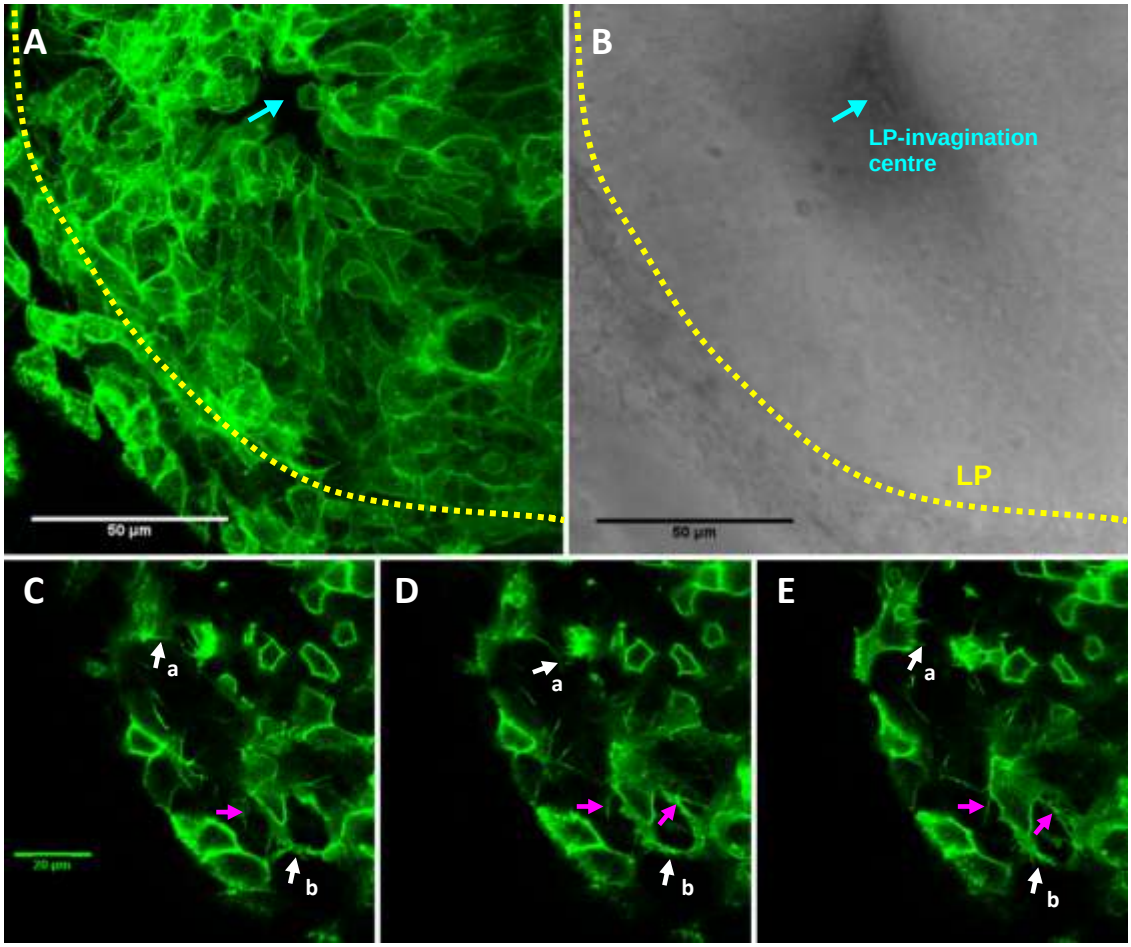

Figure 32. Mouse embryos periplacodal cells showed intense protrusion emission. (A) Z-Projection of GFP-positive cells in mouse embryo at stage E10.0. Even with a mosaic expression pattern, its is hard to distinguish protrusions in images generated by maximal Z-projection. **(B)** Bright field of the last optical slice (most basal), showing the lens placode (yellow dotted line) and the centre of lens invagination (cyan arrow). **(C-D)** Sequence of non continuous frames of one optical slice showing the dynamic of periplacodal protrusions. One of the protrusions is very unstable. It extends between frame 1 (C) and frame 7 (D) and appears retracted in frame 14 (E) (white arrow 'a'). Two protrusions are stable, they do not extend or retract between the frames (magenta arrows). One protrusion is in contact with another one, forming a bridge in frame 1 and 2 (C and D) and then they lose contact in frame 14 (E) (white arrow 'b'). This image was acquired with approximately one minute of interval between the frames. LP= lens pit

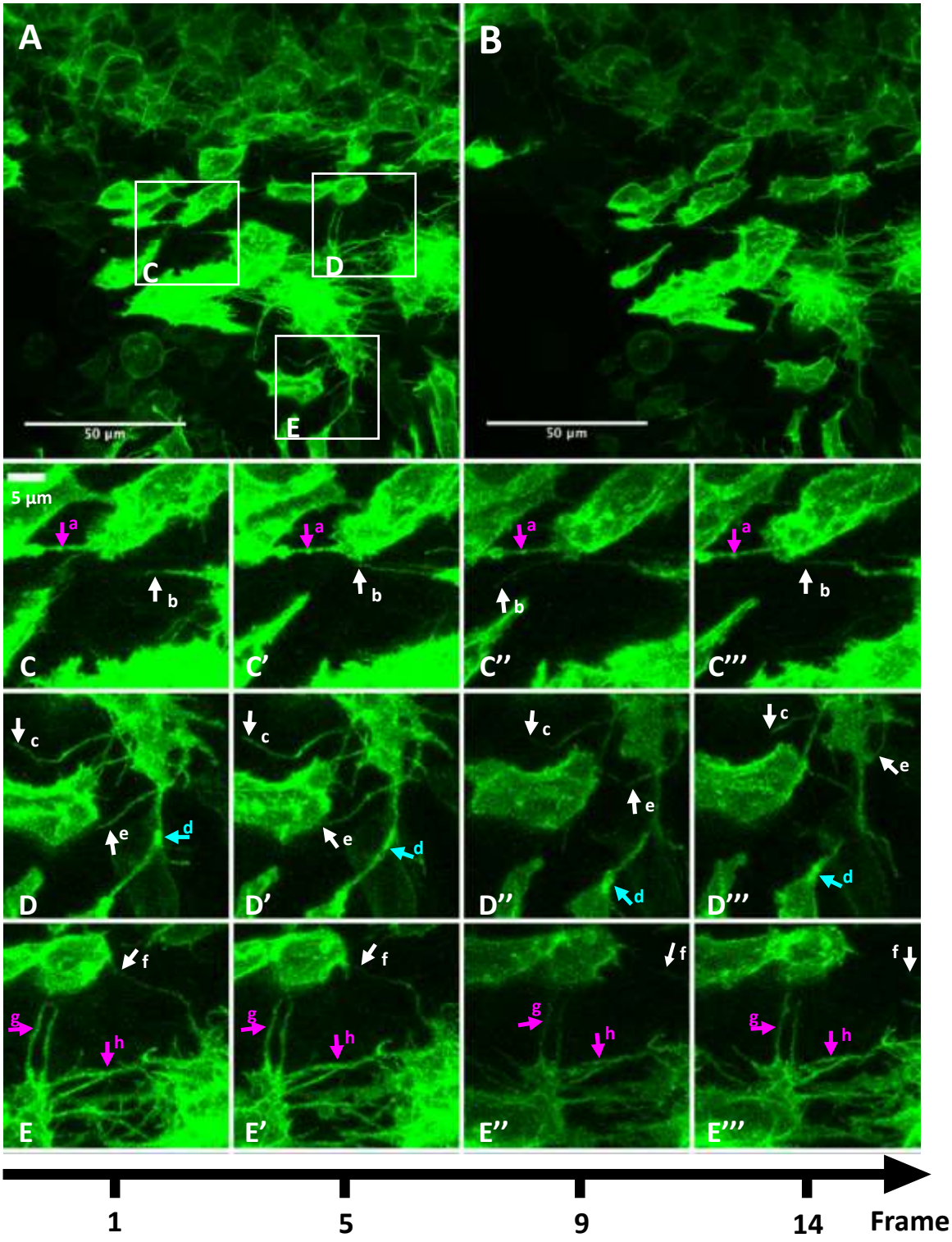

Figure 33. Periplacodal protrusions showed great diversity in length and behaviour in mouse embryos. (A-E) Z-Projection of confocal live imaging of GFP-positive cells in mouse embryo periplacodal region at stage E9.75. **(A-B)** Frame 1 (A) and frame 14 (B) shows stable and unstable protrusions with different lengths. **(C-E)** Sequence of frames in higher magnification of the regions delimited in A. White arrows point to unstable protrusions and magenta arrows point to stable protrusions. **(C-C''')** Protrusion 'a' is an intercellular stable communication and it seems to be a membrane puncta traffic. **(D-D''')** Protrusion 'd' (cyan arrow) contacts another protrusion in frame 1-5 and loses contact in frame 9-14 after retraction. There also seems to be membrane puncta transport (tip of cyan arrow). **(C-E''')** Protrusions 'b', 'c', 'e' and 'f' are unstable. They extend and retract between the frames, reaching long short extensions. This image was acquired with approximately one minute of interval between the frames.

3.3.4 Thin membrane protrusions presence in other epithelial surface

As we did not find a clear correlation between periplacodal protrusions and the placode invagination movement, we then searched for protrusions in other surface ectoderm cells of chick and mouse embryos (Fig. 34). Surprisingly, cells from other regions also exhibit protrusions in both models (Figure 34). In chick embryos, we analysed epithelia electroporated cells from the surface of the anterior head ectoderm and hindbrain (Fig. 34 A and B). In mouse embryos, we analysed the epithelial surface from otic placode region, somites and anterior head ectoderm (Fig. 34 C and D). This data shows that the protrusions - originally identified in periplacodal cells - are actually characteristic of ectoderm, suggesting an important role in the development of the embryonic epithelial surface.

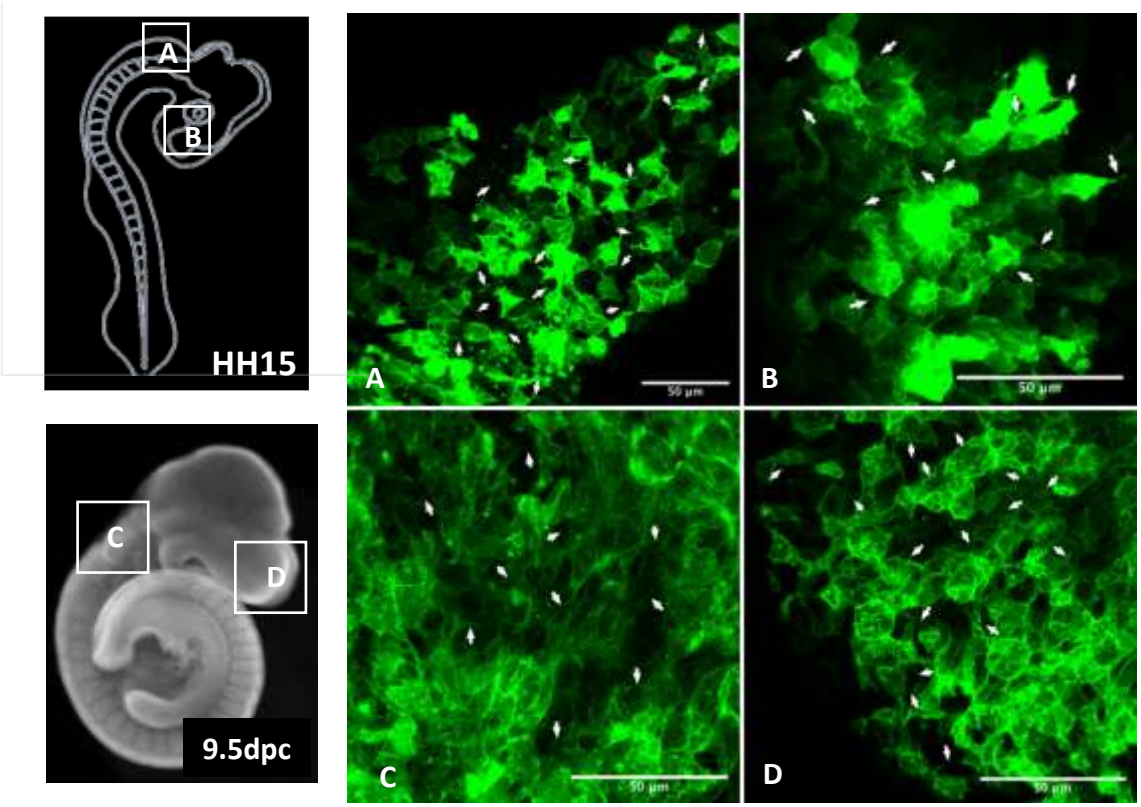

Figure 34. Other surface epithelia have thin membrane protrusions. (A-D) Confocal live images showing cellular protrusion emission (white arrows). Squares from the scheme on the right corresponds to the regions of images A-D. **(A-B)** Chick embryo at stage HH15 electroporated with mGFP. In A, cells from anterior head ectoderm region and, in B, cells from the hind brain surface. **(C-D)** Mouse embryo at stage E9.5 expressing mTmg-GFP. The scheme on the right points to regions correspondent to the images shown in C and D. In C, cells from otic placode region and, in D, cells from anterior head ectoderm.

3.4 DISCUSSION

Thin membrane protrusions have been increasingly identified as an additional manner of establishing morphogen gradients besides the classical models of secretion and diffusion. Protrusions allow precise and localized information exchange (reviewed in Yamashita et al., 2018). Thin membrane protrusions can be classified in three groups according to their morphology and behaviour: cytonemes, tunneling nanotube (TNT)-like protrusions and microtubule-based nanotubes (MT nanotubes) (reviewed in Yamashita et al., 2018).

To place the membrane protrusions observed in periplacodal cells during lens placode invagination in the context of these previously describe protrusions, we focused here on their behavior and cytoskeletal composition. Our quantification analyses showed a large variation in length (0.7 and 22 µm), and a relation between maximum length and velocity, where longer protrusions extend and retract rapidly and shorter protrusions have slower dynamics. Our first hypothesis was that these protrusions were related to the cell movement involved in lens morphogenesis and could generate the necessary tension/force for placodal lens closure. In vertebrate embryos, the emission of protrusions have been associated to morphogenetic processes. During convergent-extension movements for the formation of the neural plate in Xenopus embryos there is a polarized protrusions emissions that is necessary for the exert traction between intercalating cells (Davidson and Keller, 1999). Protrusions are also observed during neural tube closure in various other developmental models (reviewed in Nikolopoulou et al., 2017). In mouse embryos, filopodia and ruffles (lamelipodia) are found during different moments of neurulation (Rolo et al., 2016). At the onset of neural tube closure, the protrusions are mostly filopodia and they are longer than other regions (Rolo et al., 2016). In chick and Xenopus embryos, the non-neural ectoderm that borders the neural plate needs to join together at the final stages of neural tube formation (reviewed in Nikolopoulou et al., 2017). In chick embryos, the non-neural ectoderm cells emit filopodia-like protrusions during contact and, in Xenopus, those protrusions are more like ruffles (reviewed in Nikolopoulou et al., 2017). In both cases the protrusions participate on the neural tube closure (reviewed in Nikolopoulou et al., 2017). In this scenario, the protrusions should then be organized in force-generating vectors relative to the lens invagination movement. After measuring the angle of protrusions emission relative to the centre of the invagination point, we didn´t find a

preferential direction relative to the centre of lens placode invagination, suggesting that these protrusions did not generate a net force or tension that could affect tissue morphogenesis.

Our next hypothesis was that these protrusions played a role in intercellular communication. We observed membrane puncta transport through in these protrusions. When we measured an individual puncta movement speed, we observed that it moved at 80nm/s. This data places membrane puncta transport as a possible function for our protrusions. Firstly, during chick limb bud development, mesenchymal cells emit protrusions that transport Shh at an average speed of 120nm/s (Sanders et al., 2013). Also, in somite development, the dermomyotome extends protrusions that transport membrane puncta that contain the Wnt receptor Frz7 at 65nm/s (Sanders et al., 2013; Sagar et al. 2015). Thus, the speed of transport that we observed is within the previously identified transportation events and could be an indication that this is one of the functions of the periplacodal protrusions.

Since both of these previously described protrusions are formed by actin (Sanders et al., 2013; Sagar et al., 2015), we then investigated the presence of actin in our periplacodal protrusions. Our results showed that the periplacodal region contains both Tubulin- and Cofilin-positive protrusions. We then conclude that the mGFP-labelled protrusions are composed of both actin and Tubulin-positive protrusions. This heterogeneity in cytoskeletal composition could explain why we did not detect in mGFP-labelled protrusions a direct relation between their half-life and length.

Indeed, when we analysed separately the half-life of the Tubulin or Cofilin-positive protrusions, a clearer picture emerged. Tubulin labelled both long and short protrusions, but all with longer half-lives. Cofilin labelled short and more unstable protrusions. These results are consistent with what is known about cell biology of actin and microtubules-based structures (Farhadi et al., 2018). F-actin and microtubules are dynamic polymers that assemble from ATP-bound G-actin monomers and GTP-bound α–β-Tubulin heterodimers respectively (reviewed in Coles and Bradke, 2015). In both, accessory proteins facilitate filament polymerisation and modulate stabilisation of the filament. Purified polymerized microtubules are more unstable than actin filaments in *in vitro* conditions (reviewed in Coles and Bradke, 2015). However, in a more complex scenario, such as in the mammalian axonal growth cone, actin filaments are abundant in immature dendritic spines and microtubules bundles are formed in mature and stable dendrites and axon of the neuron (reviewed in Coles and Bradke,

2015). Both filaments are associated with motors proteins such as myosin for actin filaments and kinesin and dynein in microtubules (Alberts, 2010). Those motor proteins have a great diversity of dynamic properties and their movement velocity can vary between 0.2 and 60 µm/s for myosins and 0.02 to 2 µm/s for kinesins (Alberts, 2010). Thus, because they are more stable, it is possible that our microtubule-positive protrusions are the main carriers of membrane puncta transport.

Unfortunately, our methodology does not allow us to visualize membrane puncta transport and cytoskeletal composition at the same time. It would be interesting to take more measurements of membrane puncta transport velocity and to associate them with the cytoskeleton composition. This would give us clues as to what kind of transport occurs in our context and would help investigate what is being transported.

Interestingly, we detected similar thin membrane protrusion in different regions of the surface ectoderm, suggesting that these protrusions play a role in the overall development of this tissue. Protrusions are found in different ectodermal cells contexts during embryonic development in zebrafish (Luz et al., 2014) and mouse embryos (Rolo et al., 2016). In zebrafish, epithelial cells emit filopodia that participate in Wnt signalling during neuroectoderm patterning (Luz et al., 2014). In mouse embryos, the protrusions analysed during neural tube closure are also found in neighbouring cells that will later become the epidermis of the skin (Rolo et al., 2016). In mouse embryos later eye development stages, filopodia extend from epithelial cells during eyelid closure. In mouse transgenic embryos mutated for c-jun, which is a transcription regulator of EGFR, filopodia emissions decrease in number and length and the embryo displays defective eyelid closure (Zenz et al., 2003). This widespread presence of protrusions in the surface ectoderm suggest that they are relevant for embryonic skin development. If that is the case, their importance could be evolutionarily conserved, as we observed the same richness in protrusions in different regions of the mouse embryo surface ectoderm.

3.5 CONCLUSION

Our data showed an intense thin membrane protrusion emission by periplacodal cells during lens placode development in chick and mouse embryos. In both models, there was a great variation of length, dynamics and we also observed the traffic of membrane puncta through the protrusions. Our quantification analyses of membrane labelled-protrusions showed no correlation between length and direction of emission or with half-life of the protrusions. We also analysed Cofilin- and Tubulin-positives protrusions, which had a shorter and longer half-life respectively. These data suggest a heterogeneous population of periplacodal protrusions. Finally, we also identified these protrusions in other ectodermal surfaces, suggesting that they play a role in surface ectoderm development.

4. REFERENCES

Araya, C., Carmona-Fontaine, C., & Clarke, J. D. W. (2016). Extracellular matrix couples the convergence movements of mesoderm and neural plate during the early stages of neurulation. Developmental Dynamics, 245(5), 580–589.

Bailey, A. P., Bhattacharyya, S., Bronner-Fraser, M., & Streit, A. (2006). Lens Specification Is the Ground State of All Sensory Placodes, from which FGF Promotes Olfactory Identity. Developmental Cell, 11(4), 505–517.

Borges, R. M., Lamers, M. L., Forti, F. L., dos Santos, M. F., & Yan, C. Y. I. (2011). Rho signaling pathway and apical constriction in the early lens placode. Genesis, 49(5), 368–379.

Bokel C, Brown NH. (2002). Integrins in development: moving on, responding to, and sticking to the extracellular matrix. Dev Cell 3:311–321.

Brown, N.H., Gregory, S.L., and Martin-Bermudo, M.D. (2000). Integintegrin inactivation occur on timescales of minutes, rins as mediators of morphogenesis in Drosophila. Dev. Biol. 223, 1–16.

Byers B, Porter KR. (1964). Oriented microtubules in elon- gating cells of the developing lens rudiment after induction. Proc Natl Acad Sci USA 52:1091–1099.

Chauhan, B., Plageman, T., Lou, M., & Lang, R. (2015). Epithelial Morphogenesis: The Mouse Eye as a Model System 1, 111, 375–399.

Chiquet M (1999) Regulation of extracellular matrix gene expression by mechanical stress. Matrix Biology 18(5):417–426.

Cholkar, K., Dasari, S. R., Pal, D., & Mitra, A. K. (2013). Eye: Anatomy, physiology and barriers to drug delivery. Ocular Transporters and Receptors: Their Role in Drug Delivery.

Coles, C. H., & Bradke, F. (2015). Review Coordinating Neuronal Actin – Microtubule Dynamics. Current Biology, 25(15), R677–R691.

Collomb, E., Yang, Y., Foriel, S., Cadau, S., Pearton, D. J. and Dhouailly, D. (2013). The corneal epithelium and lens develop independently from a common pool of precursors. Dev. Dyn. 242, 401– 13.

Danilchik M., Williams M., Brown E. (2013). Blastocoel-spanning filopodia in cleavage-stage Xenopus laevis: potential roles in morphogen distribution and detection. Dev Biol 382:70–81.

Dhouailly, D., Pearton, D. J. and Michon, F. (2014). The vertebrate corneal epithelium: From early specification to constant renewal. Dev. Dyn. 243, 1226–1241.

Diaz-de-la-Loza, M. del C., Ray, R. P., Ganguly, P. S., Alt, S., Davis, J. R., Hoppe, A., Thompson, B. J. (2018). Apical and Basal Matrix Remodeling Control Epithelial Morphogenesis. Developmental Cell, 46(1), 23–39.e5

Farhadi, L., Fermino Do Rosario, C., Debold, E. P., Baskaran, A., & Ross, J. L. (2018). Active Self-Organization of Actin-Microtubule Composite Self-Propelled Rods. *Frontiers in Physics*, *6*(July), 1–16.

Fata, J. E., Werb, Z., & Bissell, M. J. (2004). Review Regulation of mammary gland branching morphogenesis by the extracellular matrix and its remodeling enzymes, 1–11.

Ffrench-Constant, C., & Hynes, R. O. (1988). Patterns of Fibronectin gene expression and splicing during cell migration in chicken embryos. Development (Cambridge, England), 104(3), 369–382.

Frantz, C., Stewart, K. M., & Weaver, V. M. (2010). The extracellular matrix at a glance. Journal of Cell Science, 123(24), 4195–4200.

Furuta, Y. & Hogan, B. L. (1998) BMP4 is essential for lens induction in the mouse embryo. Genes Dev. 12, 3764–3775.

Gilbert SF. Developmental Biology. 10th ed. Sinauer Associates; 2013.

Grocott, T., Johnson, S., Bailey, A. P., & Streit, A. (2011). Neural crest cells organize the eye via TGF-β and canonical Wnt signalling. Nature Communications, 2, 266–269.

Hamill, K. J., Kligys, K., Hopkinson, S. B., & Jones, J. C. R. (2009). Laminin deposition in the extracellular matrix: a complex picture emerges. *Journal of Cell Science*, *122*(24), 4409–4417.

Hendrix RW, Zwaan J. (1974). Changes in the glycoprotein concentration of the extracellular matrix between lens and optic vesicle associated with early lens differentiation. Differentiation 2, 357-362.

Hendrix RW, Zwaan J. (1975). The matrix of the optic vesicle- presumptive lens interface during induction of the lens in the chicken embryo. J Embryol Exp Morphol 33:1023–1049.

Hendrix, R. W. & Zwaan, J. (1974). Correlation between changes in extracellular matrix and early lens differentiation. Anat. Rec. 178, 372.

Hilfer, S. R., & Randolph, G. J. (1993). Immunolocalization of basal lamina components during development of chick otic and optic primordia. The Anatomical Record, 235(3), 443–452.

Hintze, M., Prajapati, R. S., Tambalo, M., Christophorou, N. A. D., Anwar, M., Grocott, T., & Streit, A. (2017). Cell interactions, signals and transcriptional hierarchy governing placode progenitor induction. Development, 144(15), 2810–2823.

Huang J, Rajagopal R, Liu Y, Dattilo LK, Shaham O, Ashery- Padan R, Beebe DC. (2011) The mechanism of lens placode for- mation: a case of matrix-mediated morphogenesis. Dev Biol 355:32–42.

Inaba M, Buszczak M, Yamashita YM. (2015). Nanotubes mediate niche-stem-cell signalling in the Drosophila testis. Nature 523:329–32

Jalali S.,del Pozo MA,ChenK,MiaoH,LiY,Schwartz MA,ShyyJY, Chien S. (2001). Integrin-mediated mechanotransduction requires its dynamic interactionwith specific extracellularmatrix (ECM) ligands. In: Proceedings of the national academy of sciences of the United States of America vol 98(3), pp 1042–1046

Jenkins RG, Su X, Su G, Scotton CJ, Camerer E, Laurent GJ, Davis GE, Chambers RC, Matthay MA, Sheppard D. (2006). Ligation of protease-activated receptor 1 enhances avb6 Integrin-dependent TGF-b activation and pro- motes acute lung injury. J Clin Invest 116: 1606–1614.

Jidigam, V. K., Srinivasan, R. C., Patthey, C., & Gunhaga, L. (2015). Apical constriction and epithelial invagination are regulated by BMP activity. Biology Open, 4(12), 1782–1791.

Joki N, Kaname S, Hirakata M, Hori Y, Yamaguchi T, Fujita T, Katoh T, Kurokawa K (2000) Tyrosine-kinase dependent TGF-beta and extra- cellular matrix expression by mechanical stretch in vascular smooth muscle cells. Hypertens Res - Clin Exp 23(2):91–99

Kadoya, Y., Salmivirta, K., Talts, J.F., Kadoya, K., Mayer, U., Timpl, R., et al. (1997). Importance of nidogen binding to Laminin gamma1 for branching epithelial morphogenesis of the submandibular gland. Development 124, 683–691.

Kleinman, H. K., Philp, D., & Hoffman, M. P. (2003). Role of the extracellular matrix in morphogenesis. Current Opinion in Biotechnology, 14(5), 526–532.

Kornberg, T. B. (2017). Distributing signaling proteins in space and time: the province of cytonemes. Current Opinion in Genetics and Development.

Kornberg, T. B. and Roy, S. (2014). Cytonemes as specialized signaling filopodia. Development 141, 729–36.

Kwan, K. M. (2014). Coming into focus: The role of extracellular matrix in vertebrate optic cup morphogenesis. Developmental Dynamics, 243(10), 1242–1248.

Lallier, T.E., DeSimone, D.W. (2000). Separation of neural induction and neurulation in Xenopus. Dev. Biol. 225, 135–150.

Lecuit T, Lenne PF. (2007). Cell surface mechanics and the control of cell shape, tissue patterns and mor- phogenesis. Nat Rev Mol Cell Biol 8:633–644.

Lee AA, Delhaas T, McCulloch AD, Villarreal FJ (1999) Differential responses ofadult cardiac fibroblasts to in vitro biaxial strain patterns. J Mol Cell Cardiol 31(10):1833–1843.

Linask, K. K. & Lash, J. W. (1986). Precardiac cell migration: Fibronectin localization at mesoderm- endoderm interface during directional movement. Devi Biol. 114, 87-101

Linker, C., De Almeida, I., Papanayotou, C., Stower, M., Sabado, V., Ghorani, E., Streit, A., Mayor, R. and Stern, C. D. (2009). Cell communication with the neural plate is required for induction of neural markers by BMP inhibition: evidence for homeogenetic induction and implications for Xenopus animal cap and chick explant assays. Dev. Biol. 327, 478-486.

Litsiou, A., Hanson, S., and Streit, A. (2005). A balance of FGF, Wnt and BMP signalling positions the future placode territory in the head. Development 132, 4051–4062.

Logan, C. Y., & Nusse, R. (2004). the Wnt Signaling Pathway in Development and Disease. Annual Review of Cell and Developmental Biology, 20(1), 781–810.

Loganathan, R., Rongish, B. J., Smith, C. M., Filla, M. B., Czirok, A., Be, B., & Little, C. D. (2016). Extracellular matrix motion and early morphogenesis, 2056–2065.

Luz M., Spannl-Muller S., Ozhan G., Kagermeier-Schenk B., Rhinn M., Weidinger G., Brand M. (2014). Dynamic association with donor cell filopodia and lipid-modification are essential features of Wnt8a during patterning of the zebrafish neuroectoderm. PLoS One 9:e84922

Lwigale, P. Y. (2015). Corneal development: ifferetn cells from a common progenitor. Prog. Mol. Biol. Transl. Sci. 134, 43-59.

Mao, Y., & Schwarzbauer, J. E. (2005). Fibronectin fibrillogenesis, a cell-mediated matrix assembly process. Matrix Biology, 24(6), 389–399.

Marsden M, DeSimone DW. (2001). Regulation of cell polar- ity, radial intercalation and epiboly in Xenopus:Novel roles for integrin and Fibronectin. Development 128: 3635–3647.

Martin, A. C., & Goldstein, B. (2014). Apical constriction: themes and variations on a cellular mechanism driving morphogenesis. Development, 141(10), 1987–1998.

Matsuda, M., & Keino, H. (2001). Possible roles of β-catenin in evagination of the optic primordium in rat embryos. Development Growth and Differentiation, 43(4), 391–400.

McKeehan, M. S. (1951). Cytological aspects of embryonic lens induction in the chick. J. Exptl. Zool. 117, 31.

Melo, M. de O., Moraes Borges, R., & Yan, C. Y. I. (2017). Par3 in chick lens placode development. Genesis, 55(6), 1–11.

Mouw, J. K., Ou, G., & Weaver, V. M. (2014). Extracellular matrix assembly: A multiscale deconstruction. Nature Reviews Molecular Cell Biology, 15(12), 771–785.

Munger, J. S., & Sheppard, D. (2011). Cross Talk among TGF-β Signaling Pathways, Integrins, and the Extracellular Matrix. Cold Spring Harbor Perspectives in Biology, 3(11), a005017–a005017.

Munger, J. S., & Sheppard, D. (2011). Cross Talk among TGF-β Signaling Pathways, Integrins, and the Extracellular Matrix. Cold Spring Harbor Perspectives in Biology, 3(11), a005017–a005017.

Munger, J.S., Huang, X., Kawakatsu, H., Griffiths, M.J., Dalton, S.L., Wu, J., Pittet, J.F., Kaminski, N., Garat, C., Matthay, M.A., Rifkin, D.B., Sheppard, D. (1999). The integrin alpha v beta 6 binds and activates latent TGF beta 1: a mechanism for regulating pulmonary inflammation and fibrosis. Cell 96, 319–328.

O'Callaghan CJ, Williams B. (2000). Mechanical strain-induced extra- cellular matrix production by human vascular smooth muscle cells: role of TGF-beta(1). Hypertension 36(3):319–324

Parsons MJ, Pollard SM, Saude L, Feldman B, Coutinho P, Hirst EMA, Stemple DL. (2002). Zebrafish mutants identify an essential role for laminins in notochord formation. Development 129:3137–3146.

Patthey, C., Edlund, T. and Gunhaga, L. (2009). Wnt-regulated temporal control of BMP exposure directs the choice between neural plate border and epidermal fate. Development 136, 73-83.

Pieper, M., Ahrens, K., Rink, E., Peter, A. and Schlosser, G. (2012). Differential distribution of competence for panplacodal and neural crest induction to non-neural and neural ectoderm. Development 139, 1175-1187.

Prols F, Sagar, Scaal M (2016) Signaling filopodia in vertebrate embryonic development. Cell Mol Life Sci 73: 961-974.

Rajagopal, R., Huang, J., Dattilo, L. K., Kaartinen, V., Mishina, Y., Umans, L., Beebe, D. C. (2010). The type I BMP receptors, Bmpr1a and Acvr1, activate multiple signaling pathways to regulate lens formation. NIH Public Access, 335(2), 305–316.

Ramirez-Weber FA, Kornberg TB (1999) Cytonemes: cellular processes that project to the principal signaling center in Drosophila imaginal discs. Cell 97: 599-607.

Riedl, J., Crevenna, A. H., Kessenbrock, K., Yu, J. H., Bista, M., Bradke, F., Jenne, D., Holak, T. A., Werb, Z., Sixt, M., et al. (2008). Lifeact: a versatile marker to visualize F-actin. Nat. Methods 5, 605–7. S

Rifes, P., & Thorsteinsdóttir, S. (2012). Extracellular matrix assembly and 3D organization during paraxial mesoderm development in the chick embryo. Developmental Biology, 368(2), 370–381.

Roy S, Huang H, Liu S, et al. (2014) Cytoneme-mediated contact-dependent transport of the Drosophila decapentaplegic signaling protein. Science 343: 1244624.

Rozario, T., & DeSimone, D. W. (2010). The extracellular matrix in development and morphogenesis: A dynamic view. Developmental Biology, 341(1), 126–140.

Rustom A., Saffrich R., Markovic I., Walther P., Gerdes HH. (2004). Nanotubular highways for intercellular organelle transport. Sci- ence 303:1007–1010.

Sagar, Prols F, Wiegreffe C, Scaal M. (2015). Communication between distant epithelial cells by filopodia-like protrusions during embryonic development. Development 142:665–71

Sanders, T. a, Llagostera, E. and Barna, M. (2013). Specialized filopodia direct long-range transport of SHH during vertebrate tissue patterning. Nature 497, 628–32.

Schook, P. (1980). Morphogenetic movements during the early development of the chick eye. An ultrastructural and spatial reconstructive study. A. Invagination of the lens placode. Acta Morphol. Neerl. Scand. lg, 133—57

Schwarzbauer, J. E., & DeSimone, D. W. (2011). Fibronectins, their fibrillogenesis, and in vivo functions. Cold Spring Harbor Perspectives in Biology, 3(7), 1–19.

Sjödal, M., Edlund, T., & Gunhaga, L. (2007). Time of Exposure to BMP Signals Plays a Key Role in the Specification of the Olfactory and Lens Placodes Ex Vivo. Developmental Cell, 13(1), 141–149.

Smith, M. L., Gourdon, D., Little, W. C., Kubow, K. E., Eguiluz, R. A., Luna-Morris, S. and Vogel, V. (2007). Force-induced unfolding of Fibronectin in the extracellular matrix of living cells. PLoS Biol. 5, e268.

Smyth, N., Vatansever, H.S., Murray, P., Meyer, M., Frie, C., Paulsson, M., et al., 1999. Absence of basement membranes after targeting the LAMC1 gene results in embryonic lethality due to failure of endoderm differentiation. J. Cell Biol. 144, 151–160.

Stanganello, E., Hagemann, A. I. H., Mattes, B., Sinner, C.,Meyen, D.,Weber, S., Schug, A., Raz, E. and Scholpp, S. (2015). Filopodia-based Wnt transport during vertebrate tissue patterning. Nat. Commun. 6, 5846.

Sternlicht, M.D., Kouros-Mehr, H., Lu, P., Werb, Z. (2006). Hormonal and local control of mammary branching morphogenesis. Differentiation 74, 365-381.

Streit, A. (2008). The cranial sensory nervous system: specification of sensory progenitors and placodes. StemBook, (August).

Svoboda, K. K. H., & O'Shea, K. S. (1987). An analysis of cell shape and the neuroepithelial basal lamina during optic vesicle formation in the mouse embryo. Development, 100(2), 185–200.

Vogel V, Sheetz M (2006) Local force and geometry sensing regulate cell functions. Nat Rev Mol Cell Biol 7: 265–275.

Wawersik, S., Purcell, P., Rauchman, M., Dudley, A. T., Robertson, E. J. and Maas, R. (1999). BMP7 acts in murine lens placode development. Dev Biol 207, 176-188.

Weil, M., Jacobson, M. D., & Raff, M. C. (1997). Is programmed cell death required for neural tube closure? Current Biology, 7(4), 281–284.

Yamashita, Y. M., Inaba, M., & Buszczak, M. (2018). Specialized Intercellular Communications via Cytonemes and Nanotubes.

Zenz R, Scheuch H, Martin P, Frank C, Eferl R, Kenner L, Sibilia M, Wagner EF. (2003). c-Jun regulates eyelid closure and skin tumor development through EGFR signaling. Developmental Cell 4:879–889.

5. SUPPLEMENTARY

5.1 OPTIMIZING LASER MICRODISSECTION OF CHICK EMBRYO CRYOSECTIONS

- **Collection of embryos and cryosection**

Embryos were collected by the filter paper method and washed in PBS 1x solution. The embryo stage was analysed in the dissecting microscope and the heads were cut and separated according to the stage of the lens placode (ectoderm, placode, invaginating placode, lens formed).

For the cryosection, the heads were fixed in PFA 4% for 25 minutes, on a rotating platform. Three 10-minute washes were carried out in 1x PBS solution and placed in 20% sucrose overnight solution, diluted in 1x PBS. The next day, the heads were embedded in O.C.T compound (Tissue-Tek) with 20% Sucrose (1:1) and positioned inside the cryocube on dry ice. The cryocubes were stored at -80 ° C. The embryo heads were sectioned (10 mm or 20 mm) on a cryostat (Leica) and mounted on glass slides.

- **Laser capture microdissection (LCM) of cryosections**

LCM was performed using a PALM Microbeam (Zeiss) with 40x Objective. Slides were transported to the instruments room and kept on dry ice. Using the *free hand drawing* and *CloseCut* tool, we delimitated all tissues (pre-placode ectoderm, placode or invaginating placode) that were cut with 72-75 laser points. The areas varied between 3000 and 5000 μm^2 and for each 1000 μm^2 we placed one point off catapulting (LPC). The *Auto LPC* tool automatically calculates the energy of catapulting laser (Supplementary Figure 1 C).

The equipment catapults the cut tissues directly to a 0.6 µl tube cap with a drop of water. After dissecting the tissues of interest, the tubes were kept and transported on ice. We extracted and purified the DNA from the samples and performed PCR with specific primers. Students of our laboratory previously designed the primers used in this experiment and they amplify two genomic DNA sequences for the Slug and Snail gene (Supplementary Figure 1 D).

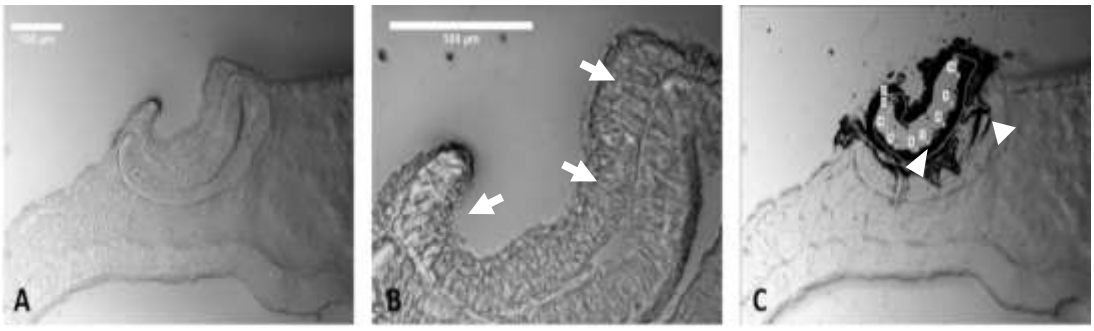

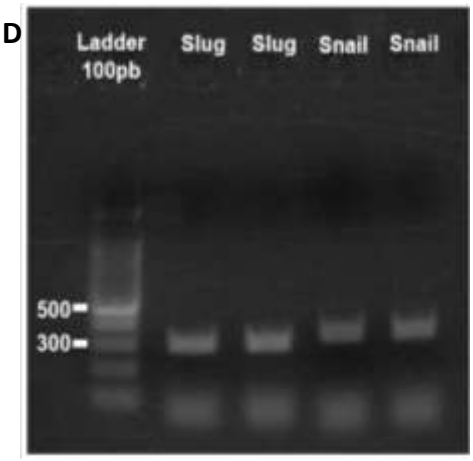

Supplementary Figure 1. Cross section of cryopreserved chick embryo tissues at stage HH15 in the eye region before and after laser microdissection under PALM MicroBeam Zeiss microscope. A. Low magnification of the cross section prior to microdissection. **B.** Higher magnification showing region of the lens invaginating placode (white arrows). C. Low magnification, after laser microdissection, with empty space in the region of the placode (white arrowheads). Small dots represent LPC points. **D.** Agarose gel 2% with PCR results after amplification of genomic sequences. Specific primers were used for the Slug genes (2 first wells) and Snail (2 last wells). Amplified Sequence Size: Slug = 303 bp; Snail = 335 bp.